BIOPHYSICAL AND GENE EXPRESSION CHANGE IN LIVING CELLS BY FORCE-INDUCED MECHANOTRANSDUCTION

BY

YEH CHUIN POH

DISSERTATION

Submitted in partial fulfillment of the requirements
for the degree of Doctor of Philosophy in Mechanical Engineering
in the Graduate College of the
University of Illinois at Urbana-Champaign, 2013

Urbana, Illinois

Doctoral Committee:

Professor Ning Wang, Chair
Associate Professor Yingxiao Wang
Professor Iwona M. Jasiuk
Assistant Professor Brendan A. Harley

ABSTRACT

Within the past decade, there has been abounding scientific evidences supporting the notion that mechanical forces are crucial in regulating the physiologic functions of cells and tissues. The importance of engineering principles in studying the biological behaviour of cells is no longer in question. Instead, much research is now focused on how mechanical forces are transduced into biochemical activities and biological responses at the cellular and molecular level – a process known as mechanotransduction. This work uses both engineering and biological principles to investigate the different biophysical and gene expression changes of individual cells in response to exogenous forces. We attempt to unravel the mechanism at which forces are transmitted from the apical surface of the cell in to the nucleus.

The work presented here provides the first unequivocal evidence that a local surface force can directly alter nuclear functions without intermediate biochemical cascades. We show that a local dynamic force via integrins results in direct displacements of coilin and SMN proteins in Cajal bodies and direct dissociation of coilin-SMN associated complexes. Fluorescence resonance energy transfer changes of coilin-SMN depend on force magnitude, an intact F-actin, cytoskeletal tension, Lamin A/C, or substrate rigidity. Other protein pairs in Cajal bodies exhibit different magnitudes of fluorescence resonance energy transfer. Dynamic cyclic force induces tiny phase lags between various protein pairs in Cajal bodies, suggesting viscoelastic interactions between them. These findings demonstrate that dynamic force-induced direct structural changes of protein complexes in Cajal bodies may represent a unique mechanism of mechanotransduction that impacts on nuclear functions involved in gene expression.

We further extend our study to mouse embryonic stem cells (ESCs). Increasing evidence suggests that mechanical factors play a critical role in fate decisions of stem cells. We

demonstrate that forces transmitted through different natural extracellular matrix proteins or cellcell adhesion molecules such as fibronectin, laminin or E-cadherin, have different effects on cell spreading, cell stiffness, Oct3/4 gene expression, and cell proliferation rate. Surprisingly, it was also observed that mouse ESCs do not stiffen when substrate stiffness increases. These cells do not increase spreading on more-rigid substrates either. However, ESCs do increase their basal tractions as substrate stiffness increases. ESCs therefore exhibit mechanical behaviors distinct from those of mesenchymal stem cells and of terminally differentiated cells, and decouple its apical cell stiffness from its basal tractional stresses during the substrate rigidity response. We further elucidate how mechanical forces influence the differentiation of ESCs into spatially organized endoderm, mesoderm, and ectoderm germ layers. ESCs cultured within 3D soft fibrin gels in the absence of Leukemia Inhibitory Factor (LIF) promotes in vivo tissue morphogenesis during vertebrate gastrulation. The results presented demonstrate that mechanical forces play different roles in different force transduction pathways to shape early embryogenesis.

To my parents, for their love and support.

ACKNOWLEDGMENTS

This dissertation and the completion of my doctorate will not be possible without the guidance of my advisor Prof. Ning Wang. I would like to express my heartfelt gratitude to him, whose advice and counsel were invaluable throughout my doctoral training. His teaching, assistance, supervision, and generous sharing of ideas are only a fraction of the things that I have to thank him for. The opportunity to do research in Wuhan, China and to experience the oriental culture of my Chinese heritage would not be possible if not for the collaboration that Prof. Wang has with Huazhong University of Science and Technology. Primarily, he has been a great example of professionalism and his approach to research will guide me in my future academic career.

Despite being thousands of miles away, I would like to thank my family for always being a source of encouragement and support. To my father, who has been an inspiration to me since I was young. A role model that I hope to emulate, both intellectually and spiritually. It is he who first sowed the thought of pursuing a doctorate in me. To my mother, who has been a constant comfort and just a phone call away. A gentle soul that I can only aspire to be like. Her supportive personality and caring character guided me through thick and thin. I owe it to my parents for the daily thoughts and prayers throughout my university education, for "it may be that my sons have sinned and cursed God in their hearts". To my three brothers, Yeh Han, Yeh Tze and Yeh Ern, all of whom reassured me that higher education was worth pursuing. To my sister-in-law, Louisa, for keeping me motivated with the regular scientific discussions. Family is undeniably my chief pillar of support.

Many of my colleagues have directly or indirectly contributed to this work. I would like to thank members of Prof. Ning Wang's Cell Mechanics Lab. Sungsoo Na, Farhan Chowdhury, Douglas Wu, Arash Tajik, Youhua Tan, Rishi Sigh, Yuhei Uda, Russell Borduin,

Chen Junwei, Yi Haiying, Hong Ying, Zhang Shuang, Chen Junjian, Zhang Yuejin, Jia Qiong, Wang Lili, and Wei Fuxiang have helped in one way or another. A special thanks to Sungsoo Na for the initial training in cell biology and basic experimental techniques. The conversations that we had and the delicious lunch his wife made will definitely be missed. I would also like to thank Prof. Fei Wang, and Prof. Peter Yingxiao Wang for the technical assistance they have provided all these years. In the same spirit, I would like to acknowledge members of my doctoral committee. Their insightful suggestions and valuable comments made the work presented here more complete and thorough.

My uncle in Michigan, Chek Teck Poh and the rest of his family, Auntie Elsa, Alex and Andrew, have been my family away from home. I thank them for the wonderful thanksgiving celebrations and family trips over the past few years. They have been a great support emotionally and financially throughout my college education. I would also like to thank the brethren of Damansara Reformed Baptist Church for their regular prayers. The thought of them praying for me and the warm welcome I receive every time I visit Malaysia, is a constant reminder of where I am from and the importance of a local church family.

My stay in America the past eight years would not have been the same without the love and support of the Pakala family. They have been a tremendous encouragement in times of need. I thank Uncle Leino for the wise advice and regular prayers that kept me along the straight and narrow path. Auntie Sally has been a motherly figure to me. I thank her for all the delicious food and the Sunday evening phone calls that kept me grounded. Thanks also to Alexandra Pakala for the many visits to Champaign with Perry Anderson. Their occasional presence created many fond memories that are very much appreciated.

I truly value the interactions I have had with fellow students at the University of Illinois. I thank all members of AIESEC for the great social and professional experience. I have grown especially close to Oksana, Victor, Kaitlyn, Nisha, Tyler, Sherry, and Hari. They gave me a means of relaxation from the vigorous journey of a graduate student. I would also like to thank my friend David Hoelzle for his help and example in using LaTeX to format this dissertation. A big thank you to Yeong Hoong Chieh and Colin Das for being the best roommates anyone could ever have. To the rest of the individuals who have made my life at the University of Illinois an enjoyable experience – Griselda Alvarez, Sadia Hussien,

Wilbur Chang, Dave Szybilski, Chris Choi, Annette Gueth, Mbikayi, Newton Kazadi, James McKnight, Andrea Vozar, Myung EunShin, Safiyyah Mohsin, Alina Amir, Nadiah Affendi, Intan Wan Suhaila, Ezamil Suhaimi, Mike Poellmann, Vikas Chandra, Neera Jain, Nanjun Liu, Justin Koeln – thank you for being a friend.

TABLE OF CONTENTS

LIST OF FIGURES

LIST OF ABBREVIATIONS

ESCs	Embyonic Stem Cells
mESCs	Mouse Embyonic Stem Cells
hESCs	Human Embyonic Stem Cells
EB	Embryoid Body
FN	Fibronectin
LN	Laminin
RGD	Arg-Gly-Asp peptide
Lat A	Latrunculin A
Bleb	Blebbistatin
Colch	Colchicine
LIF	Leukemia Inhibitory Factor
bFGF	Basic Fibroblast Growth Factor
TGF-β	Transforming Growth Factor Beta
E-cadherin	Epithelial cadherin
NMMIIA	Nonmuscle Myosin IIA
SMN	Survival Motor Neuron
PBS	Phosphate Buffer SOlution
MTC	Magnetic Twisting Cytometry
CFP	Cyan Fluorescent Protein
GFP	Green Fluorescent Protein
YFP	Yellow Fluorescent Protein

CHAPTER 1

INTRODUCTION

1.1 Mechanics in the context of biology

Biology has become one of the most important interdisciplinary field of research, where physics, chemistry, mathematics, and engineering meet. However, why should we study the effects of mechanical forces on cellular behavior? This daunting question has plagued the biological world for many decades as it involves a plethora of complex theoretical and experimental techniques. The answer lies evidently in our daily life. Mechanical properties influence the biological behavior of cells and tissues. Physical activity such as breathing, beating of heart, blood shear flow, and walking regulate regulate development, morphogenesis, cell migration, proliferation, and even survival. Bones of astronauts are known to turn brittle and less dense after a prolonged period of antigravity in space. For many types of cancer, the first indication of the disease is an increase in tissue mechanical stiffness. It is therefore undeniable that mechanical forces play a significant role in biological processes.

Mechanobiology – the science that focuses on the effects of mechanical properties on cells and tissues, is a field that has recently captivated the attention of many researchers. As chemicals, drugs, and soluble factors fail to explain certain biological phenomena, researchers have turned to engineering, mathematics, and continuum mechanics to shed new insights on the complex laws that govern biological systems. Professor Yuan-Cheng Fung (regarded as the father of biomechanics) pioneered the work on tissue remodeling in response to mechanical forces in the 1960s. Since then, much progress has been made on how forces are transduced at the cellular and subcellular levels. Although it has been established that cells experience a variety of mechanical stimuli under physiologic conditions, how cells sense and integrate these forces at the molecular level (a process known as mechanotransduction as

explained in Section 1.4) to produce coordinated behaviors remains an unanswered question. In 1993, Ning Wang and colleagues showed for the first time that transmembrane integrins are mechanosensors and the cell cytoskeleton plays a major role in force transmission [1]. This work proved that forces are not just localized at the apical membrane of the cell, but are distributed throughout the cell via cytoskeleton filaments. Even small changes in the magnitudes or distribution of these forces within the cytoskeleton may lead to compensatory remodeling of cell-matrix and cell-cell contacts and may initiate a variety of cell behaviors. A considerable amount of work has already shown that stress and tension play a vital link in many biological processes that may involve cell-matrix integrins, and cell-cell cadherins. The question that arises, which we intend to seek an answer to, is: what is the mechanism of mechanotransduction at cell junctions, and to what extent do the mechanical forces act to regulate biological function?

1.2 What is mechanotransduction?

Mechanotransduction is the process by which living cells sense mechanical stimuli and convert them into intracellular biochemical signals that elicit physiological or pathological responses. It has been established that mechanical forces play vital roles in shaping the normal functions of all tissues and organs of human beings [2]. The mechanical environment of cells crucially influences many cell functions [3]. However, it remains largely mysterious how mechanical stimuli affect tissue and organ functions. Specifically, it is not clear how mechanical forces are transmitted into biochemical signals inside the living cells; i.e., the mechanism of mechanotransduction. It is of great importance to understand how cells sense and adapt to mechanical stresses because cell shape, cell behavior and cytoskeletal structure are influenced by the mechanical environment the cells are in [2, 4]. These mechanical stresses can be generated by cell-cell interaction through E-cadherin molecules, by pressure generated in vessel walls, by shear stress due to blood flow, or by the cell exerting on the extracellular matrix (ECM) adhesions through the contractility of the cytoskeletal known as tractional forces [5, 6]. Over the years, it has been clearly demonstrated that in determining cell morphology, transcriptional programs, and cell fate, the stiffness of a cells substrate and cell

traction forces provide as much input as do chemical messengers [7, 8]. It has also been shown that several molecules and cellular structures are involved in mechanotransduction. For example, stress activated ion channels, transmembrane proteins that mediate cell-matrix or cell-cell contacts, focal adhesion complexes, membrane lipids, glycocalyx proteins, and also G-protein coupled receptors can serve as mechanosensors and transducers [2].

1.3 Models for Mechanotransduction

Over the years, several models of mechanotransduction have been proposed such as stretch-activated membrane ion channel opening and local plasma membrane protein unfolding [9]. The main thrust of these models is that mechanotransduction, similar to the soluble factor induced signal transduction, initiates at the cell membrane by inducing local conformational changes or unfolding of membrane-bound proteins at the site of a local force followed by a cascade of passive diffusion or active translocation processes for downstream signaling. This is consistent with the theory of the classical continuum mechanics of St. Venants principle that a local force must cause only a local deformation. In a conventional continuum material, the magnitudes of a local applied force decrease as the square of the distance from the force impact. Therefore it is widely accepted that applied local forces are mostly dissipated at the focal adhesions on the cell surface [9] such that there should be little direct deep cytoplasmic deformation and no direct nuclear deformation beyond the close vicinity of the applied force. This view is supported by the finite element analysis of cell models based on principles of continuum mechanics [10]. In contrast, it has demonstrated that a local load of physiologic magnitudes applied at the cell apical surface via integrin receptors is propagated along the cytoskeleton to remote sites in the cytoplasm [11–13] and into the nucleus [14, 15]. Forces were also found to be concentrated at discrete sites deep in the cytoplasm and nucleoplasm [11–15], tens of micrometers away from the site of mechanical stress application. These findings is contrary to the predictions of existing models and challenge the prevailing views on mechanical signaling inside a living cell. As scientific evidences are gathered over the years, it is now known that actin filaments, intermediate filaments, and microtubules are the major stress supporting structures inside the cell.

Different features of mechanotransduction have been shown in recent years, including myosin dependent substrate rigidity feedback [8, 16], myosin dependent lamellipodial contractions [17], selective recruitment of adaptor proteins by flow induced shear stress [18], stress induced alterations of focal adhesion zyxin proteins dissociation constant [19], force induced structural adaptation at focal adhesions [20], and mechanical adaptation at focal adhesions [4] or in the whole cell [21]. It was also shown that substrate stiffness strongly influences stem cell differentiation [16].

1.4 Magnetic Twisting Cytometry

The magnetic twisting cytometry (MTC) is a device used to deliver small forces to specific sites on the cell membrane. The MTC has been well-established and provides a controlled and precise mechanical forces to specific sites on the cell surface through different force transmitting proteins of interest (Fig 1.1a). Optical magnetic cell twisting is an extension of the magnetic cell twisting technique [1, 22] to any modes of forcing. Ferromagnetic beads (4.5 μm diameter) were coated with saturated amount of Arg-Gly-Asp (RGD)-containing peptides, ligands for integrin receptors (the ligand density on the bead was measured to be about 1 RGD-peptide per 2 nm^2 of bead surface area). The beads were suspended in serum free medium, and 20,000 beads were added to an individual cell well. The cells were incubated for 15 min to allow for binding of the beads to integrins on the cell surface (Fig 1.1b). Excess and unbounded beads were removed by washing with PBS before the dish of cells was placed under the microscope. Similar technique was used to coat the ferromagnetic beads with different proteins such as transferrin, poly-L-lysine, e-cadherin...etc. The binding specificity of bead binding was determined following protocols described previously [1]. The magnetic moments of each batch of self-made ferromagnetic beads were calibrated according to published methods [1]. The technique of applying twisting torques to cells in a dish under a microscope had been described in detail [23]. The beads were magnetized by a strong (1,000 G) and short (<100 μs) magnetic field pulse oriented at the horizontal direction using the magnetizing coils (Fig 1.1c). The twisting current was driven by a current source controlled by a computer (Fig 1.1a, 1.1c). The magnetic twisting field can be varied from 0

to 75 Gauss (G)(Fig 1.1d). The stress applied to the cell in Pascals (Pa) where 1 Pa equals to 1 picoNewton per micrometer square (pN/μm^2) is defined as the ratio of the applied torque (in pN/μm) to six times the bead volume (μm^3). The applied stress (in Pa) can be obtained by multiplying the bead constant (in Pa/G) with the applied twisting field (in G). The bead constant is a magnetic property of the bead and differs from each batch. To calibrate and calculate the bead constant (in Pa/G), the magnetic beads can be immersed in a medium with known viscosity and a twisting field (in G) of variable magnitude is applied while measuring the angular velocity. Calibration procedure on converting applied magnetic field to applied stress on cell surface has been described by Valberg et al [24].

1.5 Fluorescence Resonance Energy Transfer (FRET)

Fluorescence resonance energy transfer (FRET) is a mechanism that occurs between two different chromophores (the donor and the acceptor) with overlapping emission absorption spectra [27]. A chromophore is a part of a molecule that is responsible for its color. Light of a certain wave length that is incident on a chromophore can be absorbed by exciting an electron from its ground state into an excited state. The excited chromophore now emits a visible light of a different wave length. An acceptor chromophore is now able to be excited by the emission light wave of the excited donor. A donor chromophore, in its electronic excited state transfers energy to an acceptor chromophore that is of close proximity (<10 nm) through nonradiative dipole-dipole coupling. This mechanism of transferring energy from the donor to acceptor is termed FRET. There are two major methods of FRET. The first being intramolecular FRET (Fig. 1.2a, 1.3), the second being intermolecular FRET (Fig. 1.2b, 1.3). Intramolecular FRET can be measured when both the donor and the acceptor are fused to the same host molecule, separated by a flexible polypeptide linker [13]. This method yields higher efficiency and produces a much larger change in the fluorescence emission ratio. Many biosensors utilize intramolecular FRET, similar to the calcium biosensor used in Fig. 2.11 of this manuscript. Intermolecular FRET can occur when the donor and the acceptor are on different macromolecules. This form of FRET is more difficult to observe because the stoichiometry of acceptors to donors can vary with transfection efficiencies,

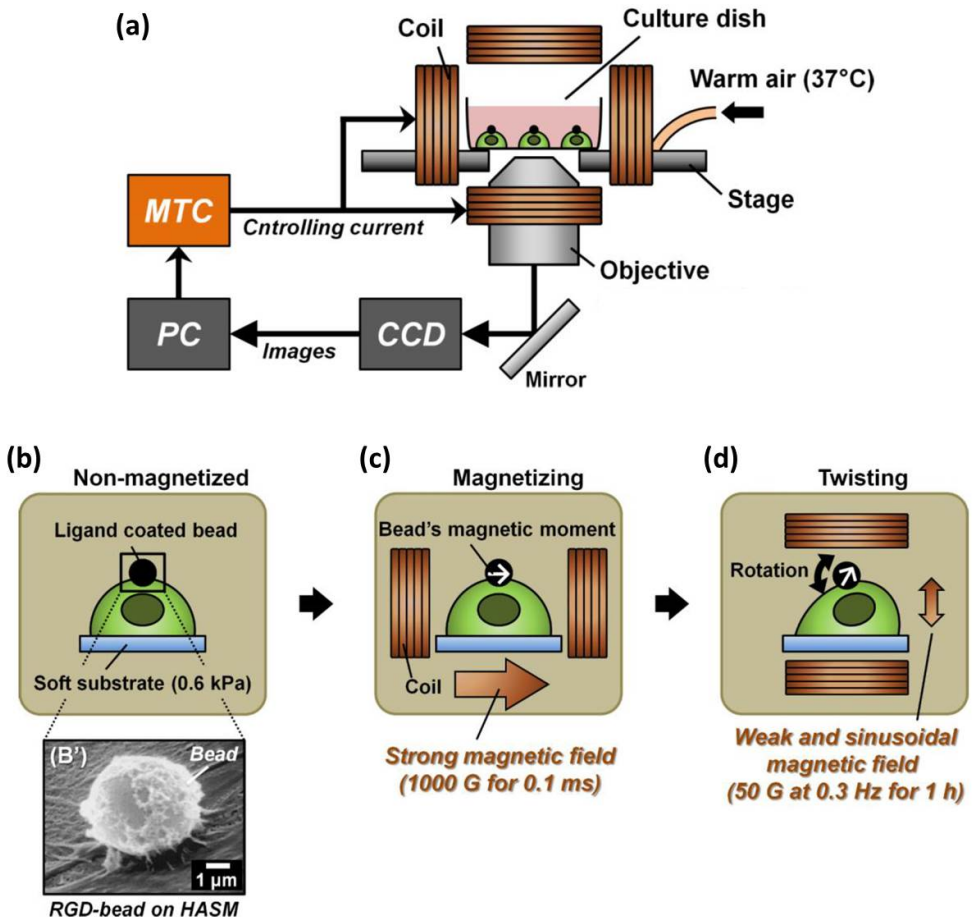

Figure 1.1: Schematic and principle of the Magnetic Twisting Cytometry. (a) Experimental setup of the MTC integrated witht he microscope system. Cells bound with magnetic beads were placed within the coils. Magnitude of firce applied to cell was controlled by the magnetic field generated by the coils. The computer controls the capture of images through the CCD camera as it is synchronized with the magnetic twisting field. (b) Ligand coated bead are bound to the cell. Inset, a representative SEM image of a RGD-coated bead adhered to the apical membrane of a smooth muscle cell (adapted from Maksym et al. [25]). (c) A strong magnetic pulse of 1000G is applied to magnetize the feromagnetic bead. (d) The magnetic field is applied from different axis, allowing twisting of the bead in the desired direction. Mechanical stress is applied as twisting occurs. *Image modified from [26].*

and also the donor and acceptor host proteins may not be constitutively bound in vivo. Optimal conditions occur when all the donors are paired with an acceptor, as any unpaired protein adds noise to the signal. Additionally, if the distance or orientation between the pairs are unfavorable, FRET may not occur, even if the two proteins form a complex [28]. In Chapter 2, intermolecular FRET is used in the study of different protein interactions

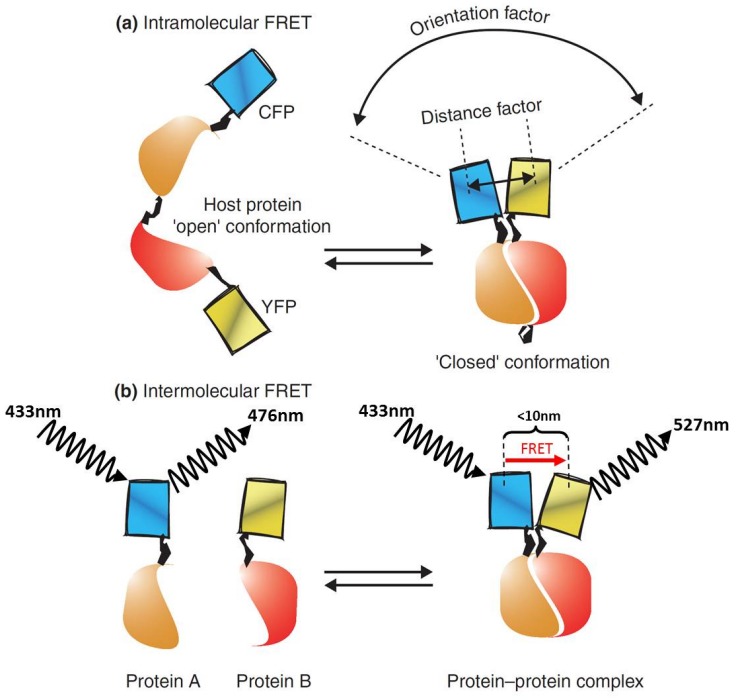

Figure 1.2: Schematic of FRET mechanism. (a) Intramolecular FRET can occur when both the donor and acceptor chromophores are on the same host molecule, which undergoes a transition, for example, between 'open' and 'closed' conformations. In each square box corresponding to CFP or YFP (shown in cyan or yellow, respectively), a diagonal line represents the chromophore. The amount of FRET transferred strongly depends on the relative orientation and distance between the donor and acceptor chromophores: the parallel orientation and the shorter distance (<10 nm) generally yield larger FRET. (b) Intermolecular FRET can occur between one molecule (protein A) fused to the donor (CFP) and another molecule (protein B) fused to the acceptor (YFP). When the two proteins dissociate, FRET diminishes. The donor CFP is excited with a light of wavelength 433nm and emits a light of wavelength 476nm. The fluorescence emission of CFP overlaps the excitation of YFP. When the two proteins bind to each other, or when both CFP and YFP are within a proximity of <10nm, FRET occurs. A large amount of energy transfer occurs from CFP to YFP, causing a significant decrease in CFP emission and an increase in YFP emission. (*Adapted from [27]*)

within the nucleus. In both cases, the fluorescent intensity of both donor and acceptor are monitored simultaneously and the intensity ratio of donor and acceptor is used to quantify the activation or interaction between proteins of interest (Fig. 1.3). FRET-based imaging microscopy is commonly used as a sensitive probe of protein-protein interactions and protein conformational changes in vivo [27].

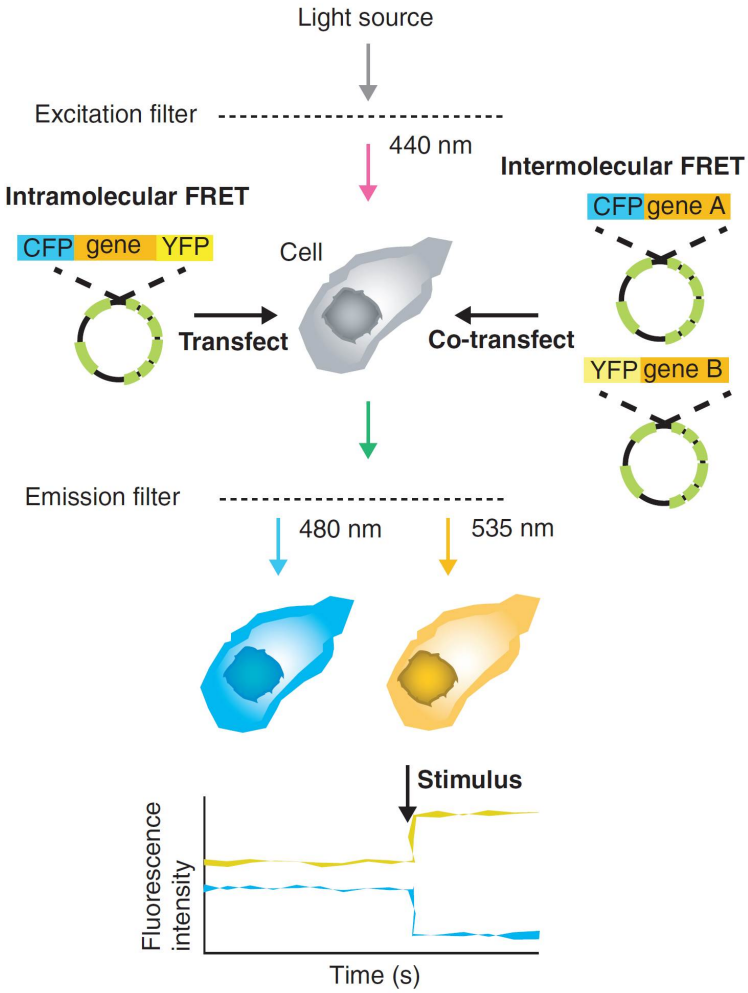

Figure 1.3: FRET imaging microscopy experiment. In FRET experiments, a single transfection (intramolecular FRET) or co-transfection (intermolecular FRET) of the constructs must first be performed. The occurrence of FRET can be observed by exciting the sample at the donor excitation wavelengths while measuring the fluorescence intensities emitted at wavelengths corresponding to the emission peaks of the donor versus those of the acceptor. If the acceptor and donor are at a distance <10nm and favorable orientation, donor emission intensity decreases (CFP, cyan) while the acceptor emission (YFP, yellow) intensity increases. The ratio of fluorescence intensity provides a good quantification of different protein interactions. (*Modified from [27]*)

1.6 Thesis Organization

This thesis can be divided into two major sections. The first being how cells transmit forces in to the nucleus and potentially give rise to gene expression change. The second section involves embryonic stem cell (ESC) differentiation. More specifically, how mechanical

properties such as stress, substrate rigidity, and microenvironment induce differentiation of ESCs. The first and second section therefore ties together by the process at which forces are transmitted into the nucleus and induce differentiation of ESCs. The content and tone of each section changes considerable depending on the chapter.

Chapter 2 demonstrates that local mechanical forces applied at the cell surface can directly alter protein-protein interactions in a nuclear body within the nucleus [15]. If a physiologic load could not directly deform intra-nuclear structures, then signaling inside the nucleus would occur only via diffusion or translocation. The results presented elucidates the the force transmitting structural pathway from the the apical membrane of the cell in to the nucleus. We demonstrate the first experimental evidence that a local physiologic force can alter protein complexes within a sub-nuclear body, representing a unique mechanism of mechanotransduction that impacts on nuclear functions involved in gene expression.

Despite the growing evidence that extracellular physical microenvironment and mechanical stresses help direct stem cell fate [8, 29, 30], the biological responses to a local force in embryonic stem cells remain underexplored. Chapter 3, 4 and 5 describes how externally applied forces, matrix mechanical properties (e.g. substrate rigidity, dimensionality), and cell-generated (contractile) forces influence the differentiation of embryonic stem cells. In Chapter 3, we demonstrated that mechanical signals may be mediated by both integrin-ECM and cadherin-dependent cell-cell adhesions. Since, differential binding between cell-matrix integrins and cell-cell cadherins is widely believed to mediate cell sorting during embryogenesis, we show that mouse embryonic stem cells increases cell spreading and cell stiffness,decreased cell proliferation rate, and downregulated Oct3/4 gene expression. The same cyclic force applied via cellcell adhesion molecule E-cadherin, however, had no effects on cell spreading, Oct3/4 gene expression, and the self-renewal of mouse ES cells, but induced significant cell stiffening. Chapter 4 explores the biophysical effects of embryonic stem cells on cell-ECM mediated substrate rigidity. It is known that differentiated cells stiffness and traction forces increase with the stiffening of culture substrate. In contrast, we found that embryonic stem cells' stiffness remains the same despite the change in substrate rigidity, whereas their basal traction increases. We further explored the difference in 2D and 3D culture in Chapter 5. Our interesting and surprising results show that 3D soft fibrin gels

facilitate the differentiation and organization of germ layers. The work presented in this chapter not only provides further insights on embryogenesis, but also equips researchers with a versatile technique to further explore the mysteries surrounding germ layer organization.

Chapter 6 provides concluding statements and future work. The Appendices provide complete details of the processes, equipment, and computer code used in this work and are designed to aid researchers who are building on this work. In the vast field of biophysics and cell mechanics, this thesis is a humble attempt to unravel the complex mechanism by which cells sense mechanical forces and convert them in to biochemical signals, thereby giving rise to gene expression, morphology, proliferation, and other biophysical changes.

CHAPTER 2

DYNAMIC FORCE-INDUCED DIRECT DISSOCIATION OF PROTEIN COMPLEXES IN THE NUCLEUS

Poh et al. (2012) Nature Communications 3: 866

2.1 Introduction

It is well established that mechanical forces can influence functions of living cells, tissues, and organisms. However, despite significant progress in past decades in understanding cellular mechanotransduction [31–36], it is still not clear how mechanical forces applied at the cell surface alter nuclear functions of the cell. One prevailing model suggests that a local force applied at the cell surface might be able to influence the nuclear functions indirectly via induced translocation and/or diffusion of signaling molecules from the cytoplasm into the nucleus [9]. Alternatively, a local surface force, via force propagation along cytoskeletal-nuclear linkages, is speculated to directly alter nuclear functions by affecting activities of molecules inside the nucleus [33]. It has been demonstrated that a surface force/deformation via integrins can alter the gross shape of the nucleus [37], resulting in direct deformation of nucleoli [14], and that the nuclear lamina containing Lamin A/C are important in nuclear mechanical properties [38–41]. These findings suggest that it is possible that mechanical forces at the cell surface might directly alter nuclear functions via force propagation from the extracellular matrix (ECM) to the nucleus, but so far experimental evidence is lacking. We hypothesize that a local surface force can directly alter nuclear functions via changing the protein-protein (and likely protein-RNA) associations. In this report we provide evidence for force-induced direct dissociation of major multi-protein complex in the Cajal body (CB), a prominent nuclear body. CBs are evolutionarily conserved nuclear domains found in yeast, plant, and animal cells and are critical for the biogenesis and recycling of several classes

of small nuclear ribonucleoprotein (snRNP) complexes involved in pre-mRNA splicing and preribosomal RNA (pre-rRNA) processing [42, 43], and assembly and delivery of telomerase to telomeres [42–45]. Knockout of coilin, a marker protein of a CB, reduces viability and fertility in mice [46] and loss of SMN protein leads to spinal muscular atrophy [47]. Recent advances in our understanding of the formation, dynamics, and function of CBs suggest that the CBs form as a direct reflection of activity of highly expressed genes with which they are physiologically associated [48–50]. Our present study demonstrates that local mechanical forces applied at the cell surface can directly alter protein-protein interactions in a nuclear body within the nucleus.

2.2 Results

2.2.1 A local surface force directly dissociates coilin from SMN

To investigate whether a surface force applied via integrins could directly deform nuclear proteins in the CBs, we transiently co-transfected HeLa cells with two major essential CB components critical for its structural integrity, CFP-SMN and YFP-coilin [44] (Fig. 2.1a). We quantified their displacements that were synchronized with the oscillatory loading applied via an RGD-coated magnetic bead (Fig. 2.1b). We employed an established synchronous detection approach that could detect external-stress-induced nanoscale displacements at $\sim$4 nm resolution while filtering out spontaneous movements [11, 51]. Both CFP-SMN and YFP-coilin in the same CB were directly displaced by the external dynamic force applied on the cell surface but SMN exhibited greater displacements in response to the same force (Fig. 2.1c), suggesting that differential displacements of coilin and SMN might lead to dissociation of the protein-protein complex, which is known to interact with each other inside the CB [52]. To further determine if the applied surface force had any direct impact on the dissociation of the coilin from the SMN in the CB, we applied a quick instant force (a step-function) with the magnetic bead via the integrins and quantified the FRET changes of the CFP-SMN (the donor) and YFP-coilin (the receptor) protein pairs. The FRET ratio of CFP-SMN to YFP-coilin rapidly increased within 350 ms in response to the applied stress (Fig. 2.1d). The

emission intensity of the protein pairs was anti-correlated: CFP-SMN intensity increased while YFP-coilin intensity decreased (Fig. 2.1e). This is a strong evidence for a FRET change, suggesting that SMN were dissociated away from coilin by force. Varying force magnitudes revealed that the threshold stress for the FRET change was ∼14-17 Pa and that the FRET change reached a plateau by ∼350 ms (Fig. 2.1f). Turning off the applied force did not return the FRET ratio of CFP-SMN to YFP-coilin back to the pre-force level, suggesting that the force-induced structural changes to the protein pairs were 'plastic' or 'permanent', which lasted at least 10s (Fig. 2.1g). To further examine the plasticity of dissociation of the protein complex, we quantified mean square displacements (MSDs) of both proteins before, during and after a cyclic stress application. Both coilin and SMN inside the same CB exhibited constrained diffusion behaviors and had almost identical spontaneous MSDs before stress application (Fig. 2.1h), suggesting that they were tightly associated and moved as a single entity. Both responded synchronously to the cyclic stress (Fig. 2.1h), suggesting that the proteins were directly displaced by the applied stress, but coilin had much greater spontaneous MSDs than SMN after stress application (Fig. 2.1h), indicating that coilin was tethered less tightly than SMN after stress application. Taken together, these data strongly suggest that an external force on the cell surface induced direct differential displacements between SMN and coilin, which resulted in the increased distances and thus the FRET change between these two proteins.

We next examined if force-induced displacements of coilin or SMN in the nucleus were dependent on the distance between the site of force application and the CB. The magnitudes of SMN or coilin displacements decreased only slowly as the distance increased (Fig. 2.2); there were significant force-induced displacements of both proteins even when the local force (the bead) was placed $>27\mu$m away from the CB, suggesting the force transmission pathway from the cell surface to the CB was concentrated along the force-bearing cytoskeletal-nuclear structures and that stress field did not follow the decay pattern from the homogeneous material prediction [11].

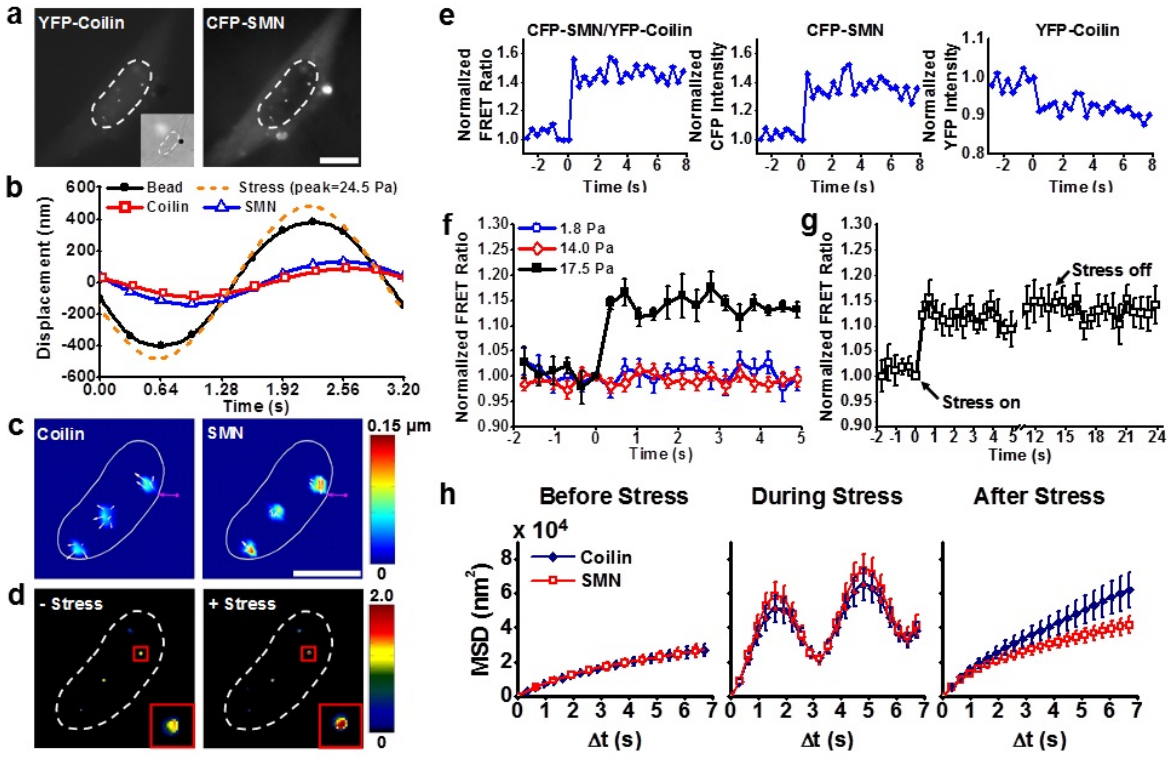

Figure 2.1: A local surface force directly dissociates coilin from SMN in the CB in the nucleus. (a) Fluorescence images of a HeLa cell transfected with CFP-SMN and YFP-coilin (inset is the brightfield image of the cell; black dot shows the bead). Nucleus is outlined with dashed line. Scale bar = 10μm. (b) Displacements of the magnetic bead and of the CB proteins SMN and coilin as a function of cyclic forces (0.3 Hz). Displacements of the bead, coilin, and SMN were all synchronized with the applied stress (peak magnitude=24.5 Pa). Bead displacement was $\sim 5^\circ$ phase lagged behind the stress; there were $\sim 30^\circ$ phase lags for SMN and coilin behind the bead displacement; SMN was displaced slightly more than coilin but its phase lag was somewhat less than coilin. (c) Displacement maps of coilin and SMN within the nucleus of the same cell. SMN exhibits larger displacements upon stress than coilin. White arrows indicate direction of displacement and the color bar indicates the displacement magnitude. Pink arrow represents the direction of bead center displacement (not drawn to scale). Scale bar = 10μm (d) Florescence resonance energy transfer (FRET) ratio map of force-induced dissociation of coilin and SMN. Inset shows an enlarged CB with FRET changes when stress is applied. (e) A representative time course plot of CFP-SMN and YFP-coilin anti-correlation in response to force. (f) FRET ratio change between coilin and SMN by mechanical is stress-magnitude dependent and rapid (<0.35s). Each load was applied to a cell only once. n = 5 CBs for stress of 17.5 Pa; 40 for 14 Pa; 95 for 1.8 Pa. (g) Stress-induced structural change to CB protein pairs is plastic. FRET ratio of CFP-SMN and YFP-coilin pairs do not return to pre-stress ratio when load was released. A step load of 24.5 Pa was applied. n=13. All data points in (e), (f) and (g) were normalized to time zero when a step load was applied. (h) The dynamics of coilin and SMN were quantified

before, during, and after application of an oscillatory stress (24.5 Pa peak stress at 0.3 Hz). ($p<0.05$ when $\Delta t>5.12$ s). n = 106 CBs. Mean +/- s.e.; data are pooled from >4 independent experiments for each sub-figure.

2.2.2 Structural basis for dissociation of coilin from SMN by force

To further investigate the structural basis of stress transmission into the nucleus, we quantified changes of FRET ratio of CFP-SMN to YFP-coilin when different cytoskeletal or nuclear structural components were specifically disrupted or knocked down. Treatments of Latrunculin A, an F-actin disrupter, or blebbistatin, a myosin II inhibitor, but not colchicine, a microtubule-disrupting agent, prevented the force-induced FRET changes (Fig. 2.3a, 2.4), suggesting that intact F-actin and myosin II, but not microtubules, are indispensable for force transmission from the cell surface to the CB in the nucleus. Knocking out Lamin A/C, a critical nuclear filament underneath the nuclear envelope, also abolished force-induced FRET changes (Fig. 2.3a), indicating the essential role of Lamin A/C in force transmission to the CB. Consistent with the necessary role of Lamin A/C in force transmission into the nucleus, using mCherry-Lamin A as a marker of the nuclear envelope, we observed defor-

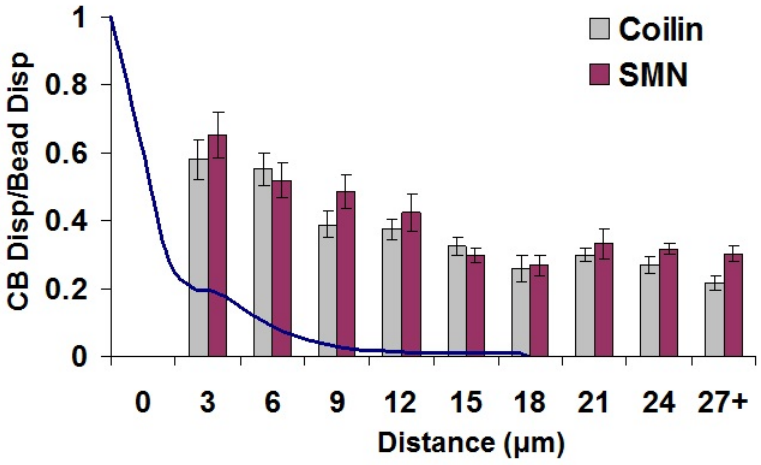

Figure 2.2: Stress propagation to Cajal bodies does not follow decay patterns of homogeneous materials. CB protein (coilin or SMN) displacements normalized against bead displacement on the cell surface as a function of distance from the bead center (n=136 CBs). The solid line is a model prediction of displacements obtained using finite element analysis under similar loading conditions, assuming a continuum homogeneous solid body (replotted from ref. 24). Mean +/- s.e.; data are pooled from 8 separate experiments.

mation of the nuclear envelope in response to the local force on the cell surface (Fig. 2.3b, 2.3c). Knocking out plectin, a linking protein connecting intermediate filaments to the nuclear envelope, did not have any effect on stress-induced FRET change (Fig. 2.3a, 2.4), suggesting that plectin does not play an essential role in mediating force to the CB. Taken together, these results suggest that the applied stress was directly transmitted into the CB across the nuclear envelope via F-actin-LINC (linker of nucleoskeleton and cytoskeleton)-nuclear lamina structural pathways.

It is known that substrate rigidity has profound influence on cellular functions [29]. Force-induced FRET changes were observed in HeLa cells plated on 2 kPa and 8 kPa substrates, similar to those FRET changes observed in cells plated on rigid dishes, but not in cells plated on 0.6 kPa substrates (Fig. 2.3d). HeLa cells have a maximum stiffness (cell stiffness measured on a rigid dish) of $\sim$1.51 kPa (Fig. 2.3e) and express ample actin bundles and high tractions on 2 and 8 kPa but not on 0.6 kPa substrate (Fig. 2.3f, 2.3g). Together with the above data after F-actin disruption and myosin II inhibition, these data suggest that substrate rigidity regulates force-induced nuclear protein dissociation via controlling tension of the actin bundles in the cytoskeleton for long distance force propagation.

2.2.3 Other protein pairs exhibit different force-induced changes

Next, we analyzed how the local surface force affects interactions between the major interacting partners of coilin and SMN in CBs. Coilin and SMN are self-interacting proteins and their interaction is mediated by WRAP53 which is also able to self-interact [53]. Importantly, both coilin and SMN interact with spliceosomal snRNPs [54]. In addition, coilin interacts with the nucleolar chaperone Nopp140 on its N-terminus [55] and with the U4/U6 snRNP assembly factor SART3 [56]. In the absence of external stress, spliceosomal snRNP core SmE-SmG proteins had lowest baseline CFP/YFP emission ratios ($\sim$0.3), followed by coilin-coilin, coilin-SmE, coilin-Nopp140, WRAP53-WRAP53, coilin-WARP53, coilin-SART3, SMN-WRAP53, SMN-coilin, SMN-SMN, SMN-SmG, and SMN-SART3 ($\sim$0.8) (Fig. 2.5a), suggesting that baseline distances between two proteins were closest for snRNP proteins of the Sm ring SmE-SmG and farthest for SMN-SART3 complexes. Interestingly,

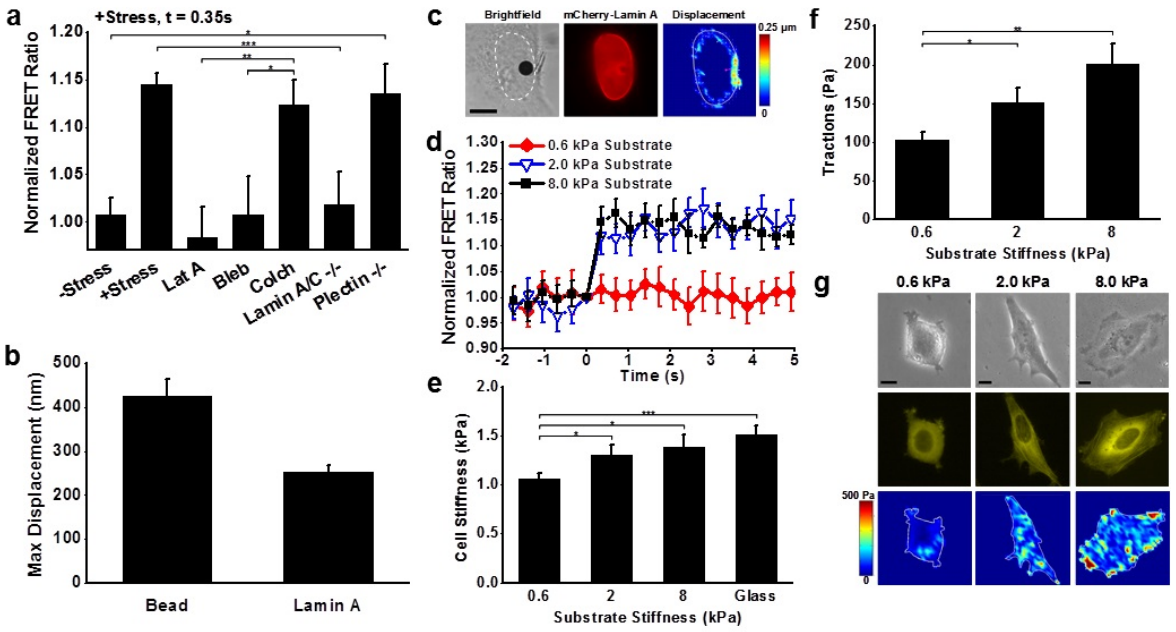

Figure 2.3: Structural basis for force-induced dissociation of coilin from SMN. (a) Normalized FRET ratio of SMN-coilin at 0.35s of stress application in cells treated with inhibitors or knockouts of cytoskeletal proteins or nuclear proteins. Disrupting F-actin with Latrunculin A (Lat A, 1 μM for 10 min, n=85) or inhibiting myonsin II with Blebbistatin (Bleb, 50 μM for 20 min, n=58) prevented force-induced FRET changes, whereas disrupting microtubules with colchicine (Colch, 10 μM for 15 mins, n=5) had no effect on force-induced FRET changes when compared with intact cells (+Stress; a step function of 17.5 Pa). Lat A disrupted actin bundles by 7 min and Colch disrupted microtubules by 10 min as confirmed by images of YFP-actin or GFP-tubulin in live cells (not shown). Lamin A/C knockouts (n=43) blocked stress-induced FRET changes. Plectin knockouts (n=10) has no effects on stressed induced FRET ratio changes. (b) Stress applied at the apical surface of cell induces deformation of the nuclear envelope. Maximum displacements (Max Displacement) are plotted for the magnetic bead and for the mCherry-Lamin A-labeled nucleus in response to a cyclic stress (24.5 Pa at 0.3 Hz); n=6 cells. The distance from the bead center to the site of the maximum nuclear envelope displacement ranges from 3.7 to 11.8 μm. (c) Brightfield, fluorescent (mCherry-Lamin A), and displacement map images of a HeLa cell nucleus. Black dot on brightfield image shows the RGD-coated magnetic bead. Nucleus is outlined with white dashed lines. Scale bar = 10μm. A local deformation is observed at the area close to the bead. White arrows indicate direction of displacement and the color bar indicates the displacement magnitude. Pink arrow represents the direction of bead center displacement (not drawn to scale). (d) Stress-induced dissociation of SMN-coilin was observed in cells on 8kPa (n=10) and 2kPa (n=8) substrates, but not on 0.6kPa (n=55) substrate. A step load was applied at time zero and all FRET ratios were normalized to that time point. Dissociation of coilin from SMN was confirmed by anti-correlation behaviors of CFP-SMN and YFP-coilin (Fig. 2.1e). (e) Stiffness (Youngs modulus) of HeLa cells increases with the

substrate stiffness. On substrate of 0.6, 2, and 8 kPa, or glass, n = 77, 96, 77, or 146 cells. (f) Root-mean-square (RMS) traction of the cell increases with substrate stiffness. n = 9, 7, and 8 cells on substrates of 0.6, 2, and 8 kPa. (g) Cells have abundant actin bundles and large tractions on stiff substrates. Phase contrast images, corresponding YFP-actin images, and traction map images of HeLa cells cultured on 0.6, 2, and 8 kPa substrates. Scale bar = 10μm. Mean +/- s.e.; data are from at least 4 separate experiments for each sub-figure (*, p<0.05; **, p<0.01; ***, p<0.001). P-values were obtained using the two-tailed Students t-test.

CFP-fibrillarin (a methylase that binds to SMN in the CB [57]) and YFP-coilin in the CB exhibited even higher baseline emission ratios than SMN-SmG, reaching almost 1.0 (Fig. 2.5a), consistent with previous published data that fibrillarin and coilin do not directly interact with each other [42] and that they might be far apart ($\sim$>10 nm) (a negative control). After a quick step-function force was applied, coilin-coilin self-interaction exhibited great-

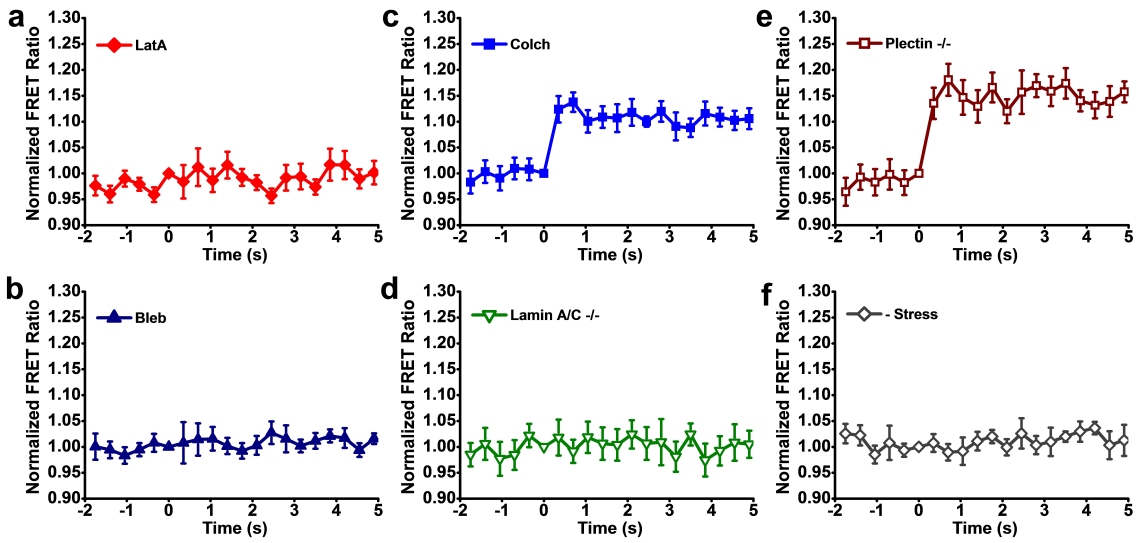

Figure 2.4: Time course FRET emission ratio of CFP-SMN and YFP-coilin upon disruption of different structural proteins. All FRET ratios were normalized to time zero when a step load was applied. Average data showing FRET ratio of cells treated with (a) Lat A, (b) Bleb (blebbistatin), (c) Colch (colchicine), (d) Lamin A/C knockout cells, (e) Plectin knockout cells, and (f) control cells without stress. Rapid dissociation of coilin from SMN was still observed in cells that were treated with colchicine or plectin knockout cells while no significant change in FRET ratios were observed in other cell conditions. n = 85 CBs for Lat A; 58 for Bleb; 5 for Colch treated cells; 43 for Lamin A/C $^{-/-}$ cells; 10 for Plectin $^{-/-}$ cells; 80 for control cells without stress. Mean +/- s.e.; data are pooled from 3 separate experiments.

est FRET ratio increases from baseline values, followed by coilin-SmE, WRAP53-WRAP53, coilin- Nopp140, SMN-coilin, coilin-SART3, coilin-WARP53, SMN-SMN, SMN-SmG, and SMN- WRAP53 (Fig. 2.5b, 2.6, 2.7). These results suggest that when these protein complexes were exposed to the same magnitudes of stress, their respective FRET ratio changes were in general inversely proportional to their baseline distances between the two proteins, except for SMN-coilin, which had larger FRET ratio changes than SMN-WRAP53, suggesting that distances between the SMN-coilin protein pairs increased more than predicted from their baseline values. Fibrillarin-coilin and SMN- SART3 pairs did not exhibit any FRET change from the baseline (Fig. 2.5b, 2.6, 2.7), consistent with the baseline data that fibrillarin-coilin and SMN-SART3 are already too far apart at baseline so that they are beyond the detection range of FRET changes. In contrast, SmE and SmG proteins strongly interact within the heteroheptameric ring of the splicesosomal snRNP core structure. Thus, it is likely that they could not be dissociated by the magnitude of the applied stress and thus did not exhibit FRET ratio change upon stress (Fig. 2.5b).

2.2.4 Dissipative behaviors of protein complexes in the Cajal body

In a time-dependent force-deformation response, a phase lag (or a time delay) between the applied cyclic stress at the cell surface and the displacement of a nuclear protein is a measure of rheological properties of the material. Any viscoelastic linkage has a phase lag of between 0° and 90°. For multiple linkages of different proteins in a complex protein aggregate that is tethered in a nucleoplasmic matrix, the phase lags would indicate how viscous these interactions are. Under an oscillatory stress of 0.3 Hz, the phase lag of coilin to the magnetic bead displacement (a measure of cytoplasmic strain, which, in turn, was $\sim 5^\circ$ lagged behind the applied force, see Fig. 2.1b) was $\sim 33^\circ$, 4° more than that of SMN ($\sim 29^\circ$) inside the same CB (Fig. 2.5c). The fact that coilin was always 4° lagged behind SMN, irrespective of which fluorescent probe (CFP or YFP) was attached to coilin (Fig. 2.5d), suggests that these phase lags were not biased by the attached fluorescent probes. The phase lag differences between CFP-coilin and YFP-coilin or CFP-SMN and YFP-SMN were almost 0° (Fig. 2.5d), suggesting that the 4°-phase difference did not originate from CFPs

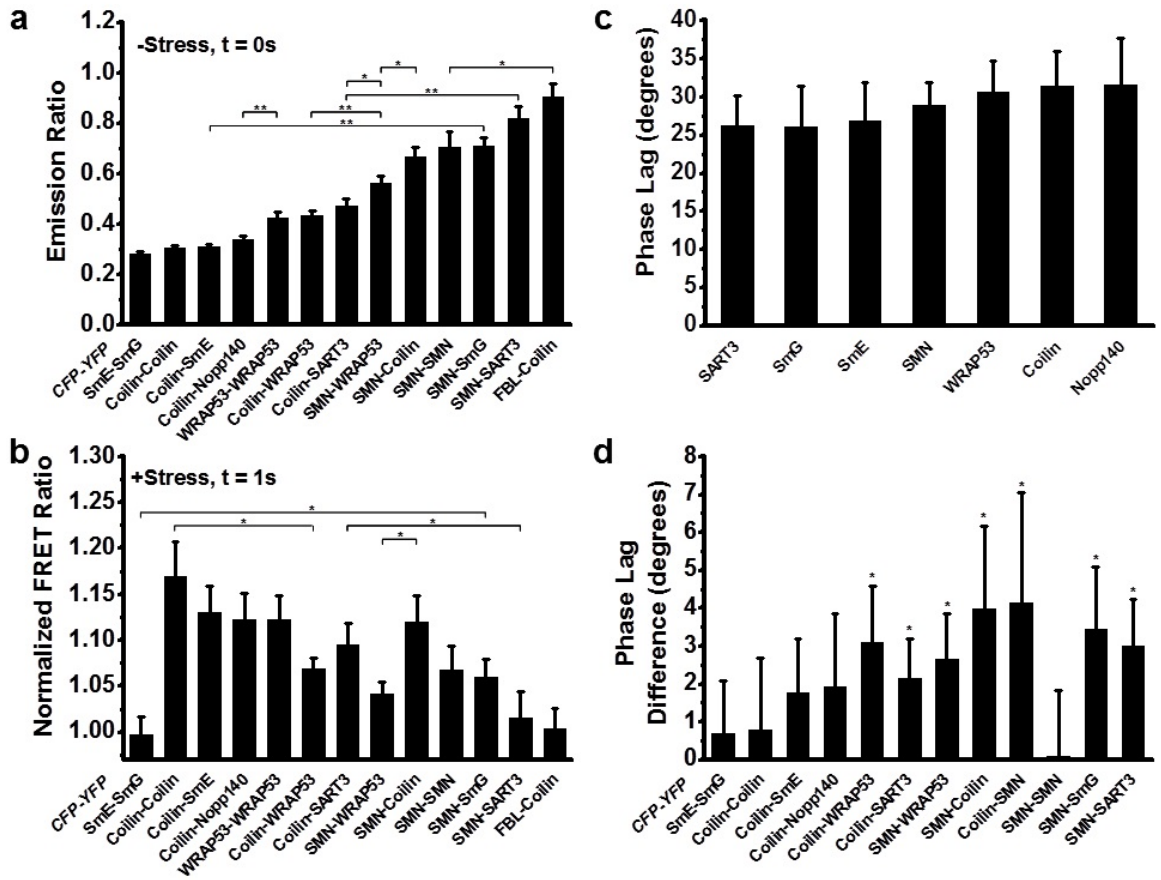

Figure 2.5: Different protein complexes in the CB have distinct association characteristics. (a) Baseline emission ratios of SmE-SmG (n=85), coilin-coilin (n=56), coilin-SmE (n=134), coilin-Nopp140 (n=64), WRAP53-WRAP53 (n=99), coilin-WRAP53 (n=140), coilin-SART3 (n=138), SMN-WRAP53 (n=64), SMN-coilin (n=53), SMN-SMN (n=48), SMN-SmG (n=100), SMN-SART3 (n=73) and Fibrillarin (FBL)-coilin (n=32) before stress application. No significant difference was observed between coilin-coilin and coilin-Nopp140 (p=0.097), SMN-coilin and SMN-SMN (p=0.58), coilin-WRAP53 and coilin-SART3 (p=0.352). (b) Normalized FRET ratio change at 1s stress. After stress was applied, normalized FRET ratios increased for coilin-coilin (n=41), coilin-SmE (n=9), coilin-Nopp140 (n=9), WRAP53-WRAP53 (n=8), coilin-WRAP53 (n=23), coilin-SART3 (n=11), SMN-WRAP53 (n=15), SMN-coilin (n=13), and SMN-SMN (n=6), SMN-SmG (n=11) but not for SmE-SmG (n=63), SMN-SART3 (n=73) and FBL-coilin (n=41). The average distance from the force to the CB was 9.87 +/- 0.1 μm. No significant difference was observed between coilin-coilin and coilin-Nopp140 (p=0.348), WRAP53-WRAP53 and coilin-WRAP53 (p=0.227), coilin-WRAP53 and SMN-WRAP53 (p=0.136), SMN-coilin and SMN-SMN (p=0.2), coilin-coilin and SMN-coilin (p=0.3). (c) Average phase lags of SART3 (n=28), SmG (n=24), SmE (n=18), SMN (n=13), WRAP53 (n=43), coilin (n=13), and Nopp140 (n=9). The differences between these average phase lags are not significant

($p>0.05$) because of variations among different cells, the paired comparison between two proteins within the same CB is statistically different. (d) An oscillatory load of 0.3 Hz is applied at the cell apical surface and the phase lag between the force applied (bead displacement) and protein displacements are compared. Phase lag of YFP labeled proteins were subtracted by the phase lag of CFP labeled proteins in the same CB, except for CFP-coilin and YFP-SMN pair, which was done in the reverse order to show the absolute value of the phase lag difference; paired comparison was used to determine the statistical significance between each protein pair. The absolute value of the difference in phase lag between coilin and SMN is approximately 4° regardless of the fluorescence pair. Number of CBs for CFP-YFP pair of SmE-SmG is 20; coilin-coilin is 13; coilin-SmE is 17; coilin-Nopp140 is 11; coilin-WRAP53 is 34; coilin-SART3 is 26; SMN-WRAP53 is 24; SMN-coilin is 44; coilin-SMN is 16; SMN-SMN is 13; SMN-SmG is 24; SMN-SART3 is 10. Mean +/- s.e.; data are pooled from at least 3 independent experiments (*, $p<0.05$; **, $p<0.01$). P-values were obtained using the two-tailed Students t-test.

or YFPs themselves. The 4°-phase difference suggests that the SMN-coilin interactions are viscoelastic and dissipative. The phase lag differences between coilin and WRAP53, between SMN and WRAP53, between coilin and Nopp140, between coilin and SmE were all $<2^\circ$, suggesting that the dissipative elements (where the input mechanical energy is dissipated into heat) between them were not as significant. SMN-SmG and coilin-SART3 pairs have significant phase lag differences between each protein pair ($\sim$2-3°, corresponding to a time delay of 20-30 ms (3° times 3200 ms divided by 360° equals 26.7 ms; one cycle is 3200 ms at a loading frequency of 0.3125 Hz)), indicating that force is dissipated when transmitted from one protein to the other. Interestingly, viscous responses were also evident when a sudden stress (a step function) is applied to the cell surface. The FRET curves exhibited creep responses showing local material deformation (two proteins pulled apart): slow responses (creep time, defined as time to reach peak FRET change, $\sim$700-1350 ms) indicate a predominantly viscous behavior (Fig. 2.8a, b, c, d); in contrast, fast responses (creep time $\sim$300 ms, confirmed by sampling at a time resolution of $\sim$150 ms in Fig. 2.8e) are likely to be associated with more elastic local nanoenvironment (Fig. 2.8f, g, h, i, j, k).

Taking together the FRET changes in an intact cell and in a cell where specific components of the cytoskeleton and of the nuclear skeleton are disrupted or knocked out, we propose a working model of the force response for the protein complex in the CB (Fig 2.9): the protein complex is stressed via the pathway of integrin-mediated focal adhesion to F-actin, to LINC,

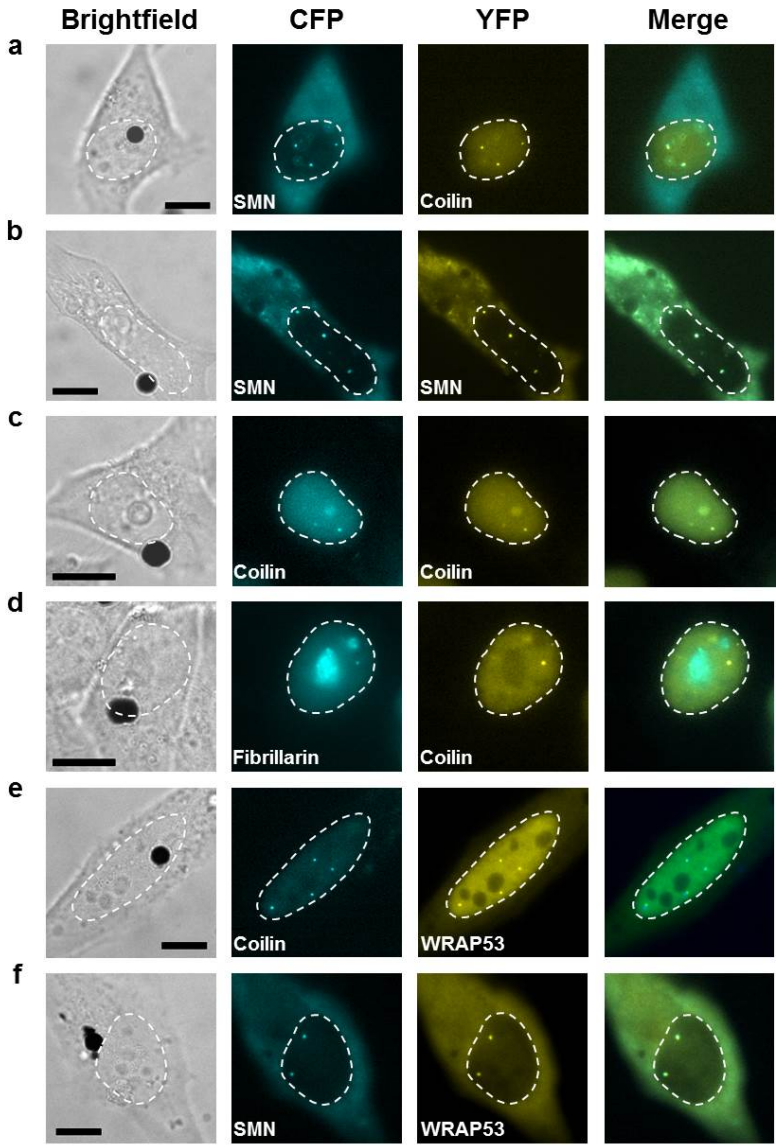

Figure 2.6: Representative images of various fluorescently-labeled Cajal body proteins. A cell transfected with CFP-SMN and YFP-coilin (a), with CFP-SMN and YFP-SMN (b), with CFP-coilin and YFP-coilin (c), with CFP-Fibrillarin and YFP-coilin (d), with CFP-coilin and YFP-WRAP53 (e), and with CFP-SMN and YFP-WRAP53 (f). Left column is bright field images, middle-left column is CFP images, middle-right column is YFP images, and right column is the merge of CFP and YFP images. A black dot in the bright field image is the RGD-coated magnetic bead. Scale bar = 10 μm.

to nuclear lamina, to a putative nucleoplasmic element (likely chromatin and/or an actin-dependent filamentous network [58]), and then to the CB. Interestingly, at a higher loading frequency of 0.83 Hz, coilin still phase-lagged SMN by $\sim 4^\circ$, although the magnitudes of

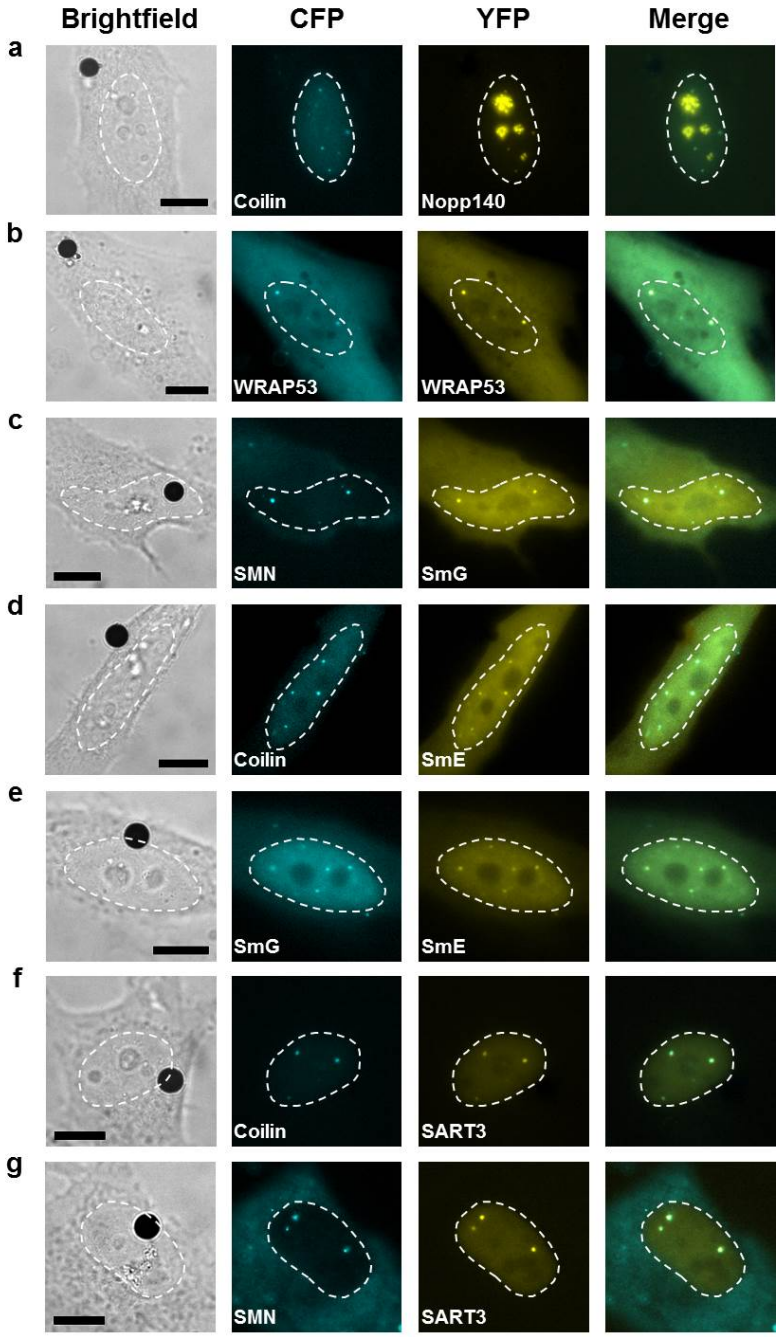

Figure 2.7: Representative images of various fluorescently-labeled Cajal body proteins. A cell transfected with CFP-coilin and YFP-Nopp140 (a), with CFP-WRAP53 and YFP-WRAP53 (b), with CFP-SMN and YFP-SmG (c), with CFP-coilin and YFP-SmE (d), with CFP-SmG and YFP-SmE (e), with CFP-coilin and YFP-SART3 (f), and with CFP-SMN and YFP-SART3 (g). Left column is bright field images, middle-left column is CFP images, middle-right column is YFP images, and right column is the merge of CFP and YFP images. A black dot in the bright field image is the RGD-coated magnetic bead. Scale bar = 10 μm.

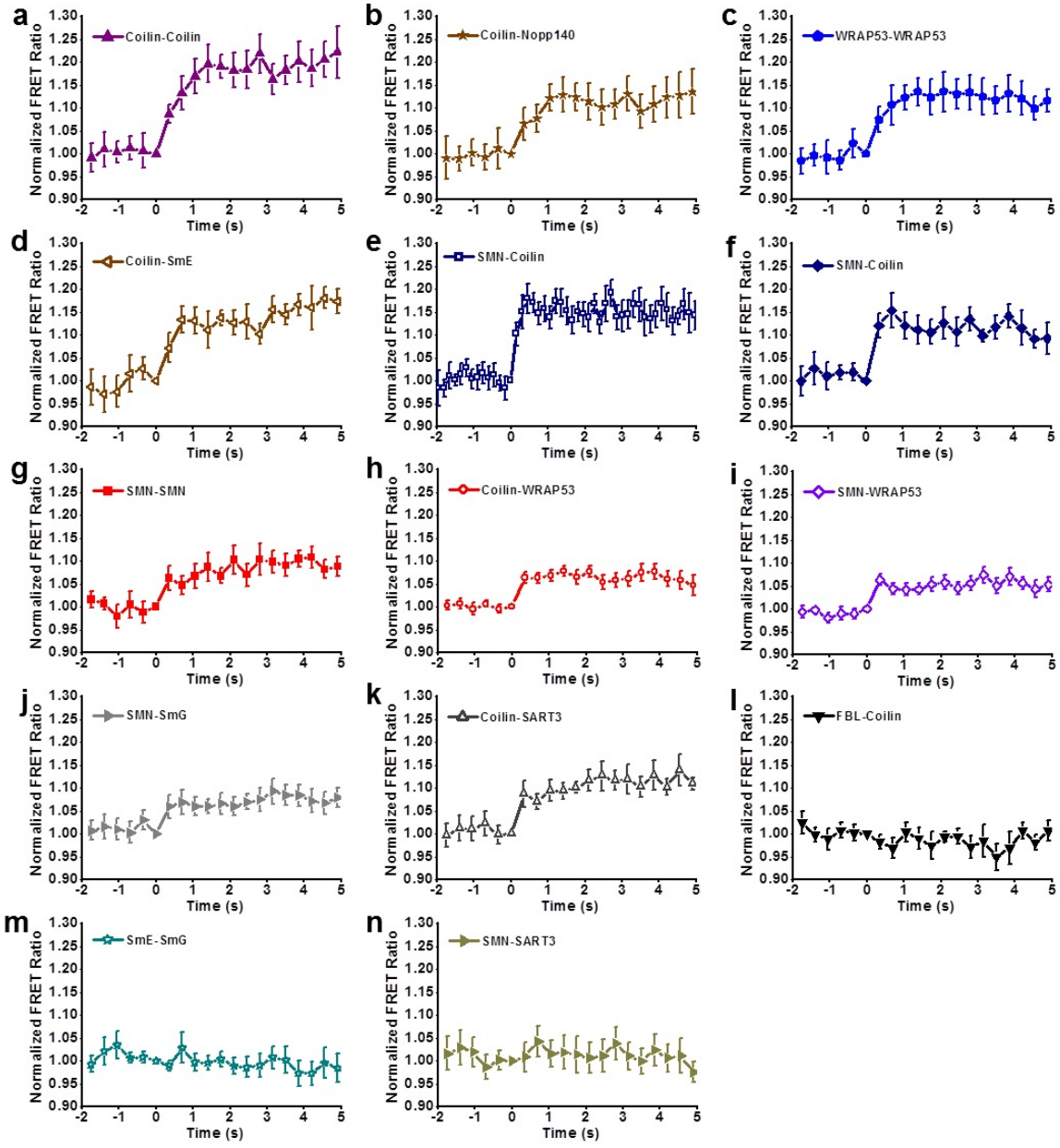

Figure 2.8: Normalized FRET of different Cajal body protein pairs as a function of stress application duration. A step load was applied at time zero and all FRET ratios were normalized to that time point. Average data are shown for slow creep responses (creep time >700 ms) of FRET changes of coilin-coilin (a) (n=41), coilin-Nopp140 (b) (n=9), WRAP53-WRAP53 (c) (n=8), coilin-SmE (d) (n=9), and for fast creep responses (creep time <300 ms) for SMN-coilin (e) (n=10) and (f) (n=13), SMN-SMN (g) (n=6), coilin-WRAP53 (h) (n=23), SMN-WRAP53 (i) (n=15), SMN-SmG (j) (n=11), coilin-SART3 (k) (n=11). No

FRET changes were observed for FBL-coilin (l) (n=41), SmE-SmG (m) (n=63), and SMN-SART3 (n) (n=73). Mean +/- s.e.; data are pooled from at least 3 independent experiments.

phase lags of both proteins decreased by $\sim 4^\circ$ (to $\sim 29^\circ$ for coilin and $\sim 25^\circ$ for SMN) (Fig. 2.10a). These frequency-dependent data suggest that a more dynamic force resulted in a more elastic cytoskeleton and/or nucleoskeleton (lower phase lags or less dissipative energy).

2.3 Discussion

In this study we have shown that a local dynamic surface force can directly alter protein-protein associations in the CB in the nucleus of a living cell without intermediate biochemical cascades. These results provide unequivocal experimental evidence supporting the proposed model of direct force propagation and transduction from ECM to the nucleus [33]. Our findings show that a local force transferred via integrins is propagated in the cytoplasm along the tensed actin cytoskeleton to the nuclear envelope, and across the nuclear envelope to the nuclear lamina, and from the nuclear lamina to a putative nuclear stress-propagating element, which might be chromatin and/or a filamentous structure, and from there to essential CB component SMN, and then to coilin, a structural element of the CB. Our recent findings on the essential roles of myosin II mediated tension and intact actin bundles in cytoskeletal force transmission are consistent with our earlier findings on long distance force transmission and transduction [11–13]. However, previous reports show that direct activation of cytoplasmic enzyme Src or Rac by force also depends on intact microtubules, whereas here we find that dissociation of SMN from coilin in the CB does not depend on microtubules, suggesting a difference in force transduction pathway in activation of molecules between the nucleus and the cytoplasm.

It is known that the nuclear stiffness of a differentiated cell is ~ 5 to 10-fold higher than that of the cytoplasm [37, 41]. One might infer that it would be difficult to displace closely interacting molecules inside the nucleus. However, our present study demonstrates that protein components in the CB can be displaced significantly by a local force of physiological magnitudes. These data suggest that a force might be focused at the cytoskeletal-nuclear

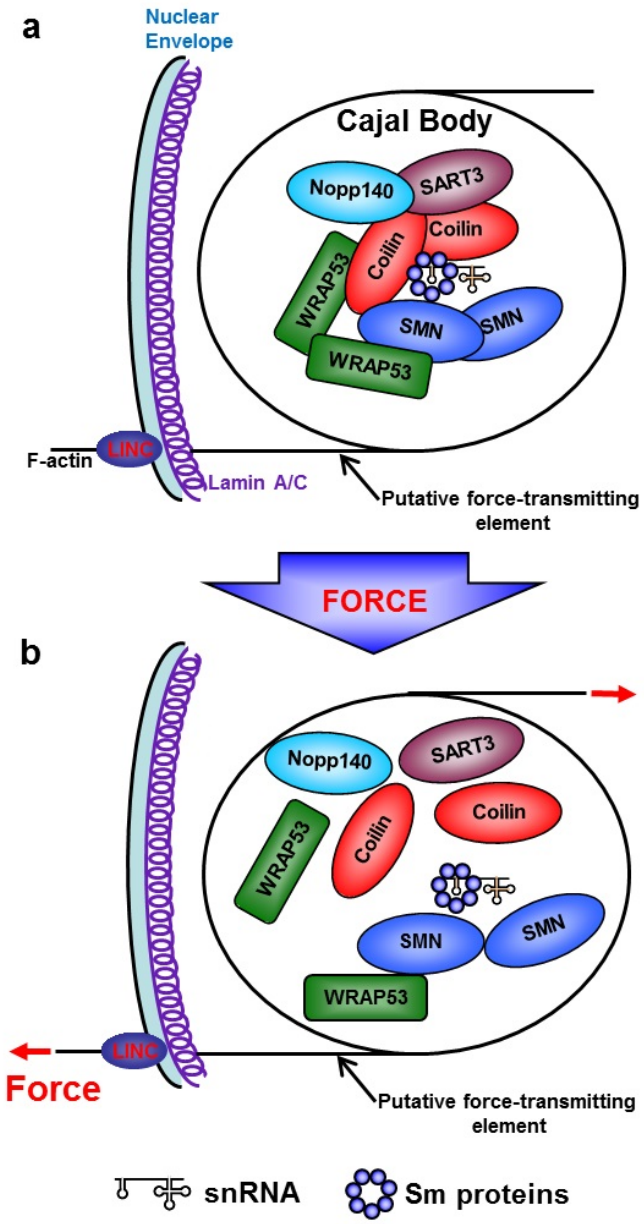

Figure 2.9: A working model of force propagation to the Cajal body. Cajal body interactome under normal physiologic conditions (a) and under an external mechanical stress at the cell surface (b). Two major multi protein-RNA complexes in the Cajal body are characterized by coilin-mediated associations and SMN-mediated associations. Based on experimental results from Figs 2.1 – 2.8 and available literature, we propose a working model that an incoming force transmits into the nucleus via tensed F-actin to LINC, across the nuclear envelope to nuclear lamina, then to a putative nuclear force transmitting element (likely chromatin and/or an actin-dependent nuclear filamentous network [58]), from there to the CB to dissociate the protein complexes. LINC=linker of nucleoskeleton to cytoskeleton. snRNA=small nuclear RNA.

coupling on the nuclear envelope such that efficient stresses are transmitted (likely via chromatin and/or the putative nucleoplasmic filaments [58]) to the CBs. It has been documented that Lamin A/C, expressed abundantly in differentiated cells, is an elastic scaffold to provide structural support to the nuclear envelope and nuclear stiffness [38, 40, 41, 59]. One might think that knocking out Lamin A/C would soften the nucleus and make it easier to deform the nucleoplasmic proteins. In contrast, our data show that cells lacking Lamin A/C fail to transmit surface forces to the CB to dissociate coilin from SMN. These data imply that the nuclear lamina also functions as necessary force-transmitting filaments to molecules inside the nucleoplasm, supported by the data of significant Lamin A deformation in response to the cell surface force, thus extending recent findings that the LINC complex plays important roles in transmitting forces to different parts of the cytoplasm [60,61]. Although F-actin, intermediate filaments, or microtubules are all physically associated with the nuclear envelope via LINC or emerin [40], our findings that plectin and microtubules do not play a significant role in force-induced dissociation of CB proteins suggest that forces are propagated into the nucleus and the CB mostly via F-actin-LINC pathway.

In a physiological environment, extracellular matrix (ECM) is a flexible polymer network that mediates external forces into the living cell and ECM stiffness is known to have profound impacts on many cellular functions [29]. Our current results, showing that protein complexes in the CB dissociate in response to force only when substrate rigidity is approximately equal to or greater than the maximum cell stiffness, are consistent with previous reports but extend the role of substrate rigidity to force-induced protein-protein dissociations in the nucleus. However, whether these force-induced changes are physiologically relevant or not needs to be determined in the future in a living tissue under a normal physiological environment.

It is known that mechanical forces can lead to conformational changes or unfolding of cytosplasmic proteins such as spectrin [34], talin [35], and vinculin [62]. It is possible that in this study the CB components such as coilin and SMN are also partially unfolded by force. However, protein unfolding alone cannot explain the results of highly elevated MSDs in coilin but not in SMN after force application. Therefore, there must be significant dissociation or physical separation of coilin from SMN such that the two proteins are constrained by different local microenvironments after force application. In addition, the magnitudes of

stress-induced displacements for coilin and SMN are too large to be accounted for by protein unfolding alone. Our findings on the phase lag differences in different protein complexes have demonstrated for the first time viscoelastic interactions for multiple CB-interacting proteins.

What might be the physiological relevance of our findings in understanding the CB structure and function? Our FRET data during force application suggest that we have identified two major multi-protein-RNA complexes in the CB. The first complex is characterized by protein associations with high affinity mediated by coilin and its self-interacting ability. The second complex is mediated by the SMN protein and its self-oligomerizing activity with low affinity associations. Interestingly, the critical interaction for the CB integrity between coilin and SMN is not very strong, which may explain the separation of coilin-containing CB residual body from SMN-containing gem when coilin-SMN interaction is impaired [44]. It appears that WRAP53, which likely recruits the SMN protein complex to CB and mediates the interactions between SMN and coilin [53], has a stronger affinity to coilin than to SMN. This suggests that WRAP53 is being stabilized by coilin in the CB. Since coilin mediates strong associations with its interacting partners, spliceosomal snRNPs, Nopp140, SART3, not surprisingly, these coilin interactions are more significantly affected under mechanical stress than SMN protein-mediated ones. Thus our results provide the first in-depth in vivo readout of the major CB structural-functional interactome under normal and stress conditions. A recent view on CB's function suggests that the CB acts as a depot for final modifications of spliceosomal snRNPs delivered to CBs by the SMN protein complex from the cytoplasm before they function in pre-mRNA splicing in the nucleoplasm. SMN is hyperphosphorylated in the cytoplasm and able to recruit proteins to the SMN protein complex in the cytoplasm. Then WRAP53 mediates the import of the SMN protein complex with snRNPs to CBs [59] which is recruited to CBs by hypophosphorylated coilin [63]. Importantly, in the following step snRNPs are exchanged between the SMN complex and coilin in CBs. Coilin is hyperphosphorylated on its C-terminus, which disrupts its interaction with SMN, promoting the release of SMN from the CB and enhancing coilin-snRNP interaction. Thus, snRNPs are transferred from SMN to coilin and become available for further modifications in CBs. As a consequence, coilin is dephosphorylated, possibly by phosphatase PPM1G, which facilitates the release of snRNPs for their functions in pre- mRNA splicing [54].

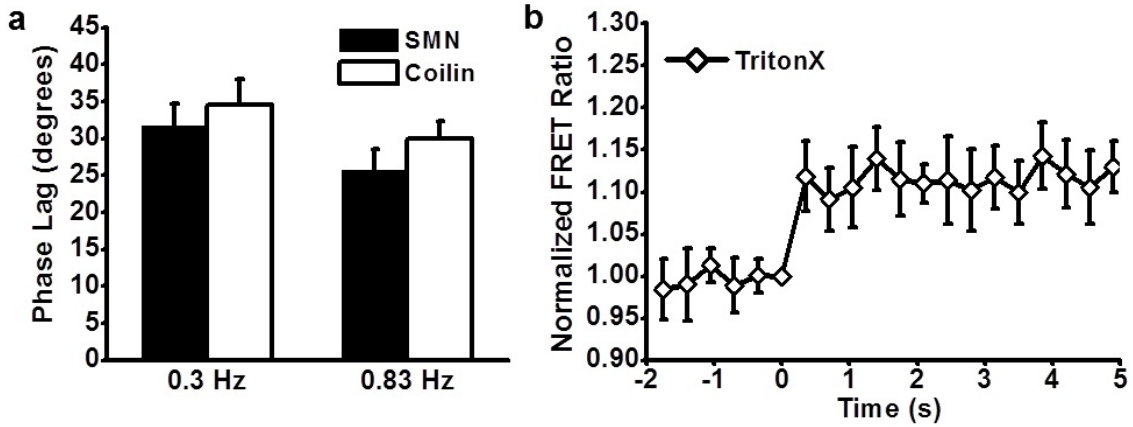

Figure 2.10: Cajal body protein phase lags are loading-frequency dependent and their dissociation does not depend on opening of ion channels. (a) At 0.83 Hz (n=20 CBs), phase lags between coilin or SMN and the bead displacement decreased by 4 ° when compared with loading at 0.3 Hz (n=44 CBs from different cells). (b) After a magnetic bead was bound, the cell was treated with 0.1% Triton X for 3.5 min to remove the plasma membrane. Upon stress application, a change in FRET ratio was observed. n=3 cells. Mean +/- s.e.; data are pooled from 3 independent experiments.

Can the results on dissociation of nuclear protein complexes be explained by indirect steps such as opening of ion channels at the plasma membrane? It is shown previously that calcium influx and propagation in the cytoplasm after a local stress takes several seconds for calcium to reach a remote site of 10-20 μm away [64], whereas we found dissociation of SMN from coilin within 0.35 sec at a distance of 10-20 μm. Therefore, it would be difficult to explain our findings by calcium influx after ion channel opening. Importantly, stress induced FRET ratio change of SMN-coilin was still observed after short-time exposure ($\sim$3.5 min) to 0.1% Triton X to remove the plasma membrane (Fig. 2.10b, 2.11), suggesting that ion channel opening may not be important in force-induced dissociation of proteins complexes in the CB. It should be noted, however, that our current findings do not rule out the important roles of slow processes (e.g., diffusion and/or translocation) induced by force in cellular remodeling and biological responses, which might be synergistic, non-synergistic, or antagonistic with those by soluble growth factors.

In this study FRET changes have also been observed in mouse skin fibroblasts (besides HeLa cells) in response to force, suggesting that the force-induced dissociation of protein complexes in the nucleus may represent a generalized response from different types of differ-

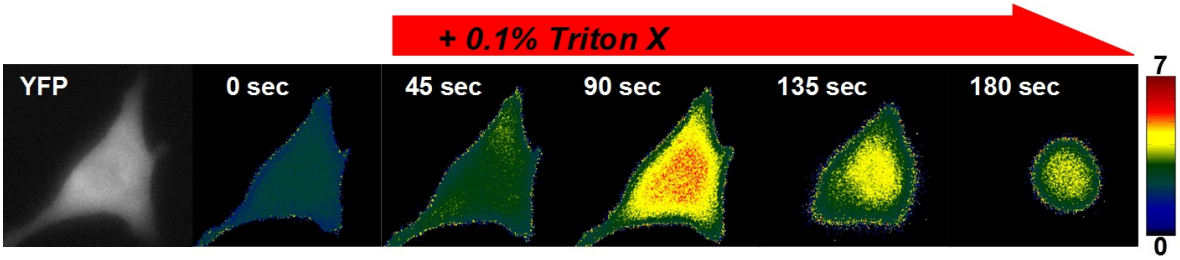

Figure 2.11: Representative figure of Triton X treatment. HeLa cell was first transfected with Calcium biosensor. Both CFP and YFP intensities were captured for FRET analysis. Upon treatment of 0.1% Triton X to puncture the phospholipid membrane, an influx of calcium is observed as indicated by the increase in FRET color scale. After 90s, the cell membrane is punctured and there's free flow of Calcium ions between the cytosol and extracellular fluid, as seen by the decrease in fluorescence. By 3.5 min, most of the plasma membrane is removed, inhibiting all functions of the membrane including those of ion channels.

entiated cells, and not just from HeLa cells. Interestingly CBs that exhibit FRET changes in response to force are the ones that show spontaneous constrained-diffusion (Fig. 2.1h), whereas some CBs that do not respond to force in general exhibit simple diffusion [65], and thus may be only loosely associated with chromatin, consistent with published data that association of CBs to chromatin significantly affects their dynamics [48]. Thus CBs are likely to have an important regulatory role in expression of specific genes with which they are physiologically associated. However, at the present time, there are no any techniques available that have the capability to measure gene expression fast and specifically enough in a single cell to be explained by the direct force effect. In the future, it would be interesting to assess whether such methods can be developed to determine whether responses of CBs to force are important in regulating expression of specific genes.

Our findings that force propagation from cell surface receptors integrins to SMN-coilin in the nucleus is blocked in Lamin A/C$^{-/-}$ cells may have implications in the premature aging disease Hutchinson-Gilford Progeria Syndrom (HGPS) [66]. Recent findings have also revealed the importance of mechanical forces in ECM-integrin-cytoskeleton-myosin II dependent cancer progression [67–69]. Since CBs are predominantly present in transformed or aneuploid cancer cells, it is conceivable that mechanical forces on cell surface might have a direct impact on cell transformation via altering the dynamics of components of nuclear bodies.

In summary, we have demonstrated that dynamic force can induce direct structural changes of essential components of a major nuclear body, which may represent a unique mechanism of mechanotransduction that impacts on gene expression and genome maintenance.

2.4 Materials and Methods

Detailed protocol of this study is described in Appendix A.

2.4.1 Cell culture and transfection

HeLa cells, LMNA-knockout mouse embryonic fibroblast cells, and plectin knockout mouse skin fibroblasts were cultured and maintained in DMEM (Sigma) supplemented with 10% FBS (HyClone), 100U/ml penicillin, 100μg/ml streptomycin, and 2mM L-Glutamine at 37 °C in 5% CO2. For live cells imaging, cells were plated on glass bottom dishes coated with type I collagen (40 μg/ml) overnight. Each fluorescence protein plasmid of interest was transfected at 1 μg per 35mm glass bottom dish using Lipofectamine 2000 twenty hours prior to experiment, following protocols provided by the manufacturer (Invitrogen). The plasmids CFP-SMN [42,70], YFP-SMN [42,70], CFP-coilin [71], YFP-Coilin [71], fibrillarin-YFP [72] constructs are described as referenced. YFP-Nopp140, CFP-WRAP53, YFP-WRAP53, YFP-SART3, CFP-SmE, YFP-SmE, CFP-SmG, YFP-SmG were subcloned into either pECFP-C1 or pEYFP-C1 expression vectors as indicated. mCherry-Lamin A plasmid was a gift from Dr. P. Kalab. The cell culture media was then changed 6 hours after transfection to serum-deprived-media.

2.4.2 Magnetic twisting cytometry, cell stiffness, and tractions

The optical magnetic twisting cytometry method [1,23] was used to exert mechanical stress on the living HeLa cells. Arg-Gly-Asp (RGD)-coated ferromagnetic beads (Fe_3O_4, $\sim$4μm in diameter) were added to the cells and then incubated for 10 minutes to allow for integrin clus-

tering and formation of focal adhesions surrounding the bead. The beads were magnetized in the horizontal direction by a strong magnetic pulse (1,000 G) for a brief period (<100 μs). During imaging, cells were maintained in CO_2 independent medium without serum (Invitrogen) at 37 °C. Cell Young's modulus in Pa was estimated by quantifying the embedded area of the magnetic bead and using the cell stiffness data (in Pa/nm) [10]. Fluorescent beads (0.2μm in diameter) were embedded in the polyacrylamide gel substrate and their positions were recorded by fluorescence microscopy. The displacement field induced by each individual cell's tractional forces was determined by comparing the fluorescent bead positions before and after trypsinization (cell-free and thus force-free). The RMS (RMS=root-mean-square) traction was calculated from the displacement field with known substrate stiffness [73]. Cell tractions were quantified after the cells were plated on various stiffnesses (0.6, 2, and 8 kP, corresponding to 0.06% bisacrylamide and 3% acrylamide, 0.05% bisacrylamide and 5% acrylamide, 0.3% bisacrylamide and 5% acrylamide respectively) of collagen-I coated polyacrylamide gels [73].

For FRET imaging, the magnetic twisting field (0, 1.8, 3.5, 8.8, 14, 17.5, or 24.5 Pa) was applied as a step function (a constant magnetic field) to the magnetic beads that are bound to the surface of the cells. A Leica inverted microscope was integrated with a magnetic twisting device and a Dual-View system (Optical Insights) to simultaneously acquire both CFP and YFP emission images in response to stress. CFP/YFP Dual EX/EM (FRET) (OI-04-SEX2) has the following filter sets: CFP: excitation, S430/25, emission S470/30; YFP: excitation, S500/20, emission S535/30. The emission filter set uses a 515 nm dichroic mirror to split the two emission images. For FRET imaging, we excited at CFP wavelength and measured the emission of both CFP and YFP simultaneously on the same screen using a CCD camera (Hamamatsu C4742-95-12ERG) and a 63x 1.32 N.A. oil-immersion objective. Exposure time was 290 ms or 150 ms.

For Cajal Body (CB) dynamics imaging, an oscillatory magnetic field (24.5 Pa at 0.3 or 0.83Hz) was applied. CFP-SMN and YFP-Coilin images before, during, and after mechanical loading were captured at every 0.32 or 0.09 seconds interval over a period of $\sim$15 s respectively. Bright-field images of the cell and the magnetic bead during oscillatory load were also obtained for bead displacement analysis.

To minimize photobleaching, the cells were treated with 0.5mM Trolox (6-Hydroxy-2,5,7,8-tetramethylchroman-2-carboxylic acid; Sigma) 18 hrs [74] before imaging and illuminated with 12% light intensity by using a 120 W Hg lamp (Leica).

2.4.3 Technical issues related to FRET analyses

Are there potential spontaneous movement artifacts caused by moving structures inside the nucleus? It is known that the largest speed of Cajal body movement can reach $\sim$0.9 μm/min (15 nm/s) [65], which may account for the observed spontaneous movements of the CBs in our study. However, we have observed that in spontaneous movements of CBs before force application there is no separation of coilin from SMN, i.e. both proteins move at the same rate and thus there is no FRET change of the protein complex. More importantly, the anti-correlation behavior between CFP-SMN (increase in emission) and YFP-coilin (decrease in emission) and differential displacements between SMN and coilin in response to force provide a strong evidence that the ratio changes are force-induced FRET changes and not movement artifacts. In addition, we excited at CFP wavelength and simultaneously measured emissions from both CFP and YFP without any time delay. The CFP-SMN transfection (without transfection of YFP-coilin) and excitation yielded only a minimal leak through the YFP channel emission. Therefore the CFP/YFP ratio change is a measure of FRET change which is due to association or dissociation of one protein from the other by force. Since we compared this FRET change in the absence and the presence of applied stress, any bleaching and/or spontaneous FRET changes are accounted for or normalized.

2.4.4 Image Analysis

A customized Matlab (Mathworks) program was used to obtain CFP/YFP emission ratio and CB displacement map. For CFP/YFP emission ratio analysis, CFP and YFP images at each time point were first background-substracted, and aligned pixel-by-pixel by maximizing the normalized cross-correlation coefficient of CFP and YFP images. YFP image was then thresholded to generate a binary mask so that the pixel value inside the fluorescent particle

was set to 1, and that outside the fluorescent particle was set to 0. Aligned CFP/YFP emission ratios were displayed as a linear pseudocolor. To obtain the displacement field of Coilin and SMN, CFP and YFP images were divided into small arrays of 11 $\times$ 11 pixels that overlap by five pixels. The corresponding arrays at the same location between two adjacent images taken at different phases during the twisting cycle were compared in the Fourier domain. This sensitive method can detect displacements of the fluorescent particles to the resolution of 4-5 nm [75].

For Cajal body dynamics analysis, a custom matlab program was developed by converting the florescent image into black and white. The centroid coordinates of each fluorescence particle obtained from the binary image were used to calculate the mean square displacement (MSD) of coilin and SMN. The MSD before, during, and after mechanical loading were calculated based on equation (2.1)

$$MSD(\Delta t) = \frac{1}{N}\sum_{i=1}^{N}\left\{[r(t_i+\Delta t) - r(t_i)]^2\right\} \tag{2.1}$$

where $r(t)$ is the fluorescence particle position and Δt is the time step (0.32s in our case). The same procedure is performed on bright-field images to obtain the magnetic bead MSD.

A two-tailed Student's t-test was used for all statistics.

CHAPTER 3

FORCE VIA INTEGRINS BUT NOT E-CADHERIN DECREASES OCT3/4 EXPRESSION IN EMBRYONIC STEM CELLS

Uda and Poh et al. (2011) Biochemical Biophysical Research Communications 415:396-400

3.1 Introduction

Increasing evidence suggests that mechanical factors play a critical role in fate decisions of stem cells [8, 76, 77], in addition to soluble factors [78]. Recently, we have reported that a local cyclic force on a single mouse embryonic stem (ES) cell via Arg-Gly-Asp (RGD)-containing-peptides coated magnetic beads induced spreading, stiffening and downregulation of Oct3/4 gene (also known as Pou5f1) [73, 79], a primary marker for pluripotency [80]; lowering endogenous forces of ES cells by seeding them on soft substrates that match ES cells intrinsic stiffness promotes the self-renewal and pluripotency of ES cells [81]. However, how ES cells sense mechanical forces via different adhesion molecules remains elusive. In addition, RGD-containing peptides are synthetic peptides and it is not clear how ES cells sense force applied via natural matrix molecules such as fibronectin or laminin. In this study, we demonstrate that a local cyclic stress applied to individual ES cells using magnetic beads coated with different ligands resulted in drastically different biological responses: force applied via integrin receptors but not E-cadherin (also known as Cdh1) resulted in cell spreading, downregulation of Oct3/4 gene expression, and a decrease in cell proliferation rate, although the ES cell stiffened in response to both cellmatrix and cellcell mediated force application. Our findings demonstrate that biological responses of ES cells to force applied via integrins are different from those to force via E-cadherin, suggesting that mechanical forces might play different roles in different force transduction pathways to shape early embryogenesis.

3.2 Results

3.2.1 ES cells stiffen in response to stress via focal adhesions and Ecadherin

We first determined the binding specificity of different ligand-coated magnetic beads. Soluble ligands were added to the culture medium of ES cells for 10 minutes at different concentrations. Then ligand-coated beads were added to the culture for 15 minutes and unbound beads were washed away. Obviously beads bound to the cells were significantly decreased by the addition of soluble ligands. Binding of the ligand-coated beads to the cell surface showed dose-dependent competition with soluble ligands (Fig. 3.1A, B, C). Furthermore, binding of E-cadherin coated beads to the cells was decreased by increasing concentrations of EGTA, a calcium chelator (Fig. 3.1D). Cell-cell adhesions via homophilic E-cadherin protein-protein interactions are strongly dependent on the presence of calcium [82]. These results suggest that ligand-coated magnetic beads interact with specific cell surface receptors.

To examine how ES cells respond mechanically to a local force via specific ligand-receptor interactions, a local cyclic shear stress (17.5 Pa at 0.3 Hz) was applied to ES cells bound with beads coated with each ligand for one hour and cell stiffness was quantified. When baseline cell stiffness was measured with application of a short, 10-second stress, stiffness of ES cells bound with RGD, fibronectin, laminin, or E-cadherin coated beads was similar and $\sim$0.5 kPa (Fig. 3.2B), consistent with previously published results [73, 79]. As the stress was applied for longer periods of duration to the ES cells via different ligands, cell stiffness increased for all conditions examined, although the cell stiffening rate varied depending on the ligand coating beads (Fig. 3.2A). Since cell stiffening in response to the same magnitude of applied stress is an index of mechanotransduction-dependent cytoskeletal remodeling [83], these results indicate that both integrin focal adhesion complexes and E-cadherin complexes are bona fide mechanosensors in ES cells, consistent with previously published results in other cells types [82, 83].

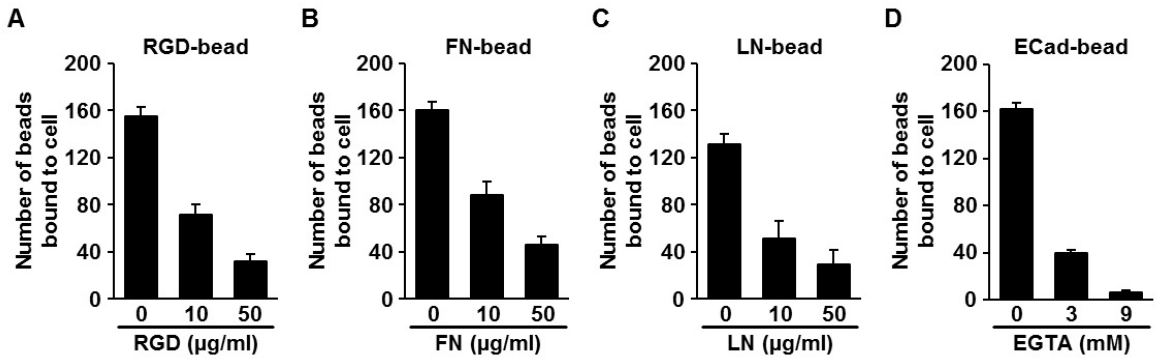

Figure 3.1: Binding of ligand-coated magnetic beads to embryonic stem cells showed ligand specificity. The number of surface-bound beads coated with each ligand indicated was quantified before (0 minutes) and 10 minutes after addition of each soluble ligand (10 and 50 μg/ml for RGD, fibronectin and laminin, and 3 and 9 mM for EGTA). (A) RGD-bead: RGD-containing peptide-coated beads; $p<0.003$ between 0 and 10 μg/ml soluble RGD; $p<0.033$ between 10 and 50 μg/ml soluble RGD peptides. (B) FN-bead: fibronectin-coated beads; $p<0.011$ between 0 and 10 μg/ml soluble fibronectin; $p<0.05$ between 10 and 50 μg/ml fibronectin. (C) LN-bead: laminin-coated beads; $p<0.015$ between 0 and 10 μg/ml; $p>0.25$ between 10 and 50 μg/ml soluble laminin. (D) ECad-bead: E-cadherin coated beads; $p<0.001$ between 0 and 3 mM soluble EGTA; and $p<0.002$ between 3 and 9 mM EGTA. Data were collected from 3 biological replicates for each condition. Means +/- s.e. are shown.

3.2.2 Force via integrins but not E-cadherin induces ES cell spreading and slows the cell proliferation rate

Previously we have shown that force applied via RGD-coated magnetic beads induces ES cell spreading [73]. However, it is not clear whether natural matrix ligands such as fibronectin or laminin and cell-cell adhesion molecule E-cadherin can mediate force-dependent cell spreading in ES cells. One hour after force application, magnetic beads coated with RGD, fibronectin, or laminin induced bleb formation and caused a $\sim$50% increase in the ES cell projected area in 12 hours (Fig. 3.3B). These ES cells remained spread and flattened for up to 24 hours after stress was applied. In contrast, control cells that were not stressed or cells stressed via magnetic beads coated with E-cadherin ligands exhibited a 20% decrease in cell projected areas in 24 hours (Fig. 3.3B). It is known that normal pluripotent self-renewing mouse ES cells have a cell-doubling time of $\sim$10.5 hours [79]. Comparing the number of nuclei in control stress-free cells or cells stressed via E-cadherin coated beads at 12 hours with

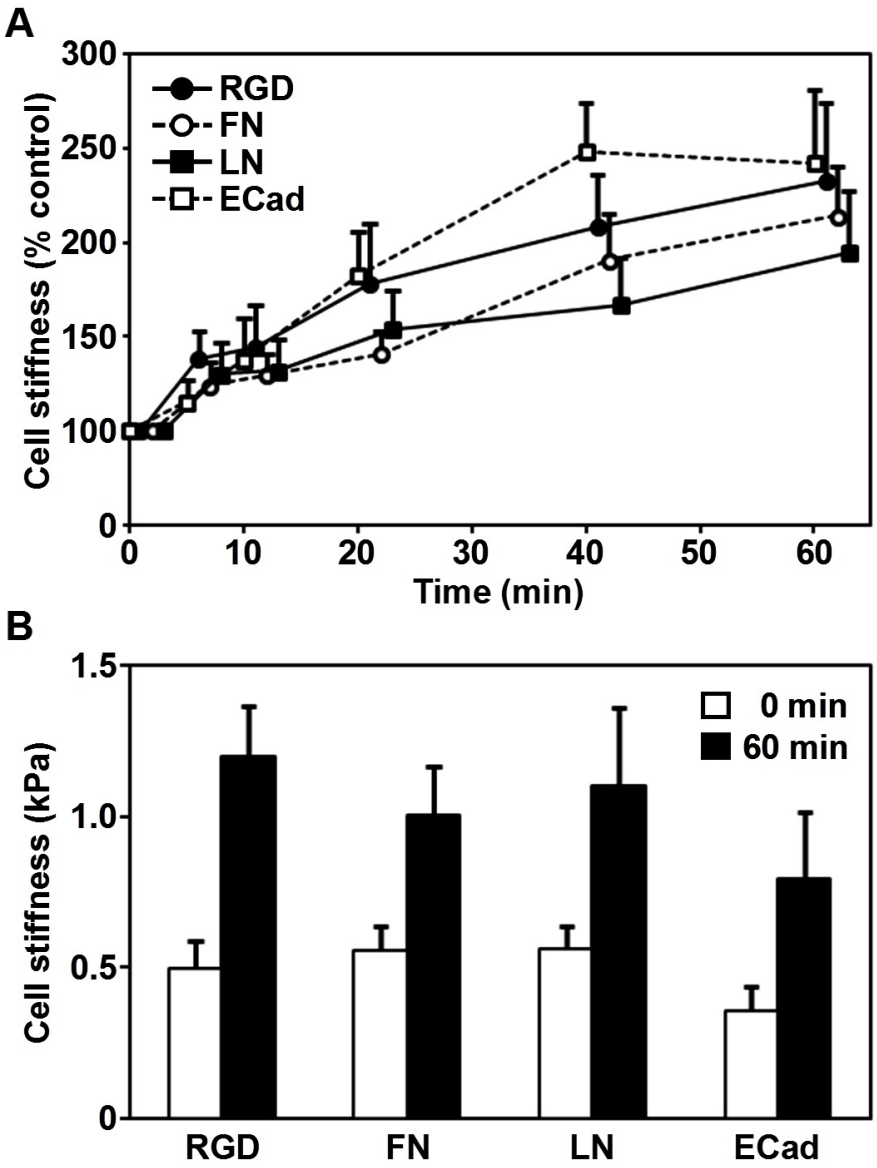

Figure 3.2: Stress induced stiffening in embryonic stem cells bound with ligand-coated beads. (A) Stiffening response is shown as a function of duration of stress application. The peak of cyclic stress is 17.5 Pa; the frequency of loading is 0.3 Hz. All stiffness measurements are normalized with respect to time zero. Means +/- s.s. are shown. (B) Absolute magnitudes of cell stiffness (shear complex modulus) are shown before (0 minutes) and after (60 minutes) stress application. Each comparison of the cell stiffness before and after stress application showed significant differences; RGD, $p<0.012$; fibronectin, $p<0.017$; laminin, $p<0.041$; and E-cadherin, $p<0.044$. Data were collected from 5, 10, 9, and 7 cells for RGD, fibronectin (FN), laminin (LN), and E-cadherin (ECad) coated beads, respectively. Means +/- s.e. are shown.

that at 24 hours, it clearly demonstrate that these ES cells double normally (Fig. 3.3A). In sharp contrast, the cells stressed via RGD, FN, or LN coated beads remained as single cells at 24 hours (Fig. 3.3A), suggesting that the force applied via integrin pathways delayed cell proliferation rates in these ES cells, possibly by impeding the self-renewing capacity of the ES cells. These results demonstrate that not all force transduction pathways in mouse ES cells are the same: forces via integrin-mediated pathways induce cell spreading and slow down cell proliferation, whereas forces via E-cadherin-mediated pathways have no effect on either cell spreading or cell proliferation rate.

3.2.3 Stress via interins but not E-cadherin induces ES cell differentiation

Recent reports show that mechanical forces influence ES cell proliferation and differentiation [8, 73, 77, 84], but it is not known if different adhesion molecules mediate different responses to force. To address this question, expression of Oct3/4, the master regulator of pluripotency in ES cells [80], was monitored using the ES cell line that express enhanced green fluorescent protein (EGFP) under the Oct3/4 promoter [73]. The individual ES cells were healthy and pluripotent before stress was applied, as indicated by the round shape and high EGFP expression (Fig. 3.4A, 1st, 5th column). When a cyclic shear stress (17.5 Pa at 0.3 Hz) was applied to the cells for 1 hr using RGD, fibronectin or laminin coated beads (Fig. 3.4A 2nd, 3rd, 4th row), EGFP expression in these cells decreased by ∼15% in 12 hours and ∼30% by 24 hours (Fig. 3.4A, B). In sharp contrast, the cells that were stressed via E-cadherin coated beads did not have any decrease in EGFP expression in 12 or 24 hours, similar to control cells in the same culture dish that were not stressed or not bound with beads (Fig. 3.4A, B). It should be noted that the apparent increase in the projected area of control cells and stressed cells via E-cadherin coated beads at 12 hours and 24 hours are not due to cell spreading, but due to increased cell numbers as a result of cell proliferation (see Fig. 3.3). To make certain that the decrease in EGFP expression was not due to a reduction in the general transcription capacity of the cell, cells were simultaneously transfected with a construct that permits expression of DsRed under CAG, a constitutively active promoter [85]. Despite the decrease in EGFP expression by force applied via the RGD-coated beads, DsRed expression

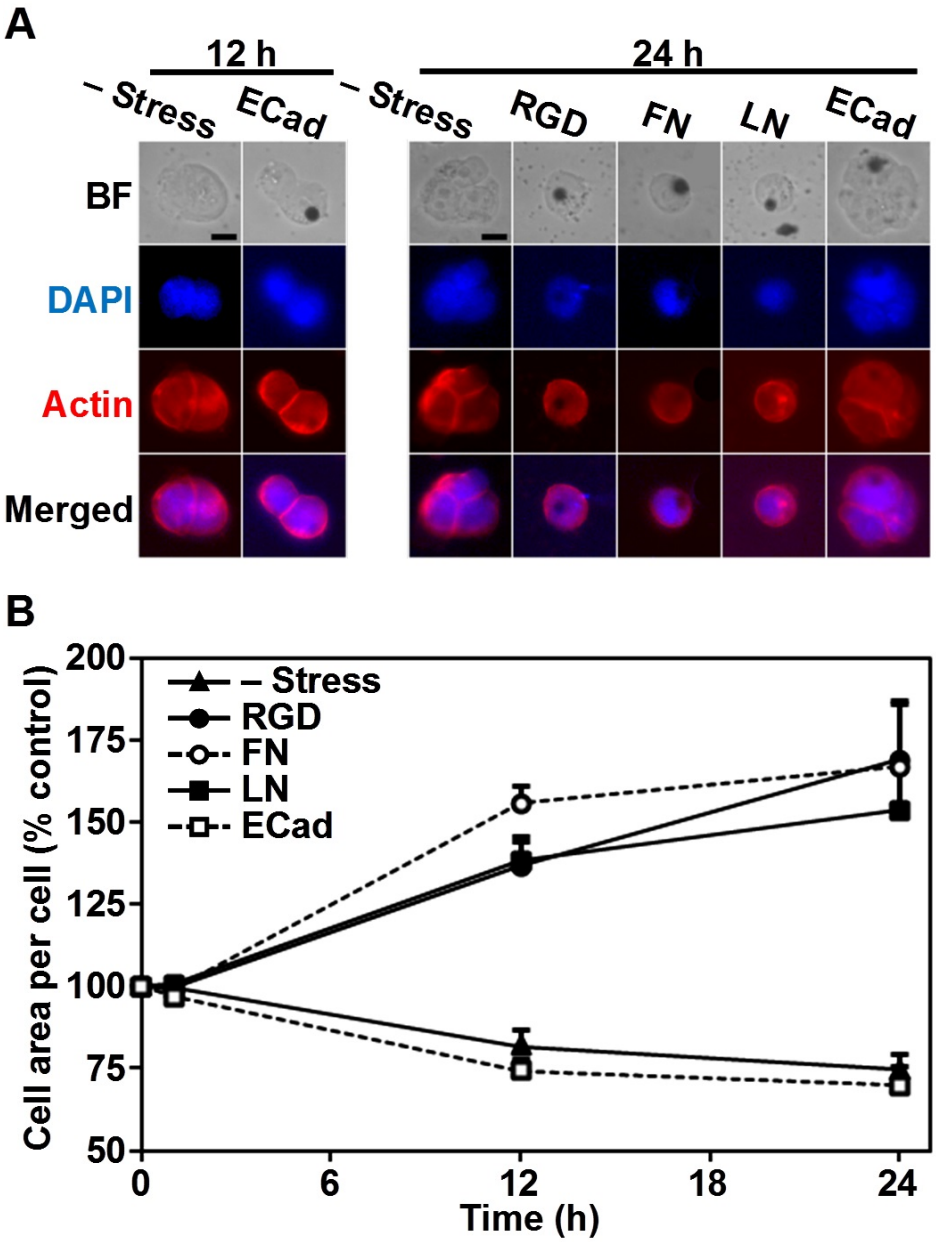

Figure 3.3: Force via integrins but not E-cadherin increased cell spreading and doubling time. (A) Representative bright field (BF; top row) images of ES cells and fluorescent images indicating the presence of the nucleus (DAPI; 2nd row) and F-actin (Actin, 3rd row) are shown at 12 hours and 24 hours without stress (Stress) or after stress was applied for 1 hour. Fluorescent images for DAPI and F-actin staining were merged on the bottom row. Cells stressed via RGD, fibronectin (FN), and laminin (LN) coated beads remained as single cells 24 hours after stress was applied. However, control cells (Stress) and cells stressed with E-cadherin coated beads continued to proliferate, which is evident from the number of nuclei at 12 and 24 hours. Scale bars, 10 μm. (B) The cell area per cell was summarized as

a function of time after stress. Cells stressed with RGD, FN, or LN-coated beads increased projected areas by 5070% by. However, control cells or cells stressed with E-cadherin (ECad) coated beads decreased cell projected areas slightly due to cell division. Values for cell areas at 12 and 24 hours are statistically significant when compared with those before application of the stress (time 0; $p<0.01$ for all conditions). Values at 12 hours did not show statistical significance when compared with those at 24 hours (for all conditions, $p>0.1$). The cell projected area before stress application was $\sim$230 μm^2. Data were collected from 10, 8, 8, 7, and 8 for Stress, RGD, FN, LN, and ECad-coated beads respectively. Means +/- s.e. are shown.

remained constant >24 hours, indicating that the ES cells were healthy [73]. These results show that force applied via integrin pathways, but not E-cadherin pathways, is capable of downregulating Oct3/4 expression, leading to ES cell differentiation.

3.3 Discussion

Despite significant progress during the past decade in the field of mechanotransduction, the mechanisms of biological responses to force remain elusive. In particular, only very recently has it been shown that cell-cell adhesion molecule E-cadherin is a direct mechanosensor [82], similar to cell-matrix adhesion molecule integrins. Here we show that the biological responses to force in mouse ES cells depend on specific pathways through transmembrane adhesion molecules: both integrin and E-cadherin pathways can mediate force-dependent cell stiffening, whereas only integrins but not E-cadherin can mediate force-dependent cell spreading and Oct3/4 downregulation. These findings suggest that integrins and cadherins play different roles in directing embryonic stem cell fate decisions.

Recently we have shown that force applied via synthetic RGD-containing peptides can cause cell stiffening, spreading, and Oct3/4 downregulation [73] [79]. In this study, we have extended these findings to investigating the effects of forces applied via natural ligands of integrins, which are fibronectin and laminin. It is known that fibronectin and laminin are essential for early embryogenesis and tissue organization [86, 87]. Fibronectin interacts with cell surface via $\alpha 5\beta 1$ and $\alpha v\beta 3$ integrins [88]. Laminin, on the other hand, interact with cell surface via $\alpha 6\beta 1$ or $\alpha 7\beta 1$ [89]. Because fibronectin forms unique fibrils in vivo [90], it will be interesting to determine in the future whether fibronectin and laminin play different

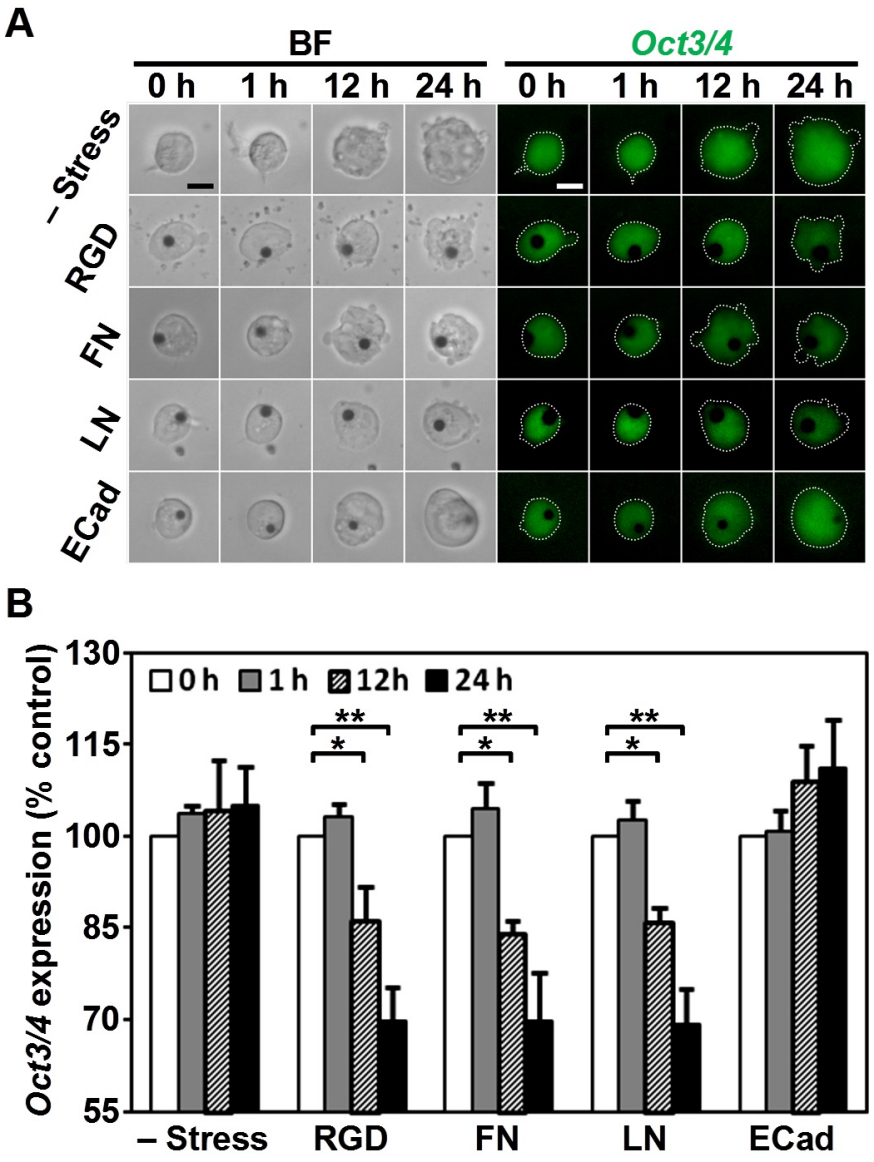

Figure 3.4: Force via integrins but not E-cadherin downregulated Oct3/4 expression (A) Representative bright field (BF, left) and fluorescence (Oct3/4, right) images of mouse ES cells bound with beads coated with ligands as indicated on left at different times as indicated on top. Expression of Oct3/4 was shown by fluorescence of EGFP driven by the Oct3/4 promoter (EGFP-Oct3/4). Cyclic shear stress was applied for 1 hr (peak stress was 17.5 Pa at 0.3 Hz). Note that the EGFP-Oct3/4 fluorescence intensity decreased in cell stressed with RGD, fibronectin (FN), and laminin (LN) coated beads at 12 and 24 hours after stress was applied. Scale bars, 10 μm. (B) Expression levels of Oct3/4 were quantified up to 24 hours after stress was applied. Force via RGD (n=9), FN (n=10), or LN (n=10) coated beads decreased EGFP-Oct3/4 at 12 or 24 hours. *p<0.05; **p<0.01. However, force via E-cadherin coated beads has no effect on EGFP-Oct3/4 expression (n=8). Cells that had no beads bound were used as a control (Stress; n = 8). Means +/- s.e. are shown.

roles in lineage differentiation of embryonic stem cells.

Why do forces applied to mouse ES cells via integrins and cadherins elicit totally different responses in cell spreading and Oct3/4 expression although similar responses in cell stiffening were observed? At this time, it is not clear what the underlying mechanisms are but there are a few clues. Both integrin-based focal contacts and cadherin-based complexes provide anchoring support to cells through links to the actin cytoskeleton. Integrin clusters via cell-ECM interactions recruit proteins such as talin [35] and vinculin [62] that can be deformed, unfolded, and activated by forces of physiologic magnitudes. E-cadherin at cell-cell adhesion sites, on the other hand, recruits proteins such as α-catenin [91], β-catenin [92], and vinculin [82]. It has been shown that vinculin facilitates E-cadherin mediated mechanosensing and stiffening in response to shear force at cell-cell junctions [82]. Vinculin knockout cells display a reduction in the stress-induced cell stiffening response through E-cadherin whereas vinculin-reconstituted cells fully restore the force-dependent reinforcement of cadherin junctions [82]. Because vinculin is implicated in force-mediated strengthening of adhesion sites and is localized in both cell-matrix adhesions and cell-cell junctions [82, 83], we hypothesize that vinculin is at least partly responsible for the stress-induced ES cell stiffening response in both integrin mediated pathways and cadherin mediated pathways. Cell spreading is a complicated process that involves plasma membrane protrusion mediated by coordinated actin polymerization, which, in turn, depends on activities of actin associated proteins such as Arp2/3 and WASP [93, 94]. Stress-induced cell spreading also requires activated Src, cdc42, and myosin II [73]. When a force is applied via the integrin pathways, it induces cell membrane protrusion as early as $\sim$30 sec of force application [73]. The ES cell continues to spread in response to the cyclic stress and the cell increases its projected area by $\sim$50 - 70% after 1 hr of force application [73] (Fig. 3.3). The significant downregulation of Oct3/4 expression, quantified by changes in EGFP fluorescence intensity in the cells, was only apparent at $\sim$ 12 hours (Fig. 3.4). This suggests that cell spreading might precede downregulation of Oct3/4 expression and might be necessary for Oct3/4 downregulation and ES cell differentiation. However, this conclusion should be dealt with caution since the fluorescence intensity in these ES cells depends on the turnovers of EGFP, which might be much slower than the actual force-induced inhibitory action on the Oct3/4 gene. The relationship between ES

cell spreading and ES cell differentiation needs to be examined carefully in the future. It will also be interesting to elucidate the mechanisms of why the same force results in totally different responses in spreading and Oct3/4 expression for integrins and E-cadherin.

E-cadherin has been implicated in promoting the pluripotency and self-renewal of ES cells. When ES cells are plated on E-cadherin coated dishes, they maintain self-renewal and pluripotency [95]. These ES cells must adhere via E-cadherin molecules and should have generated tractions and transmitted forces from the cell to the substrate via E-cadherin [96]. Therefore the fact that they maintain self-renewal and pluripotency is completely consistent with our results that the force applied via E-cadherin maintains self-renewal and Oct3/4 expression.

The first recognized differentiation event occurs at the late morula stage when the outer layer of the compacted ball of totipotent cells adopts an epithelial structure. Similar epithelialization happens during the progression of embryoid body differentiation [97, 98]. This may be due to the outer layer of cells experiencing different forces through the interaction with the surrounding microenvironment. It has been shown that forces at intercellular junctions regulate cell polarity, shape, movements, and germ cell migration during morphogenesiss [99, 100]. Taken together, it is likely that forces mediated by pathways through integrins and cadherins are crucial in cell differentiation events during embryogenesis.

In conclusion, we have shown two distinct biological responses from mouse ES cells to a small local force of physiologic magnitudes through different ligands. Cell stiffening is elicited by force in both integrin and cadherin pathways; however, cell spreading and differentiation are induced by force only in the integrin but not in the E-cadherin pathway. It will be interesting to determine the effects of force magnitude, frequency, and modes on ES cell pluripotency and the specific germ-layer (endoderm, mesoderm or ectoderm) formation.

3.4 Materials and Methods

3.4.1 Mouse ES cell culture

Undifferentiated mouse ES cells (OGR1) that express enhanced GFP (EGFP) under the promoter of Oct3/4 (Oct3/4::EGFP) were cultured and maintained in feeder free conditions with leukaemia inhibitory factor (LIF; Chemicon) as previously described [73]. For live cell imaging, individual mouse ES cells were plated sparsely on the 0.6 kPa gel substrate (0.06% bis-acrylamide, 3% polyacrylamide) [101] for ∼8 hours prior to experiment to match the substrate stiffness with the intrinsic mouse ES cell stiffness. The gel substrate was coated with collagen-I (200 μg/ml) 24 hours before plating cells. Gridded glass-bottomed dishes (MatTek) were used to track cells of interest over a long period (24 hours). To assess the general transcription status of the ES cells under stress, OGR1 cells transfected with pCAGGS DsRedT3_T2A_Puro were used [73]. The pluripotent state of cells was quantified by measuring the intensity of the EGFP expression. Cell spreading area was measured using an active contours algorithm through ImageJ (NIH).

3.4.2 Bead coating

Ferromagnetic microbeads (Fe_3O_4) ∼4 μm in diameter were coated with different ligands. For Arg-Gly-Asp (RGD) or fibronectin coated beads, 50 μg of RGD peptide or 25 μg of fibronectin (Sigma-Aldrich) per milligram of beads in 1 ml of carbonate buffer (pH9.4) were used. The beads were incubated overnight at 4 °C while being gently rotated. For laminin coated beads, 10 μg of beads and 20 μg of laminin (Sigma) were suspended in 100 μl of PBS buffer and incubated for 10 minutes. For E-cadherin coated beads, 1 mg of beads were suspended in 1 ml of coating buffer (20 mM HEPES buffer supplemented with 100 mM NaCl and 5 mM $CaCl_2$ at pH 8.0). The bead solution was mixed with 100 μg of E-Cadherin/Fc Chimera (Sigma) and incubated overnight at 4 °C while gently being rotated. After coating, RGD, fibronectin, laminin, or E-cadherin coated beads were suspended in serum-free medium or the coating buffer before storing at 4 °C or used immediately in the experiments.

3.4.3 Magnetic Twisting Cytometry (MTC)

The MTC technique has been reported before [1, 23]. After placing the dish on the microscope, a brief and strong magnetic impulse (∼1000G, <100 μs) was applied to magnetize the beads. A twisting torque with peak stress of 17.5 Pa was applied to the cells by a homogeneous sinusoidal magnetic field (0.3 Hz) perpendicular to the beads magnetic moment. This magnetic torque causes the bead to rotate, thus deforming the cells. The cell shear modulus was estimated by quantifying the embedded area of the bead and cell stiffness [10].

3.4.4 Staining

ES cells were fixed with 4% paraformaldehyde and permeabilized with 0.5% Triton X-100. Cells were then incubated with 1 μg/ml Rhodamine-phalloidin for 30 minutes. Nuclei were counter-stained with 300 nM DAPI (Invitrogen) for 1 hour. Specimens were rinsed two times with cytoskeleton buffer solution and once with dH2O.

3.4.5 Bead binding specificity

Mouse ES cells were plated on 200 μg/ml collagen-I coated glassbottomed dish (MatTek) at a density of 6.5 $\times$ 10^3 cells/cm^2. About 8 hours after incubation at 37 °C in 5% CO_2, the culture medium was replaced with a serum free medium [1]. Cells were pre-treated for 10 minutes with soluble RGD, fibronectin or laminin at a final concentration of 10 or 50 μg/ml whereas EGTA (Sigma-Aldrich) was used at a concentration of 3 or 9 mM to determine binding specificity of the ligand-coated magnetic beads. The total number of beads left on the apical surface of cells after washing was counted. A two-tailed Students t-test was used for statistics.

CHAPTER 4

EMBRYONIC STEM CELLS DO NOT STIFFEN ON RIGID SUBSTRATES

Poh et al. (2010) Biophysical Journal 99:L19-L21

4.1 Introduction

It has been previously established that living cells, including mesenchymal stem cells, stiffen in response to elevation of substrate stiffness. This stiffening is largely attributed to the elevation of the tractions at the cell base that is associated with increases in cell spreading on more-rigid substrates. We show here, surprisingly, that mouse embryonic stem cells (ESCs) do not stiffen when substrate stiffness increases. As shown recently, these cells do not increase spreading on more-rigid substrates either. However, these ESCs do increase their basal tractions as substrate stiffness increases. We conclude that these ESCs exhibit mechanical behaviors distinct from those of mesenchymal stem cells and of terminally differentiated cells, and decouple its apical cell stiffness from its basal tractional stresses during the substrate rigidity response.

Cytoskeletal stiffening as a result of elevation of cytoskeletal tension (prestress) has been established as a key feature of anchorage-dependent cells such as terminally differentiated cells [102, 103] and mesenchymal stem cells [8]. This feature is consistent with the model that a living cell behaves as a prestress-supported, integrated network [102], which may have important implications for vital cell functions such as cell spreading [101], substrate rigidity sensing [103, 104], gene expression [105], and cell proliferation and apoptosis [106]. Recently we have reported that embryonic stem cells (ESCs) exhibit unique features of high intrinsic softness that dictates stress-induced cell spreading and differentiation [73]. Unlike most other anchorage-dependent cells, these ESCs do not increase cell spreading on stiffer

substrates [73]. However, it remains unclear how these cells change their tractions and stiffness on different substrates.

4.2 Results

4.2.1 Increase in embryonic stem cell basal traction with elevated of substrate rigidity

To examine how mouse ESCs might alter their mechanical functions in response to substrate rigidity, we seeded single ESCs on collagen-I coated polyacrylamide gels of various stiffness in the presence of ESC culture medium (leukemia inhibitory factor, i.e., +LIF) which maintains their pluripotency. The individual ESCs were all undifferentiated cells, as indicated by the high expression level of Oct3/4 (pou5f1), a primary marker for pluripotency (see Fig. 4.1). As the substrate stiffness increased, cell tractions at the basal surface increased (Fig. 4.2A), consistent with all previously published results in mesenchymal stem cells or terminally differentiated cells [8, 104], although the projected areas of these ESCs did not change [73].

4.2.2 Embryonic stem cell stiffness does not increase with substrate rigidity

Surprisingly, the stiffness of the ESCs, measured at the apical surface of the cells with magnetic twisting cytometry using either Arg-Gly-Asp (RGD)-coated beads or fibronectin (FN)-coated beads, did not exhibit corresponding increases with the substrate stiffness (Fig. 4.2B). This peculiar result of the ESCs is different from those of other anchorage-dependent cells such as fibroblasts [104], although ESCs are also characterized as anchorage-dependent cells that depend on adhesion and cell shape change for survival. To investigate whether these ESCs can stiffen at all in response to mechanical stimulation, we applied periodic small stresses (17.5 Pa at 0.3 Hz) to the individual ESC seeded on collagen-I coated soft substrate of 0.6 kPa. As shown in Fig. 4.3B, the cell started to stiffen $\sim$5 min after the onset of stress application, accompanied by simultaneous elevations in tractions at the basal surface of the

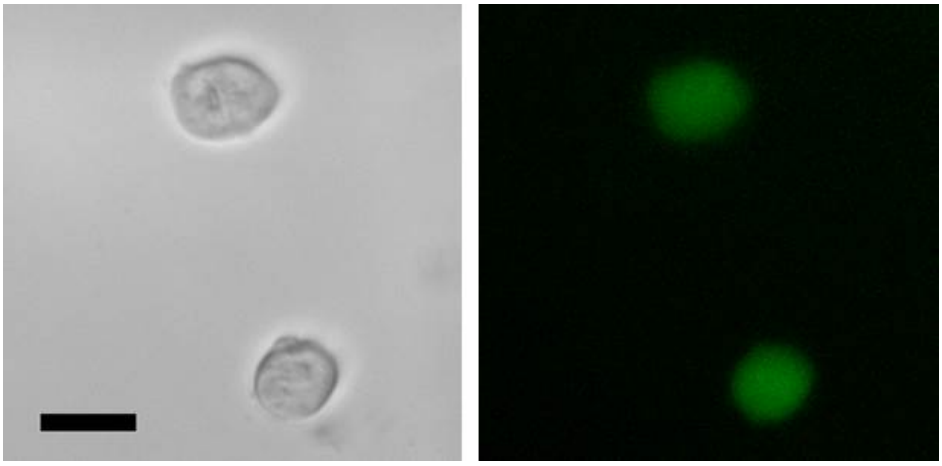

Figure 4.1: Representative fluorescent image of Oct3/4 expression, a primary marker for pluripotency, in two mouse ESCs plated on collagen-I coated 0.6 kPa substrate. Brightfield image (left) and corresponding green fluorescent protein (GFP) image (right) of Oct3/4 expression from the same cells are shown. Expression of stably transfected GFP was driven by Oct3/4 promoter in the presence of leukemia inhibitory factor (+LIF). The GFP Oct3/4 expression is specific to ESCs since it is completely inhibited in the cells that are differentiated from these cells by adding Retinoic Acid (1 μg/ml) and removing LIF (ref. 8 in the main text). All stiffness and traction measurements were done on single undifferentiated, homogeneous, pluripotent ESCs (assessed by the uniformly high GFP Oct3/4 intensity in each ESC with unique cell shape, colony-forming capability, and the short cell doubling time ($\sim$10.5 hrs)) plated on collagen-I (200 μg/ml) coated polyacrylamide gels of varying stiffness. Scale bar = 10μm.

same cells (Fig. 4.3A and 4.3C).

4.3 Discussion

Our data show that mouse ESCs clearly respond to collagen-I coated substrate rigidity by increasing cell basal tractions. However, their apical stiffness does not change with substrate rigidity. This decoupling between basal tractions and apical stiffness as substrate rigidity varies appears to be a unique feature of these ESCs, dramatically different from that of the mesenchymal stem cells or of terminally differentiated cells [8, 104].

At the time of this publication, we do not know the exact mechanism(s) underlying this stiffness-traction decoupling phenomenon. However, there are some possible explanations. It is known that the ESCs have much lower amounts of F-actin and actin bundles than their

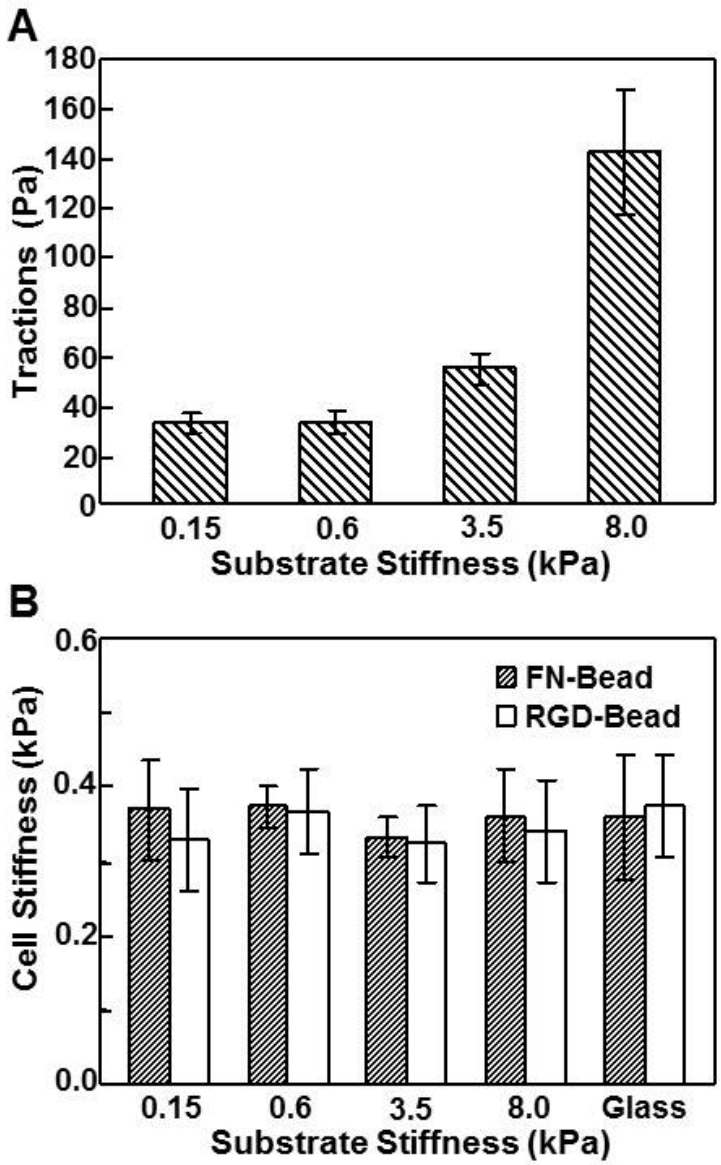

Figure 4.2: Traction and stiffness of mouse ESCs decouple on different substrate stiffness. (A) Cell root-mean-square (RMS) traction at the basal surface increases with the increase of substrate stiffness. There is no significant difference in ESC tractions between substrate stiffness of 0.15 and 0.6 kPa ($p > 0.91$), but significant differences are observed when plated on higher substrate stiffnesses: 0.6 and 3.5 kPa ($p < 0.02$) and 3.5 and 8.0 kPa ($p < 0.006$) (n = 11, 23, 13, or 13 cells on 0.15, 0.6, 3.5, or 8.0 kPa). (B) Stiffness of ESCs remained relatively constant regardless of changes in substrate stiffness (no statistical differences between different substrates). On substrate of 0.15, 0.6, 3.5, and 8.0 kPa or glass, n = 10, 10, 16, 14, or 12 cells for fibronectin-coated beads (FN-Bead); n = 15, 47, 28, 13, or 13 cells for RGD-coated beads (RGD-Bead). Mean +/- s.e.

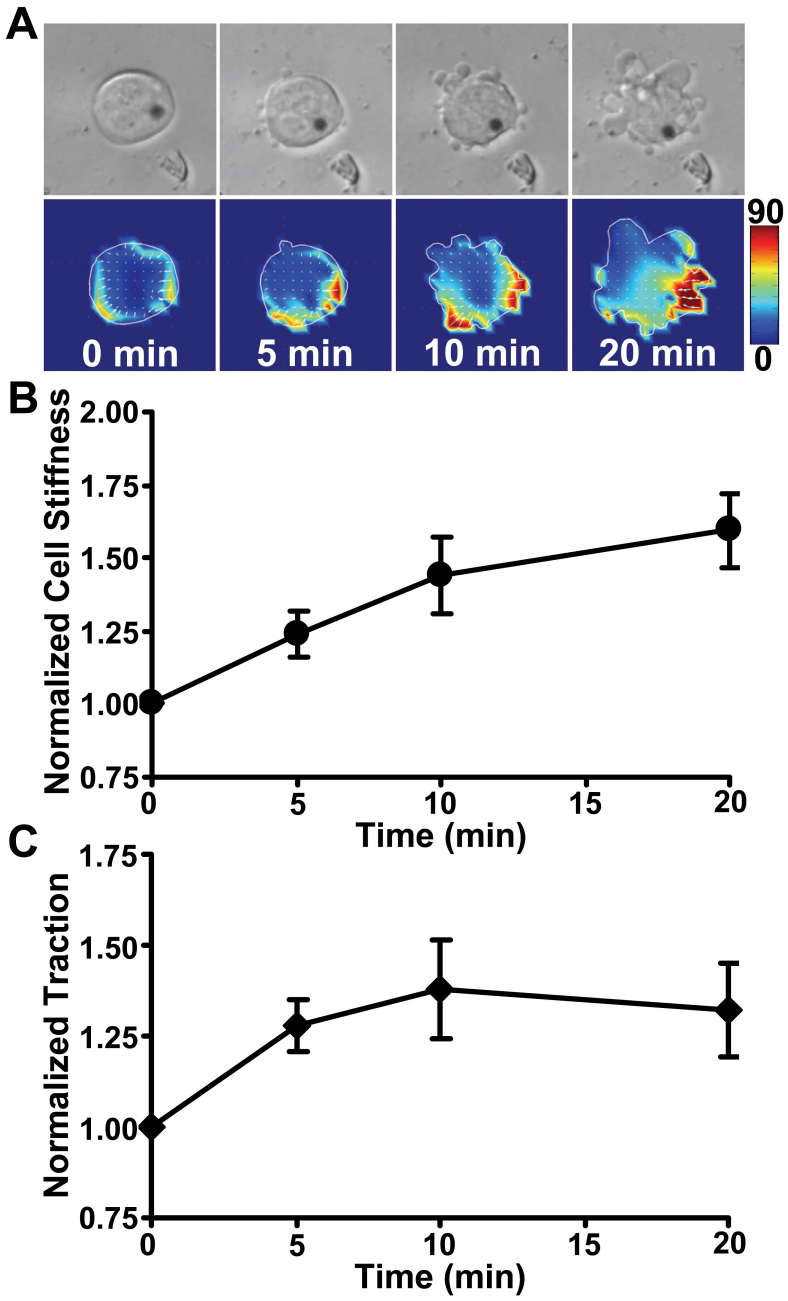

Figure 4.3: Apical cell stiffening and basal traction elevation in response to mechanical stress in ESCs. (A) Time-lapse images of a representative cell on a 0.6-kPa substrate show an increase in basal traction after onset of mechanical stress. (B) Normalized cell stiffness as a function of stress application duration shows apical cell stiffening in response to mechanical stimulation ($p < 0.03$, 0.02, and 0.006 comparing 5, 10, and 20 min with time 0; $n = 6$ cells; mean SE). (C) Normalized RMS traction in the same ESCs as in panel B in response to mechanical stress shows an elevation in basal traction. ($p < 0.007$, 0.001, and 0.024 comparing 5, 10, and 20 min with time 0; $n = 6$ cells; Mean +/- s.e.).

differentiated counterpart cells [73]. It has been established that in terminally differentiated cells, these tensed actin bundles are essential for propagating a locally applied stress through the cytoskeleton at a distance for an integrated, concerted mechanical response [11]. It is possible that the few actin bundles under the apical surface of the ESCs [107] are not sufficiently tensed so as to enable the observed elevations in tractions (i.e., myosin-II dependent tension) at the basal surface (in response to substrate rigidity) to be propagated to the apical surface.

Unlike terminally differentiated cells whose nucleus is $\sim$5 to 10 times stiffer than its cytoplasm [37, 41], the huge nucleus of the ESC [73] is as soft as its cytoplasm and does not express nuclear intermediate filaments Lamin A/C [41], a stiff nuclear matrix inside the nuclear envelope. Lack of Lamin A/C in living cells contributes to a softer cytoplasm [108], possibly by softening the anchoring sites of the LINC (linker of nuclear-cytoskeleton) [40]. As a result, the apical actin bundles might not be prestressed/tensed and/or mechanically integrated with the basal actin-myosin bundles. All these might have contributed to the lack of stiffening of the apical cytoskeleton in response to the traction elevation at the basal surface as substrate rigidity increases. Interestingly, it is reported that cell spreading and stiffening can be independently controlled when filamin-deficient, terminally differentiated cells are plated on collagen-I or fibronectin [109].

In contrast, we show here that cell basal tractions and apical stiffness are independently controlled on different rigidities of substrates, although coated with the same collagen-I concentration. Importantly, this decoupling between apical stiffness and basal tractions (and thus myosin-II dependent basal prestress) in ESCs can be abolished by applying a small oscillatory loading at the apical surface via integrins. The external stress-induced simultaneous responses in both stiffening and traction elevation shown in this report are preceded by increases in cell spreading and followed by stress-induced ESC differentiation, as evident by the observation that the pluripotent market Oct3/4 was downregulated [73].

Future studies are needed to elucidate the mechanisms of the cytoskeletal structural changes that are necessary for the observed external stress-induced coupling between stiffness and traction in ESCs.

4.4 Materials and Methods

Undifferentiated mouse embryonic stem cells (W4, 129/SvEv) were cultured and maintained in standard feeder free conditions on collagen-I coated dishes, as described previously [73]. Stiffness and traction measurements were performed on single individual cells ∼8 h after the ESCs were plated. Stiffness at the apical surface of an individual single cell was measured using either an RGD- or a FN-coated magnetic bead at 17.5 Pa and 0.3 Hz [73]. RGD or FN was coated at 50 or 25 μg/mg bead, respectively.

Because it is known that fibronectin and collagen-I bind to different integrin subsets, we point out that using the RGD-bead or the FN-bead may not engage the same set of cytoskeletal proteins as the collagen-I coated substrate at the basal surface and thus may not be so simple to relate to basal tractions. These single ESCs appear viable and healthy because they exhibit normal ES cell shape, proliferate and form ES colonies, and have normal ES cell-doubling time (∼10.5 h).

Cell root-mean-square (RMS) tractions at the basal surface were quantified by measuring embedded fluorescent submicrometer particle displacement fields in the gel following published methods [73]. The substrate stiffness of the gel was varied by altering bis-acrylamide crosslinker concentrations (0.04, 0.06, 0.1, and 0.3%) and polyacrylamide concentration (3%, 3%, 5%, and 5%) and the corresponding stiffnesses were 0.15, 0.6, 3.5, and 8.0 kPa using published protocols [101, 103].

CHAPTER 5

SOFT FIBRIN GEL PROMOTES GERM LAYER ORGANIZATION

5.1 Introduction

Understanding the mechanism of gastrulation – the early phase in embryonic development where the blastula first loses its symmetry and forms organized germ layers (i.e. endoderm, mesoderm, and ectoderm) – has long been a major challenge to the field of embryonic stem cell (ESC) research and developmental biology. A long standing objective in developmental biology is not only to direct the differentiation of ESCs into specific developmental lineages, but also to organize these differentiated lineages into spatially distinct arrangements resembling the physiological gastrulation. This study demonstrates the first successful reproduction of such germ layer organization (outside ectoderm, middle mesoderm, and innermost endoderm), and provides further insights on the mechanism of germ layer spatial positioning starting from a single pluripotent ESC.

Much research has been focused on ESC differentiation due to their pluripotency and potential therapeutic applications [110–112]. One of the methods to provide the appropriate environment for lineage commitment to ectodermal, mesodermal and endodermal fate is through embryoid bodies (EB), where an aggregate of random hotch-patched and chaotic differentiated germ cells is generated from pluripotent stem cells cultured in hung suspension [113, 114]. The ability of ESCs to form EBs is also a hallmark of the cells quality and pluripotency. However, positional signals are as important as instructive signals for a fuller understanding of the process of embryogenesis. The differential adhesion strength [115, 116] and surface contraction [117] between germ cells have been implicated in spatial positioning of germ layers. The hierarchy of these non-mutually-exclusive positional signals has provided great insights on the self-organization of germ cells [118]. Nevertheless, these models fail to

consider the mechanical properties of the extracellular microenvironment, which may in turn influence intercellular forces. Experiments of self-sorting thus far do not begin from a single cell [118], but instead utilizes pairwise sorting assays where two types of differentiated germ cells are homogeneously mixed and cultured using the hangdrop method of EBs [119]. Furthermore, the in vivo germ layer organization, where endoderm is in the innermost core, followed by mesoderm in the middle, and ectoderm at the outer periphery has never been shown.

In this study, we demonstrate that a single pluripotent mouse ESC (mESC) cultured in soft 3D fibrin scaffold in the absence of LIF (Leukemia Inhibitory Factor) – a cytokine necessary for the maintenance of mESC pluripotency and self-renewal [120, 121] – forms a rough-surface spherical colony with systematically organized germ layers. Mesoderm localizes at the outmost periphery, ectoderm in the middle, and endoderm at the center core of the colony. As mechanical properties of the extracellular microenvironment are known to influence a variety of aspects of embryogenesis [8, 79, 81, 122], we found this observation unique to 3D fibrin gels of low elasticity. The systematic organization of germ layers is regulated by the colony-matrix generated cortical tension. Changing the cortical tension by inhibiting fibrin anchoring integrins displaced the endodermal layer, and transferring the colony from 3D matrix to 2D culture gives rise to a germ layer organization similar to those in vivo. To our knowledge, the results presented in this study provide the first experimental evidence that colony tension facilitated by cell-matrix interaction dictates spatial positioning of germ cells. In addition, our results demonstrate the successful development of an accurately organized germ layer colony from a single pluripotent mESC. This study uncovers a novel method for investigating tissue morphogenesis during vertebrate gastrulation.

5.2 Results

5.2.1 Culture of mESCs in soft 3D fibrin gels promotes spatially organized formation of germ layers

Due to their nontoxicity and low immunogenicity, salmon fibrin gel that is purified from fibrinogen and activated by thrombin has been widely used as scaffolds for transplanting cells in different animal species [123, 124]. We recently showed that cancer cells cultured in 3D soft fibrin gels are able to form round tumorigenic spherical colonies that possess some key phenotypic and biophysical features of mESCs, with upregulated self-renewing *Sox2* gene expression [125]. It has also been reported that mESCs cultured for 5 days on soft 2D substrates without exogenous LIF generated homogeneous undifferentiated colonies with high levels of *Oct 3/4*, *Nanog* and Alkaline Phosphotase (AP) activities [81]. This led us to hypothesize that 3D soft fibrin gels will similarly maintain ESC self-renewal and pluripotency in the absence of LIF (–LIF). Surprisingly, a single ESC cultured in –LIF 3D soft fibrin gels for 5 days led to a significantly smaller colony with cell surface protrusions as compared to its +LIF counterpart where ESCs form smooth spheroidal colonies (Fig 5.1 a-c). Reverse transcription polymerase chain reaction (RT-PCR) results of pluripotency markers (*Nanog, Oct 3/4, Sox2*), ectoderm markers (*Fgf5, Otx2, Sox1*), mesoderm markers (*Hand1, Brachyury, Twist2*), and endoderm markers (*Gata4, Gata6, Sox17*) showed a clear indication of ESC differentiation with upregulated germ cell genes (Fig 5.1 d-e). It was further determined that soft fibrin gels of 90 Pa (1 mg ml^{-1}) were optimal for ESC proliferation and spheroid formation. Single mESCs cultured in fibrin gels of 420 and 1050 Pa (corresponding to 4, and 8 mg ml^{-1} [126]) in the presence or absence of LIF led to the formation of spherical colonies that were significantly smaller after 5 days of culture (Fig 5.1 a, 5.2 a-c, 5.2 f). Cells at the bottom of the gel near the rigid dish exhibited spread morphology (Fig 5.3 a-b). These suggest that low matrix elasticity of soft gels promotes the growth of larger spherical colonies that are primarily a result of more proliferating cells per colony.

Due to the high expression of mesodermal markers (Fig 5.1 d-e) in germ cells generated from the –LIF 3D soft fibrin gel culture, we developed a new mES cell line OGTR1, that

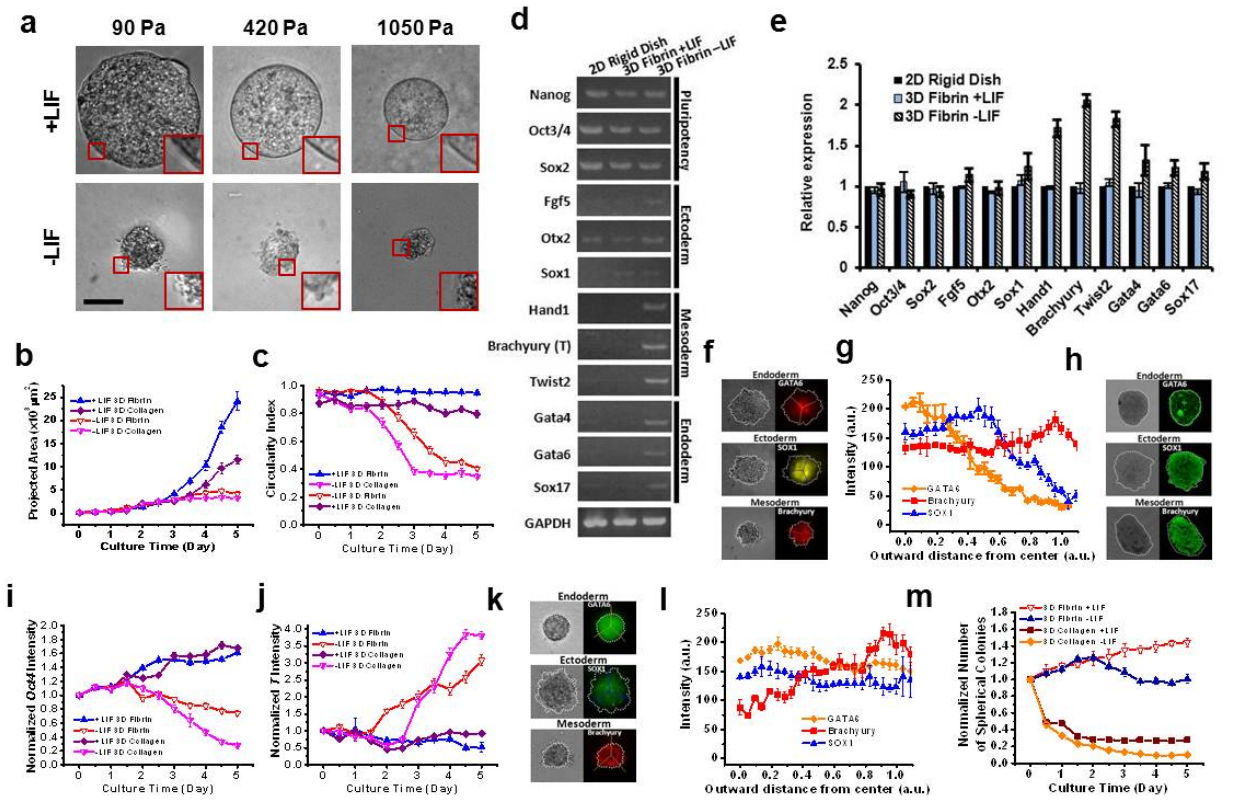

Figure 5.1: Soft fibrin gels promote organization of germ layers. (a) Brightfield images of mESC colony after 5 days of culture in 3D fibrin gels of different stiffness (90 Pa, 420 Pa, and 1050 Pa gels). Soft 90 Pa gels form larger spherical colonies with more proliferating cells per colony. Scale bar = 50μm. (b) Colony size of mESC cultured with and without LIF in soft 3D fibrin or collagen-I gels as a function of time. Fibrin matrix gives rise to larger colonies than collagen matrix. (c) The circularity of colonies was calculated using the formula of 4π[area]/[perimeter]^2. A perfect circle has a value of 1. The circularity of colonies begin to decrease at 48 hours, just as *Brachyury* expression is observed. (d) Germ cell markers are expressed in mESC spheroids in the absence of LIF. Total mRNA of mESC colonies at day 5 was extracted and used for the detection of different germ cell expression by RT-PCR. Cells cultured on regular gelatin coated 2D rigid dishes in the presence of LIF were used as a control. Three independent experiments showed similar results. (e) Semi-quantitative RT-PCR grey intensities. Grey intensities show that mesoderm cell markers are highly expressed in soft fibrin gel culture. (f) Representative immunofluorescent staining images with organized germ layers in soft fibrin gel culture. (g) Quantification of germ cell organization with 0 at the center core and 1 at the colony boundary. Endoderm is at the innermost, ectoderm in the middle, and mesoderm is at the outer periphery. (h) Embryoid bodies do not have any organized germ layers. (i) Normalized *Oct 3/4* intensity of ESCs cultured in 3D fibrin or collagen gels. Cells in collagen matrix are less pluripotent after 5 days of culture. (j) Normalized *Brachyury* (T) expression of OGTR1 mES cells show higher mesoderm cell expression in collagen gels. (k) ESCs cultured on 2D soft fibrin gels without

LIF do not form structured organization of all three germ layers. (l) Quantification of germ layers for colonies formed on 2D soft fibrin gels show mesoderm at the outermost periphery but no order for endoderm and ectoderm layers. (m) Normalized number of multicellular spheroid (round colony) as a function of culture time in soft fibrin and collagen gel. Fibrin is optimal in maintaining spherical colonies. Mean+/-s.e.

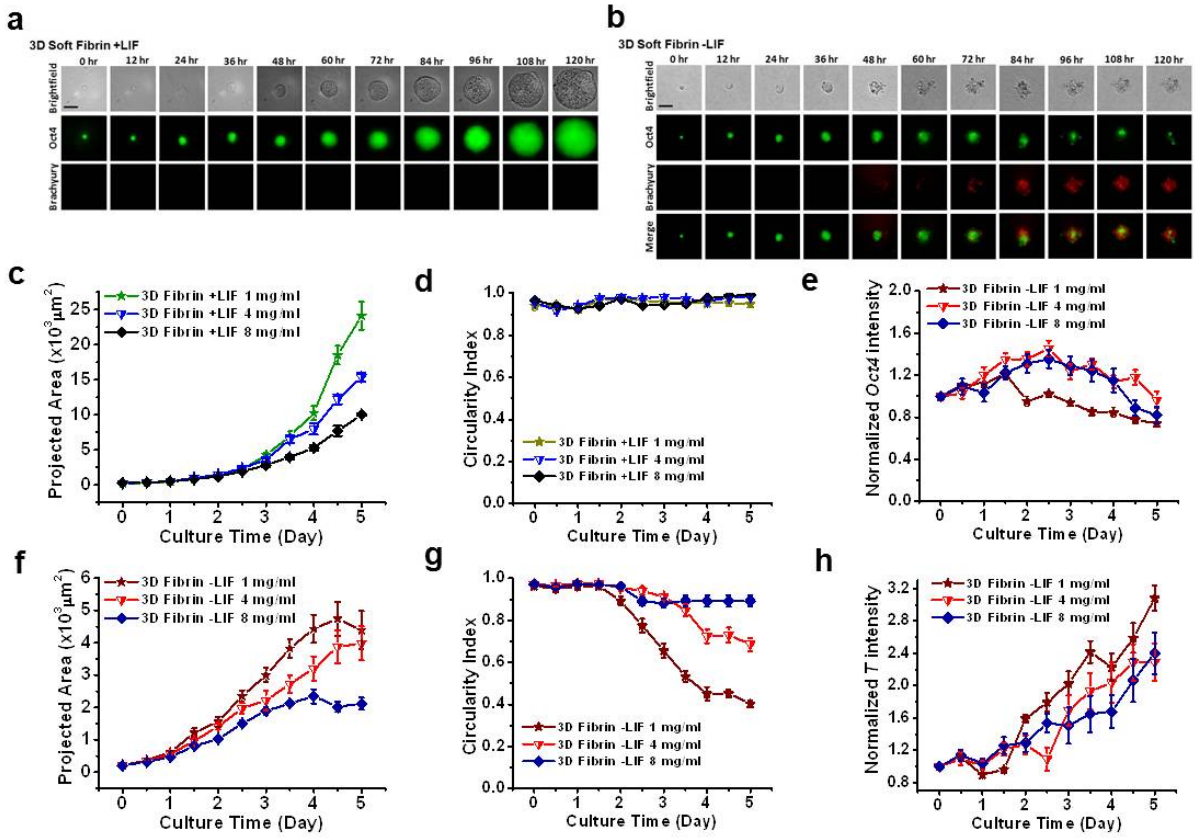

Figure 5.2: Fibrin matrix stiffness dictates ESC growth and differentiation. Representative images of single ESCs cultured in soft 90Pa 3D fibrin gels for 5 days in the presence (a) and absence (b) of exogenous LIF. Scale bar = 50μm. GFP expression is an indication of pluripotency and DsRed expression indicates differentiation towards mesodermal lineage. Summarized results of colony size show that cells cultured in LIF (c) were larger than those cultured without LIF (f). In both cases, cells colony is larger in softer gels. Circularity index for +LIF culture were close to 1 for all +LIF condition regardless of rigidity (d). Whereas under –LIF condition, circularity index decreases with the increase in fibrin gel stiffness (g). Normalized *Oct 3/4* (e) and *Brachyury* (h) fluorescence intensity of ESCs cultured in –LIF condition shows that softer fibrin gels promote differentiation. Mean+/-s.e.

stably expresses green fluorescent protein (GFP) driven by the *Oct 3/4* promoter and red fluorescent protein (DsRed) driven by *Brachyury* (T) gene, to monitor the spatial and temporal activity of both pluripotent and mesodermal cells. Interestingly, cells cultured in 3D

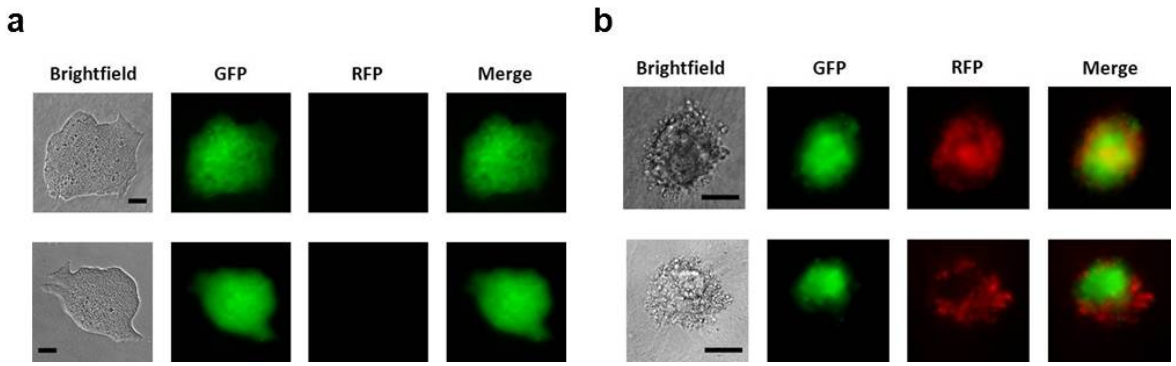

Figure 5.3: Matrix rigidity dictates spherical colony formation. Representative images of ESC colonies in both +LIF (a) and –LIF (b) culture conditions found near the bottom of the dish with spread morphology. Cells at the bottom of the gel near the rigid dish sense a stiffer environment and do not form round spherical colonies. Suggesting that matrix elasticity is more dominant than porosity in dictation spherical colony formation and germ layer organization. Scale bar = 50μm.

soft fibrin gels without LIF generated an organized mesodermal layer at the outer annulus of the colony with high DsRed::*Brachyury* expression (Fig 5.4 a, 5.2 b). Compared to gels of higher elastic modulus, soft fibrin gels gave rise to higher *Brachyury* but lower *Oct 3/4* expression. The circularity index — an indication of ESC differentiation [73, 81], was significantly lower in softer gels (Fig 5.2 d-e, 5.2 g-h). This further enforces the notion that soft fibrin gels are optimal not only for proliferation, but also differentiation and germ cell organization. By using immunofluorescence staining of endoderm (*Gata6*) and ectoderm (*Sox1*) cells, we were able to further discern the localization of all three germ layers. To our amusement, a specific and spatially organized gastrula-like colony was observed (Fig 5.1 f). Quantification of the each germ layers spatial organization showed that mesoderm forms the outermost layer, followed by ectoderm, and endoderm in the innermost (Fig 5.1 g). In contrast, conventional EBs differentiate into a random and spatially disorganized manner, forming hotch-potched clusters of germ cells within the EB (Fig 5.1 h). Monitoring the time course change of *Oct 3/4*::GFP and *Brachyury*::DsRed expression of single mESCs cultured within 3D soft fibrin gels in the absence of LIF showed that the ESCs maintained high *Oct 3/4* expression up to day 2, after which *Brachyury* expression was observed (Fig 5.1 i-j, 5.2 b, 5.2 g-h), suggesting that the gastrulation process and the formation of the primitive streak began after day 2. This is consistent with previous reports showing that EBs develop

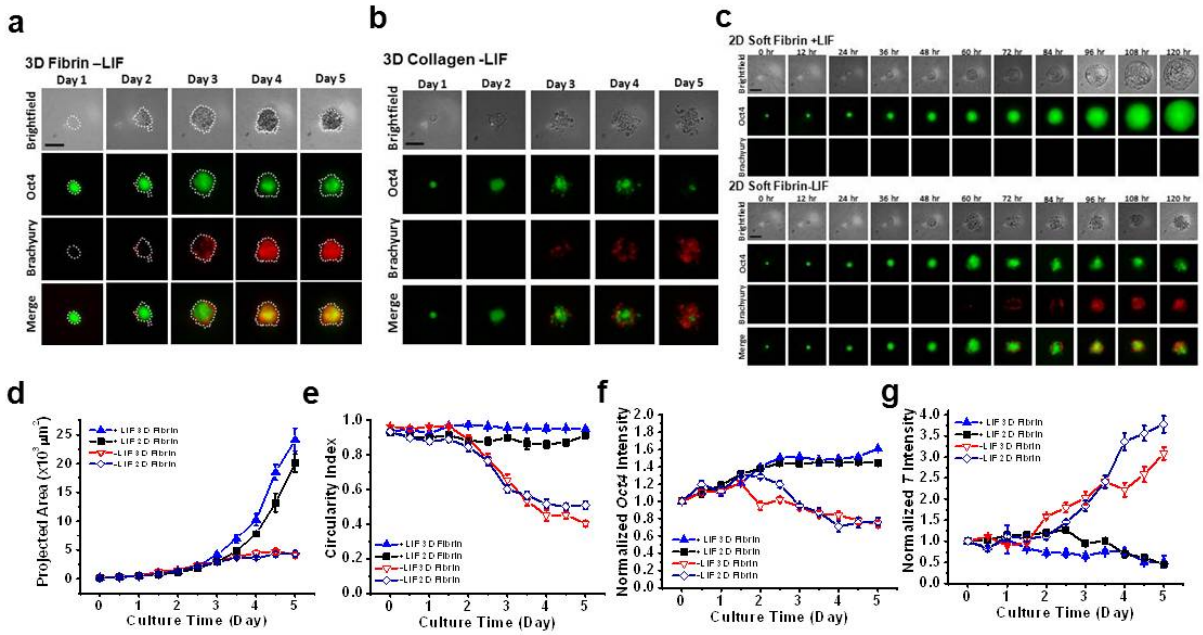

Figure 5.4: Similarity of 2D and 3D fibrin culture. (a) ESCs cultured in –LIF soft 3D fibrin generated colonies with highly expressing *Brachyury* annulus at the boundary. (b) Cells cultured in –LIF soft 3D collagen gels did not generate a structured mesodermal layer. (c) Representative images of ESCs cultured on 2D soft fibrin surface with and without exogenous LIF. A clear *Brachyury*::DsRed fluorescent ring is observed at the colony periphery of day 5 –LIF cultured cells. The colony size (d), circularity index (e), normalized *Oct 3/4* intensity (f), and normalized *Brachyury* intensity (g) are similar in both 2D and 3D fibrin culture. Scale bar = 50μm. Mean+/-s.e.

an asymmetrical shape at day 3 [127].

To examine if the observed germ layer organization is unique to 3D culture, we cultured OGTR1 cells on top of 2D soft fibrin gels and found that spherical colony size, circularity index, *Oct 3/4* expression and *Brachyury* expression were similar to those in 3D culture (Fig 5.4 c-g). Despite a clear mesodermal layer at the outermost periphery of the 2D culture colony, there was surprisingly no organization of endoderm and ectoderm cells (Fig 5.1 k-l). However, ESCs cultured on stiffer 2D fibrin substrates in the absence of LIF gave rise to spread flat colonies and lower *Brachyury* expression (Fig 5.5 a-e), suggesting that the dimensionality of cell-matrix interaction plays a crucial role in germ layer organization [128, 129]. Contrary to the hangdrop generated spherical EBs, these results show that the 3D soft fibrin scaffold is able to facilitate the generation of a spatially organized gastrula-like germ-layer colony from a single mammalian ESC. The soft fibrin matrix promotes the proliferation,

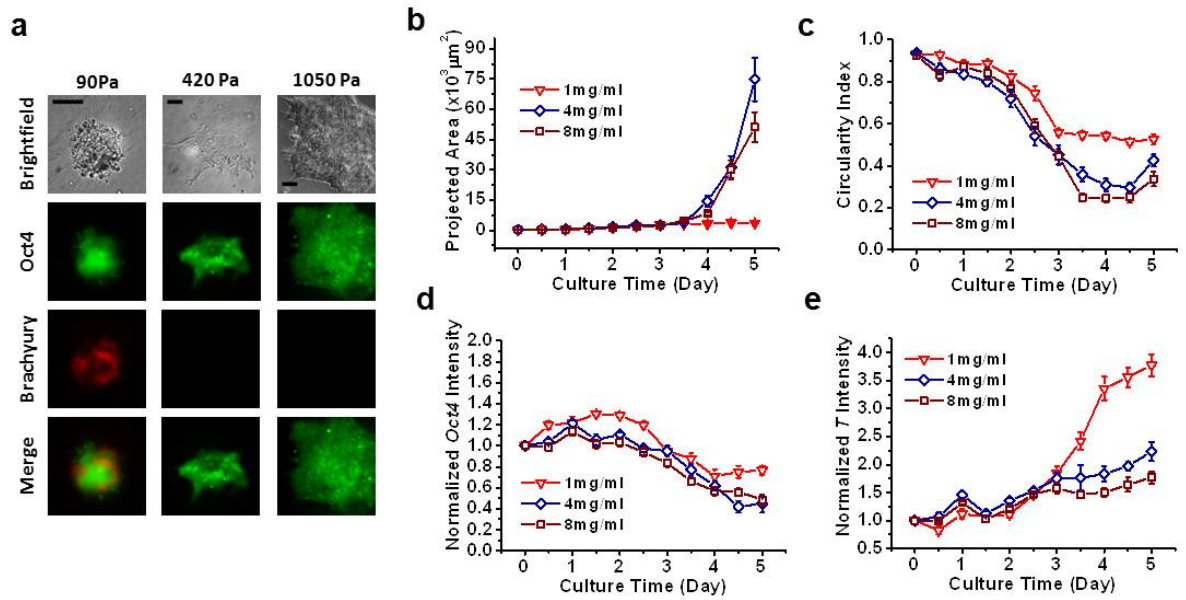

Figure 5.5: ESCs spread and form monolayers on stiff 2D substrates. (a) Representative images of ESCs after 5 days of culture on 2D fibrin of different stiffness. Only 90Pa gels generated spherical colonies with high *Brachyury* expression, while stiffer 420Pa and 1050Pa gels spread out and form monolayers. Scale bar = 50μm (b) Cells have a more spread morphology on stiffer substrates and therefore larger colony projected area. (c) Colonies on soft fibrin substrates are spherical with higher circularity index as compared to those on stiffer substrates. (d) Normalized *Oct 3/4* intensity showed little difference between cells on different substrate rigidity. (e) ESCs cultured on soft substrates differentiated in to mesoderm cells with high *Brachyury* expression. Mean+/-s.e.

differentiation, and organization of germ cells in an anchorage dependent manner. This observation was also found to be unique to fibrin gels as spherical colonies that formed within 3D collagen-I gels of similar stiffness (94 Pa) were considerably smaller in size, more differentiated, did not have structured germ layer organization, and had dramatically less number of spherical colonies (Fig 5.1 b-c, 5.1 i-j, 5.1 m, Fig 5.4 b, 5.6).

5.2.2 Control of germ layer organization through colony-matrix tension

The importance of cell biophysical properties and cell-matrix interactions in stem cell differentiation and self-renewal is becoming increasingly evident [8, 73, 130]. To determine the biophysical mechanisms of ESC colony possessing gastrula-like organized germ layers when cultured in soft 3D fibrin gels, we dissolved the fibrin matrix after 5 days of culture without

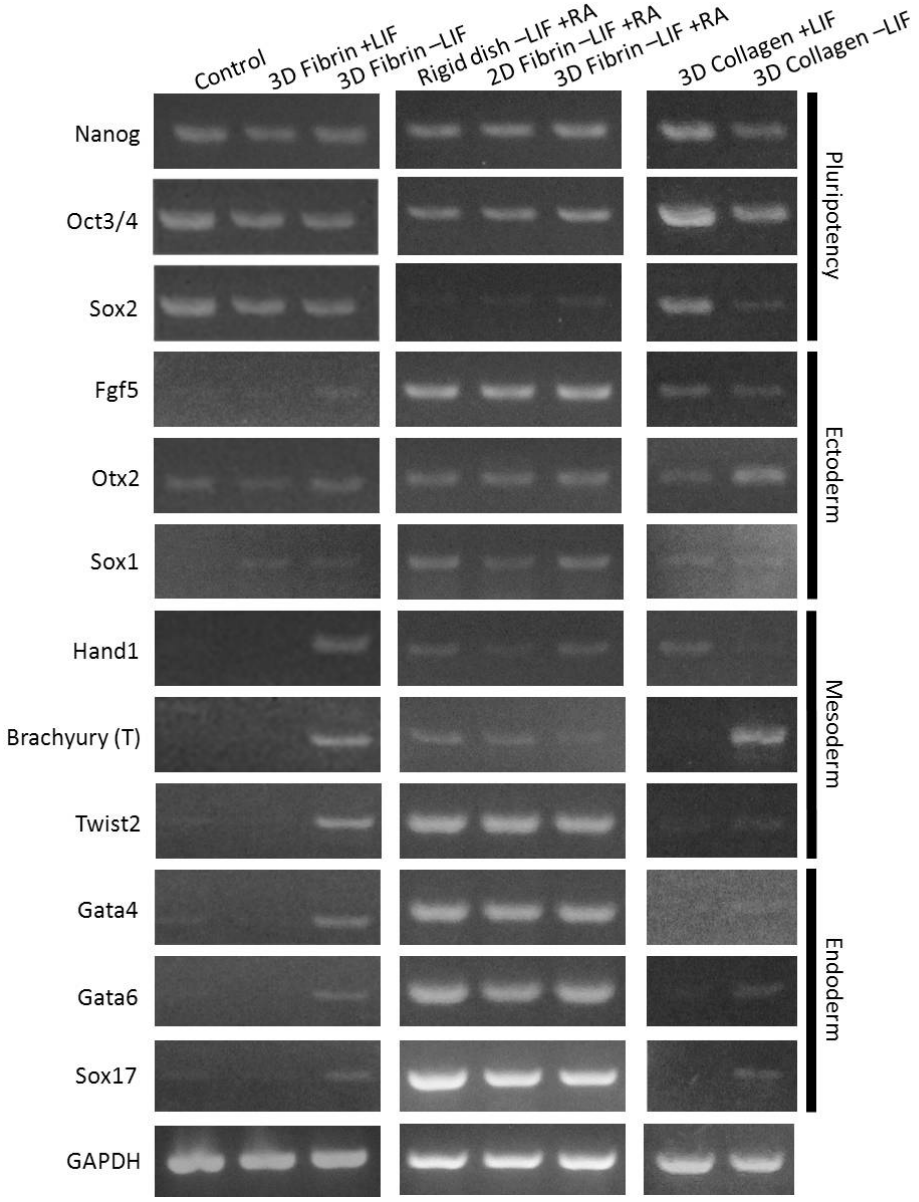

Figure 5.6: RT-PCR results of different culture conditions.

disrupting the colony integrity, re-plated the colonies on 2D substrates, and quantified the colony stiffness. Interestingly, the +LIF pluripotent colony stiffness (∼0.65 kPa) was significantly larger than the –LIF differentiated gastrula-like colony stiffness (∼0.4 kPa) (Fig 5.7 a). This is contrary to what has been previously established where differentiated cells have more actin filament fibers and are therefore stiffer than pluripotent stem cells [73]. However, cell stiffness measurements in previous reports were done on individual cells and not

colonies. We therefore disrupted the spherical colonies (after 5 day culture in 3D fibrin gel) and measured the individual cell stiffness in a similar manner. The individual cell stiffness was found to be consistent with the literature where differentiated cells were more spread and significantly stiffer (∼2.0 kPa) than their high *Oct 3/4* expressing round pluripotent counterparts (∼0.5 kPa) (Fig 5.7 b-c). As experimental evidence show that F-actin is the chief determinant in cell stiffness [1], we stained the spherical colonies for actin and observed a notable ring surrounding the round +LIF colonies (Fig 5.7 d). The absence of actin ring surrounding the rough-surfaced –LIF differentiated gastrula-like colony not only explains the lower colony stiffness, but also enforces the notion of boundary polarization inducing cortical tension in sorting and compartmentalization of different cell types [118]. Reports have shown that many different cell types in different environments have the machinery to sense and respond mechanically to "being at the boundary" [131–133]. Our results support the same notion of boundary sensing where ESC colonies maintain their pluripotency with elevated boundary cortical tension and stiffness. The lack colony boundary actin structure, loss in cortical stiffness, and decrease in circularity index leads to differentiation of ESCs. The cortical tension and circularity of colonies in stiffer scaffolds may have been extrinsically supported, thereby hampering ESC differentiation (Fig 5.2 d-e, 5.2 g-h).

Since $\alpha_v\beta_3$ integrins facilitate the cell binding to fibrin matrix [129], we wondered whether the binding of integrins to fibrin matrix plays a role in structural organization of germ layers in soft fibrin gel culture. We blocked the integrins by treating the cells with $\alpha_v\beta_3$ antagonist and found that cells continued to form spherical colonies with mesodermal cells at the colony periphery (Fig 5.8 a-e), suggesting that without anchorage of extra cellular matrix, cells may synthesize and secrete other proteins during the five day culture period for survival and growth. However, staining of other germ layers showed that the said spherical colonies had the endoderm layer at the outermost annulus, similar to that of the mesoderm layer (Fig 5.7 e-f). Interestingly, by decreasing the dosage of $\alpha_v\beta_3$ antagonist the endoderm layer moved inward, back to the –LIF gastrula-like colony with endoderm at the innermost core, ectoderm in the middle, and mesoderm at the outside (Fig 5.7 g-h). Displacement of the endodermal layer by blocking $\alpha_v\beta_3$ integrins suggest that spatial positioning of endodermal layer is colony-matrix tension dependent and not non-specific compression. Treatment of cells over

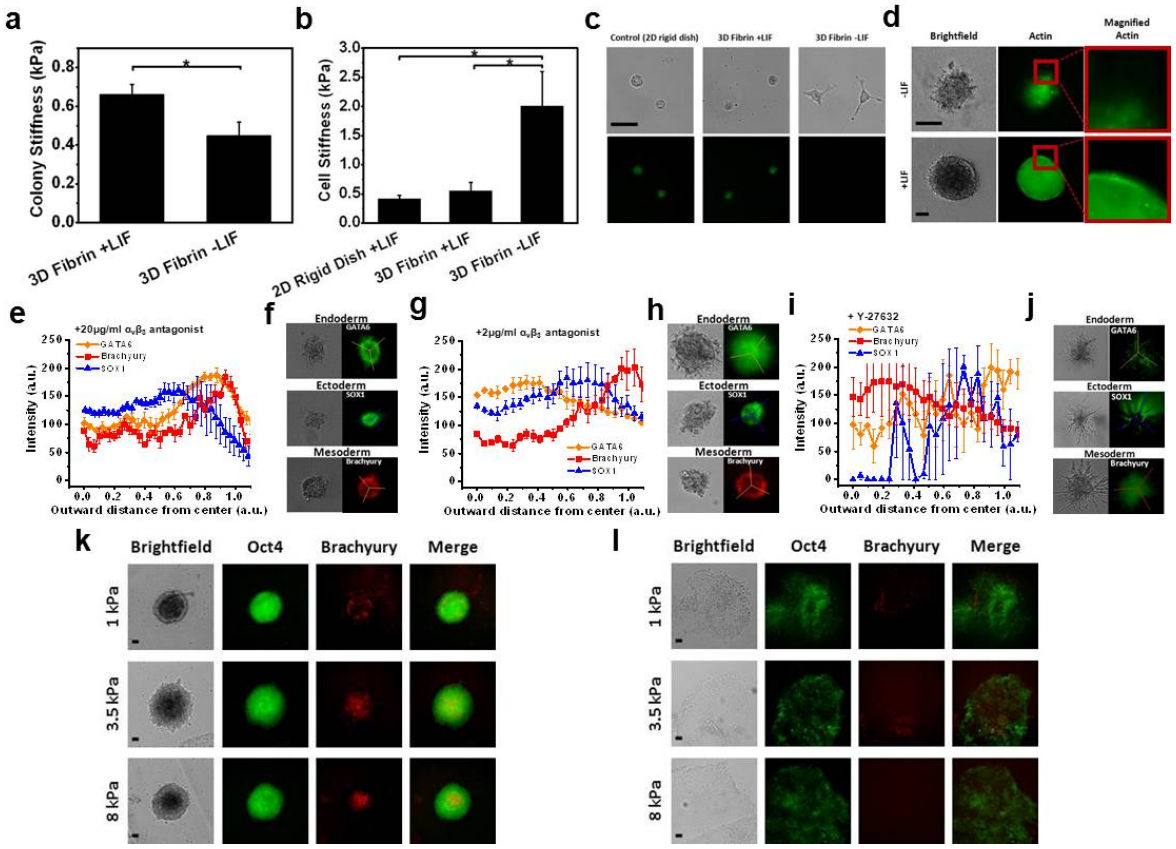

Figure 5.7: Matrix-induced cortical tension of colony influences germ layer organization. (a) Pluripotent colonies cultured in +LIF 3D fibrin was significantly stiffer than the differentiated colonies cultured in –LIF 3D fibrin. Stiffness measurements were done after 5 days of culture. (b) Individual cell stiffness showed that those cultured in –LIF 3D firin was significantly larger than those cultured with LIF. The 3D fibrin matrix was dissolved before disrupting the colonies in to individual cells. Individual cells were re-plated on 2D rigid substrate for 6 hours before stiffness measurement was obtained. (c) Representative figures of colonies re-plated as individual cells on 2D substrates. Differentiated cells from –LIF 3D fibrin exhibit a spread morphology with extended filopodia when plated as individual cells. (d) Immunofluorescent staining of actin showed distinct actin fibers surrounding the round pluripotent colony, whereas differentiated colonies cultured in –LIF 3D fibrin did not. (e) Cells treated with high dose of $\alpha_v\beta_3$ antagonist (20μg/ml) displaced the endoderm layer to the outer periphery of the colony. (f) Representative images of different germ layers after 5 days of $\alpha_v\beta_3$ antagonist treatment. (g) Decreasing the $\alpha_v\beta_3$ antagonist concentration (2μg/ml) moved the endoderm layer back to the center. Ecdoderm and mesoderm layer remained at the middle layer and outer most boundary respectively. (h) Representative images of colonies stained for different germ layers after treatment of 2μg/ml $\alpha_v\beta_3$ antagonist. (i) Inhibiting Rho-associated kinase (ROCK) with Y27632 (25μM) completely abolished all germ layer organization. (j) Representative figure showing that cellular contraction is necessary for germ layer organization. Inhibiting ROCK induced colonies with dendritic morphology.

(k) Proper mesodermal position in the middle was achieved when ESCs were first cultured in +LIF 3D Fibrin for 3 days before re-plating to 1kPa collagen-I coated polyacrylamide gels. Colonies re-plated on stiffer 2D substrates did not yield middle mesodermal layer. (l) Colonies cultured in –LIF 3D Fibrin for 3 days before re-plating on 2D substrates spread and did not maintain their spherical integrity. Data are pooled from >3 independent experiments for each sub-figure. Scale bar = 50μm. (*, p<0.05) Mean+/-s.e.

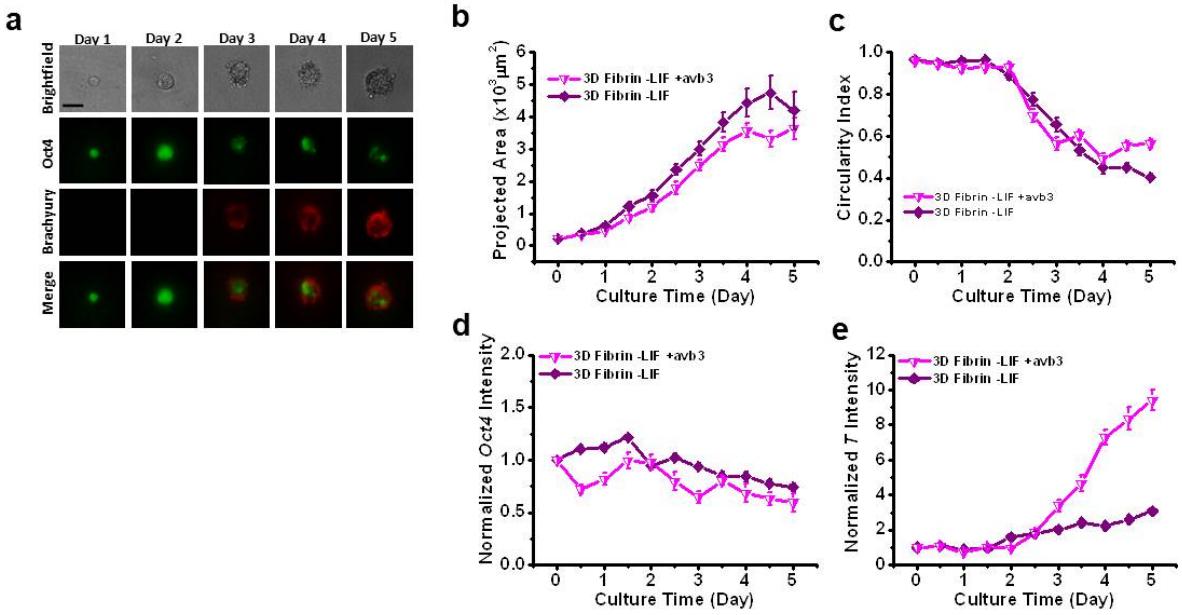

Figure 5.8: Blocking of $\alpha_v\beta_3$ integrins differentiates ESCs into mesodermal cells. (a) Representative cell treated with $\alpha_v\beta_3$ integrin antagonist did not disrupt mesoderm organization. There was no significant difference in colony projected area (b), circularity index (c), and normalized *Oct 3/4* fluorescent intensity (d). However, blocking of $\alpha_v\beta_3$ integrins induced high *Brachyury* expression (e). Scale bar = 50μm. Mean+/-s.e.

the 5 day culture period with myosin-II ATPase inhibitor blebbistatin (50μM) and Rho-associated kinase (ROCK) inhibitor Y27632 (25μM) completely disrupted the organization of germ layers (Fig 5.7 i-j, 5.9 a-f), indicating the crucial role of nonmuscle myosin-II contraction of cytoplasmic actin filaments in germ layer organization. Y27632 ROCK inhibitor treated cells took on a dendritic morphology (Fig 5.7 j, 5.9 b) that is consistent with other studies [134]. These results suggest that germ cell sorting involves active migration, in which changes in cell shape are important. It is no surprise, then, that integrins, adhesion molecules associated with migration, can be crucial for germ cell sorting.

As matrix induced colony tension controls the positioning of germ layers, we sought to reproduce the in vivo configuration where ectoderm is at the outermost periphery, followed

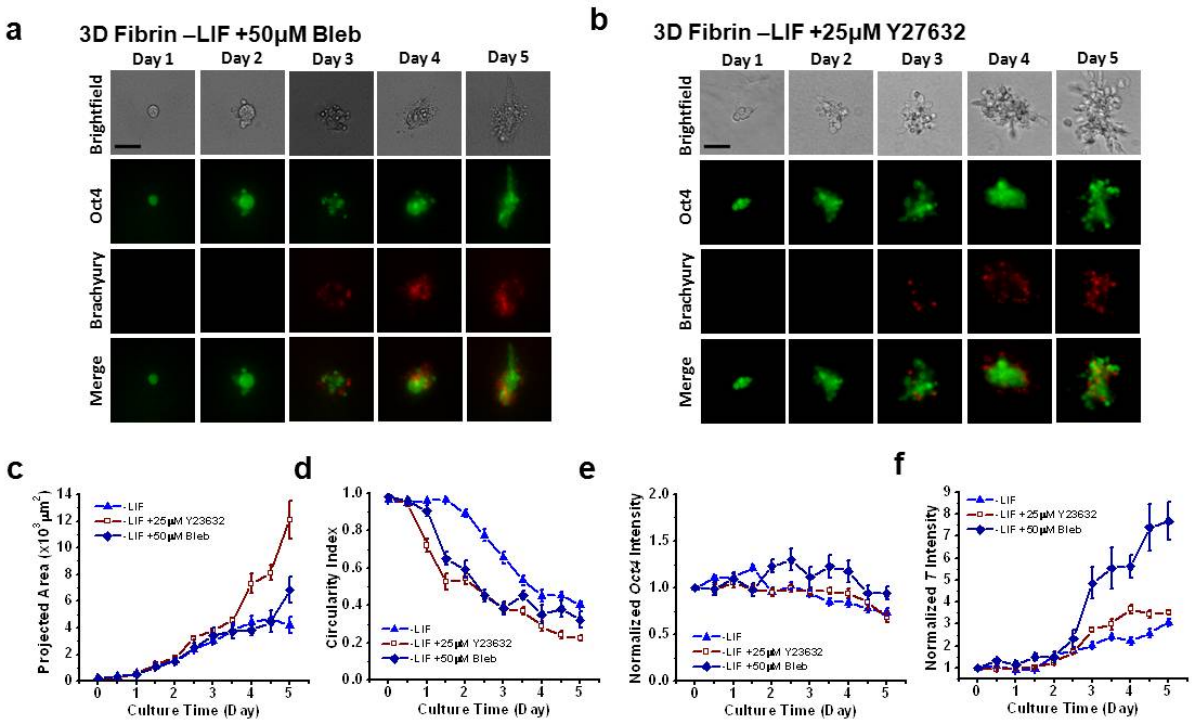

Figure 5.9: Nonmuscle myosin-II contraction of cells is necessary for germ layer organization. Representative figures of cells treated with 50μM Blebistatin (a) and 25μM of Rho-associated kinase (ROCK) inhibitor, Y27632 (b) took on a spread and dendritic morphology without organized mesoderm layer. Summarized 5 day results of colony projected area (c), circularity index (d), normalized *Oct 3/4* intensity (e), and normalized *Brachyury* intensity (f). Scale bar = 50μm. Mean+/-s.e.

by mesoderm in the middle, and endoderm at the innermost core of the colony. At the very early development stage of mice blastocyst, the ball-shaped embryo grows and develops in fluid suspension as it moves towards the uterus [135, 136]. The cells of the epiblast begin to differentiate around embryonic-day 6 after its implantation into the uterine wall [137]. We therefore postulate that cells cultured in soft 3D fibrin for the first 3 days before being "implanted" to a 2D substrate may provide the necessary cell-matrix tension to generate proper germ layer organization. However, ESCs cultured in –LIF soft 3D fibrin gels did not maintain their spherical shape when transferred to 2D substrates. Instead, the colony spreads out forming a monolayer of cells within a day (Fig 5.7 l). As differentiation of the blastocyst in physiological context begins after implantation, we tried instead to culture single mESCs in +LIF soft 3D fibrin gels. At day 3, fibrin gels were dissolved and colonies were

transferred to –LIF 1 kPa collagen coated polyacrylamide gels. Surprisingly, we observed *Brachyury*::DsRed mesodermal cells forming a middle ring 5 days after "implantation" on 2D –LIF environment (Fig 5.7 k). Colonies transferred to 2D substrates of higher stiffness (3.5 and 8 kPa) gave rise to mesodermal cells that were at the inner core (Fig 5.7 k). Endoderm and ectoderm immunostaining of colonies on 1 kPa gels showed a unique gastrula-like spherical morphology with germ layer organization accurately representing the order of each germ type (ectoderm on the outside and endoderm on the inside of the colony, with mesoderm in the middle) (Data not shown, in the process of gathering). Such germ layer organization therefore requires that ESCs form average sized pluripotent spherical colonies with high cortical tension and elevated colony stiffness, before withdrawing exogenous LIF and changing the dimensionality of colony-matrix generated tension. Our results provide clear evidence that the dimensionality of the colony-matrix mechanical tension is critical to the organization of germ layers.

5.2.3 Molecular mechanism of 3D fibrin gel mediated germ layer organization

Integrin-matrix interactions are known to regulate cadherin-dependent cell adhesion [138]. We therefore sought to elucidate the role of E-cadherin in the formation of structured germ layers in 3D fibrin gels. The –LIF gastrula-like colonies were labeled with E-cadherin at day 5 in situ using immunofluorescence. Surprisingly, E-cadherin was observed to be highly expressed at the outer periphery of the colony, co-localizing with the outer mesoderm layer (Fig 5.10 a), contrary to a recent report showing increased expression of E-cadherin at the primitive endodermal layer cells [127]. To further explore the molecular mechanisms of E-cadherin in structured germ layer colony formation, we treated the cells with 1mM EGTA over the entire 5 day culture period. EGTA removes Ca^{2+} from cadherin proteins, rendering the cell-cell mediating cadherin proteins inactive. Compact spherical colonies were still able to form with an elevated level of *Brachyury*::DsRed expressing mesodermal cell (Fig 5.11 a-e). However, organizations of all three germ layers were completely abrogated by the inhibition of cell-cell cadherin interaction (Fig 5.10 b-c). Earlier work has determined that cells undergo

cytoskeletal reorganization so that cortical tension and actin density surrounding the colony external interface is higher than those on the internal cell-cell adhesion interface [131]. Together with our results, these suggest that E-cadherin mediated signals are not only crucial in germ layer organization, but also facilitates the colony boundary polarization. Cadherins act as signaling molecules to regulate Rho family guanosine triphosphatases, providing the necessary local actomyosin contractility at cell-cell interface relative to the polarized edges at the colony boundary to facilitate the organization of germ layers [118, 139].

It is known that there are parallel circuits of LIF signaling pathways to maintain mESC pluripotency [121]. The Jak–Stat3 pathway that activates Klf4 and the PI(3)K–Akt pathway that stimulates the transcription of Tbx3, both of which leads to activation of self-renewal genes *Sox2, Nanog*, and *Oct 3/4*. However, ESCs in +LIF soft 3D fibrin culture treated with Jak inhibitor, CP690552 (2μM) [140] led to differentiation of ESC colonies and generated an outer mesoderm layer whereas PI(3)K inhibitor, LY294002 (15μM) [121] did not (Fig 5.12 a-l). This suggest that the PI(3)K–Akt pathway may not be as important in ESC differentiation and germ layer organization than the Jak–Stat3 pathway. As it was observed that ESCs in +LIF and –LIF soft 3D fibrin culture began to show a difference after 2 days (Fig 5.1 c, 5.1 i-j, 5.2 g-h), we switched the respective culture medium at day 2 to determine if cells committed to differentiation are reversible. Interestingly, cells in 3D soft fibrin culture that had medium changed from –LIF to +LIF at day 2 were reprogrammed back to its pluripotent state (Fig 5.10 d, 5.10 f-h). The *Brachyury*::DsRed expression rose for 3 days but returned to baseline after that. Circularity index decreased after day 2 but returned to a smooth spherical shape together with the decrease in *Brachyury* expression (Fig 5.10 d, 5.10 g, 5.10 i). In contrast, cells that had the medium changed from +LIF to –LIF did not show any difference compared to those in constant +LIF culture condition, except for the *Oct 3/4* intensity where constant +LIF culture condition was significantly higher (Fig 5.10 e-i).

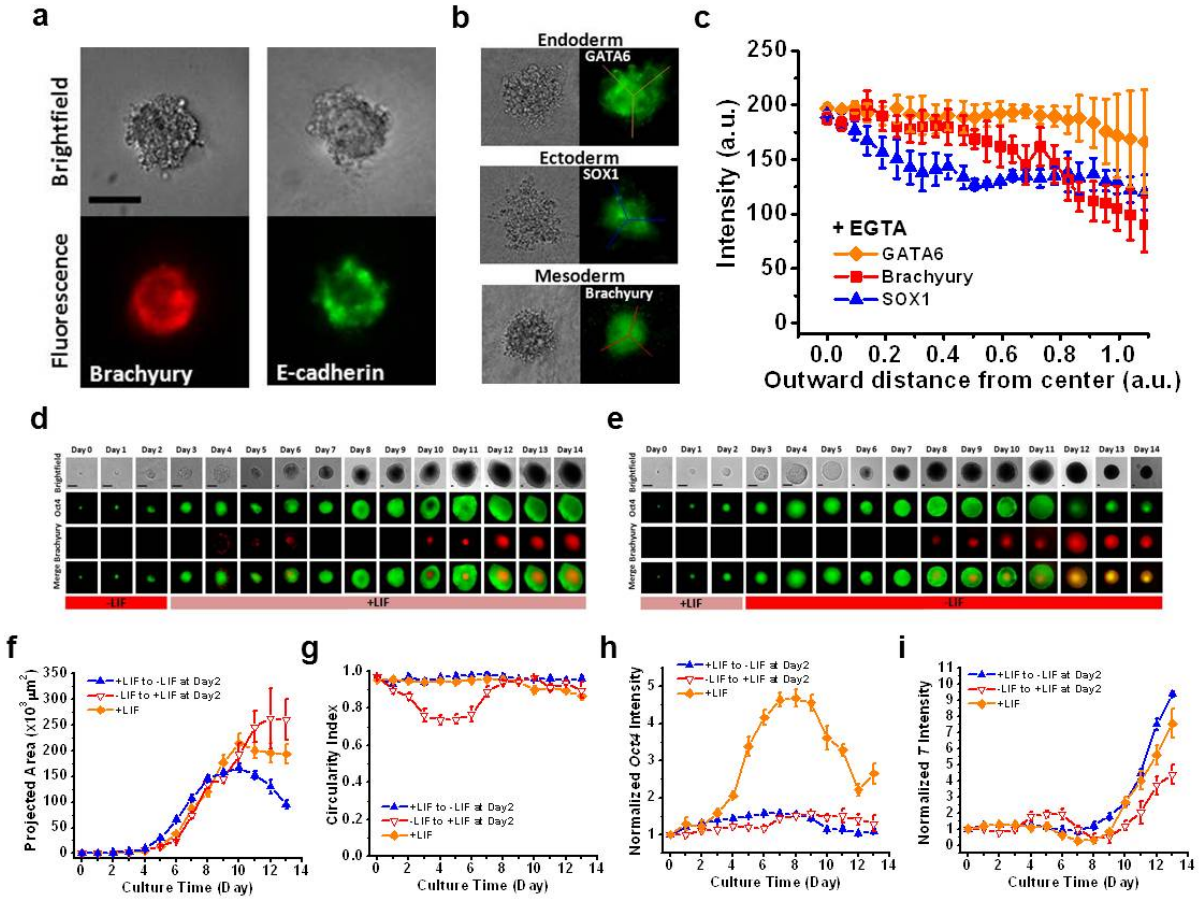

Figure 5.10: Cadherins facilitate germ layer organization and differentiated ESCs are reprogramable. (a) Immunofluorescence staining of E-cadherin shows localization at the outer colony periphery, similar to the mesoderm layer. (b) Representative figure of colonies in –LIF 3D fibrin after 5 days of cadherin inhibition through treatment of 1mM EGTA. (c) Inhibiting cell-cell cadherin interaction completely abolished germ layer organization. (d) Cell cultures that had medium changed from –LIF to +LIF at day 2 exhibit reprogramming properties. *Brachyury* expression increased for a few days before diminishing, suggesting that there might be a time delay response of 2 days. (e) Representative image of ESC cultured in soft 3D fibrin that had medium changed from +LIF to –LIF at day 2. Summarized results of colony projected area (f), circularity index (g), normalized *Oct 3/4* intensity (i), and normalized *Brachyury* intensity (i) for cells that had the medium changed from +LIF to –LIF, from –LIF to +LIF, and the control +LIF without medium change. Scale bar = 50μm. Mean+/-s.e.

5.3 Discussion

At present, how matrix-rigidity-dependent and dimensionality influence the differentiation of ESCs and organization of germ layers remains elusive. A recent report shows that the

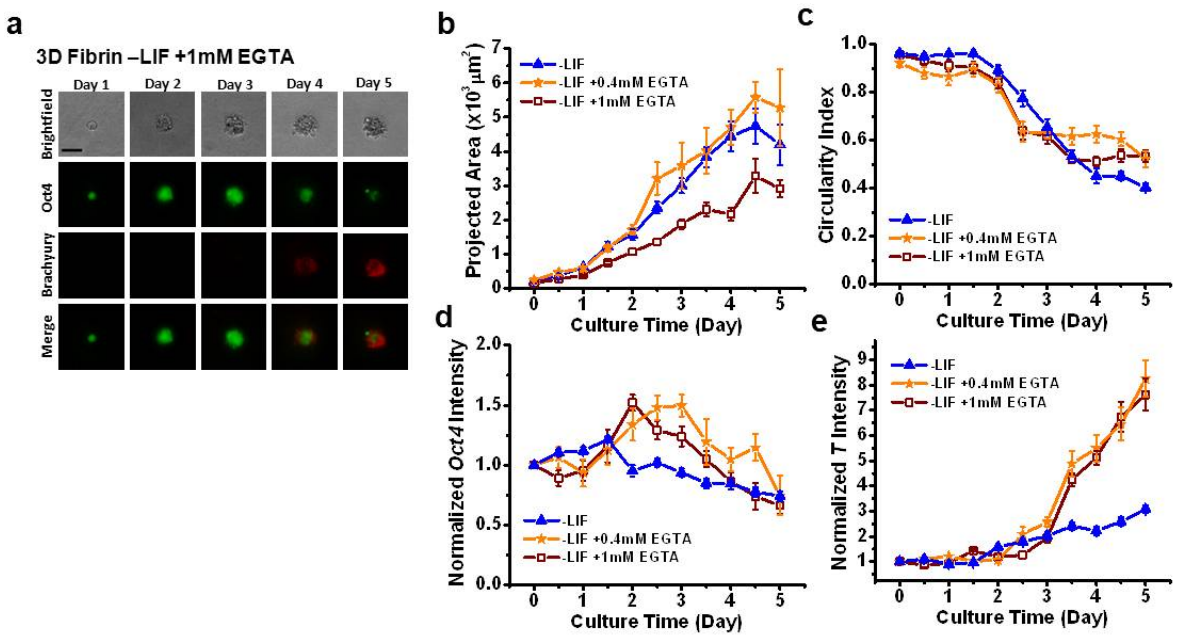

Figure 5.11: Inhibition of cadherin induce higher *Brachyury* expression. (a) Representative image of ESCs cultured in –LIF 3D fibrin gels treated with 1mM EGTA to inhibit cell-cell cadherin interaction. Inhibiting cadherin interaction disrupted formation of mesodermal fluorescent ring surrounding the colony. Summarized time course average results of the projected area (b), circularity index (c), normalized *Oct 3/4* intensity (d) and normalized *Brachyury* intensity (e). Disrupting cell-cell interaction led to a highly expressing mesodermal DsRed colony. Scale bar = 50μm. Mean+/-s.e.

Yes-associated protein (YAP)/TAZ is important in the matrix-rigidity-dependent differentiation of mesenchymal stem cells [141]. It will be interesting to see if TAZ plays a role in embryogenesis and germ layer organization within 3D soft fibrin gels. This mechanical method of mESC culture allows control of the differentiation behaviors and cell proliferation rates. The role of $\alpha_v\beta_3$ integrin is shown to facilitate tension in the positioning of the endoderm layer. The dimensionality of cell-matrix generated forces and cadherin mediated Ca^{2+} dependent cell-cell interaction is crucial germ layer organization. Taken together, the development of the OGTR1 mESC cell line and the culture of ESCs in soft 3D fibrin gels provide a novel platform for further studies in developmental biology. To our knowledge, this present study reveals for the first time that a gastrula-like spherical colony with proper germ layer arrangement of endoderm, mesoderm and ectoderm from inner layer to the outer layer can be generated from a single mammalian ESC by controlling the colony tension facilitated

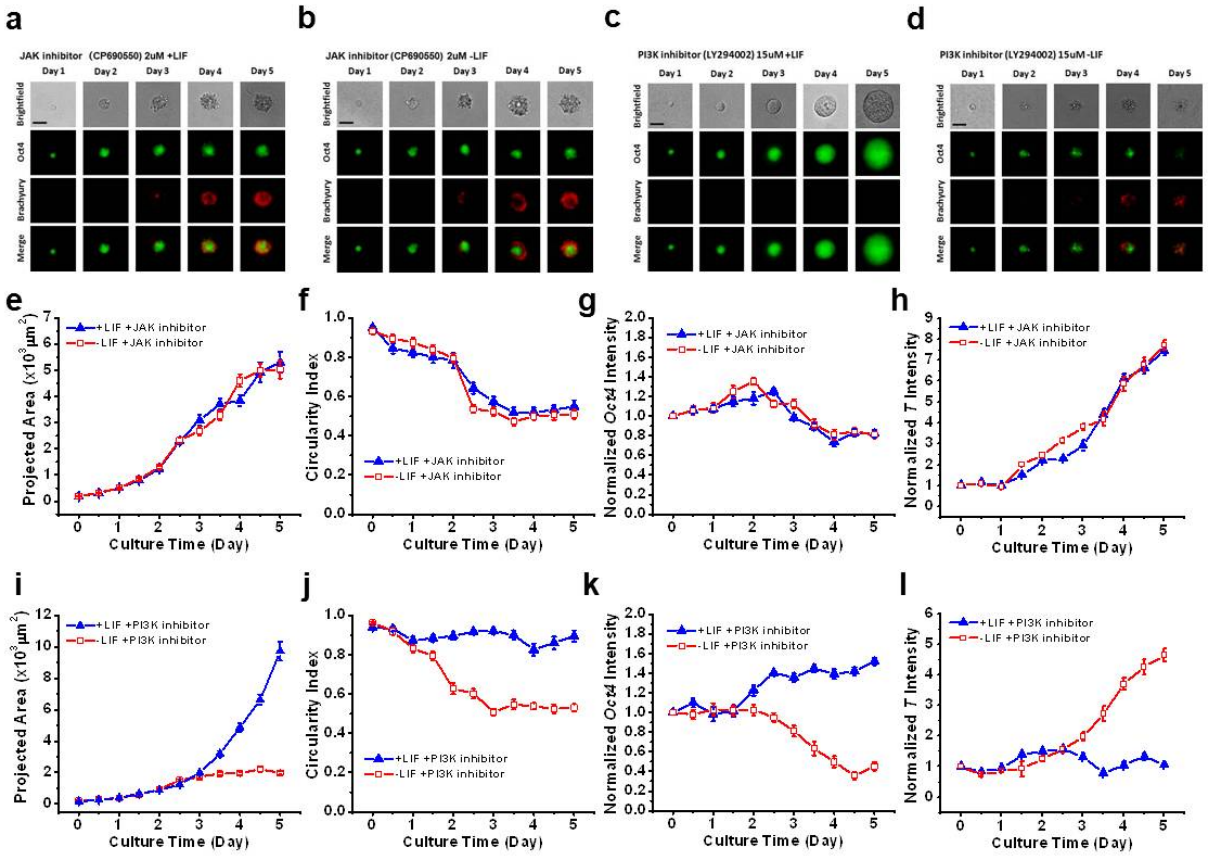

Figure 5.12: Inhibition of Jak–Stat3 signaling pathway induces ESC differentiation. Representative image of ESC culture with 2μM JAK inhibitor, CP690550 in the presence of exogenous LIF (a) and in the absence of exogenous LIF (b). In both cases, ESCs differentiate and form a distinct mesodermal ring at the colony periphery, indicating the disruption of LIF signaling pathway to maintain ESC self-renewal and pluripotency. (c) ESC cultured in +LIF 3D fibrin with the treatment of 15μM PI(3)K inhibitor, LY2940022 did not induce any observable differentiation. (d) There was no observable effect of PI(3)K inhibitor on ESCs cultured in –LIF 3D fibrin. Summarized time course average results of the projected area (e & i), circularity index (f & j), normalized *Oct 3/4* intensity (g & k) and normalized *Brachyury* intensity (h & l) for cells treated with 2μM JAK inhibitor, CP690550 and 15μM PI(3)K inhibitor, LY2940022 under both +LIF and –LIF culture conditions. Inhibition of Jak–Stat3 signaling pathway induces differentiation of ESCs whereas PI(3)K–Akt pathway does not. Scale bar = 50μm. Mean+/-s.e.

by anchorage dependent cell-matrix interaction. However, information on vertebrate gastrulation and early stage embryogenesis is far from complete. Whether directed cell migration and epithelialization within the colonies are factors that influence progenitor cell sorting remains to be determined. A recent report showed that local activation of Wnt signaling

pathway induces polarization of EBs leading to a slight self-organization as it spontaneously begins the gastrulation process [142]. It will be interesting to know how Wnt expression influences primitive streak formation and germ layer formation during gastrulation in 3D soft fibrin matrix.

5.4 Materials and Methods

5.4.1 mESC culture

A mouse embryonic stem cell (mESC) line, namely OGTR1, that expresses EGFP and DsRed under the promoter of *Oct 3/4* (*Oct 3/4*::GFP) and *Brachyury* (T::DsRed) respectively was used in this study. These undifferentiated mESCs were cultured and maintained in medium consisting of high glucose-Dulbecco's Modified Eagles Medium (Invitrogen) supplemented with 15% ES-qualified fetal bovine serum (FBS; Invitrogen), 2 mM L-glutamine (Invitrogen), 1 mM sodium pyruvate, 0.1 mM nonessential amino acids (Invitrogen), 1% penicillin/streptomycin, 0.1 mM beta-mercaptoethanol (Sigma), and 1000 U/ml recombinant LIF (ESGRO; Millipore) at 37 °C in 5% CO2. Cells were passaged every 2–3 days at a ratio of 1:6 using TrypLE (Invitrogen). Culture medium was changed daily.

5.4.2 Cell and colony stiffness measurement

Cell and colony stiffness were measure using the magnetic twisting cytometry (MTC) that has been established [1, 73, 79, 143]. A feromagnetic bead of $\sim 4\mu$m in diameter is coated with RGD peptide and bound to the apical surface of cell. By controlling the surrounding magnetic field, we are able to control the magnitude of force applied to the cell. The bead displacement amplitude can then be correlated to the applied mechanical force to determine the cell stiffness.

5.4.3 Dissolving fibrin gels

The 3D fibrin gels were dissolved using a solution mixture of Collagenase (Sigma C0130) and Dispase II (Sigma D4693) [144]. 0.1% of Collagenase and 0.5% of Dispase II were diluted with PBS. Adding 400μL of the solution to a well (24 well plate size) containing 250μL fibrin will take 2 hours to dissolve in at 37 °C.

5.4.4 3D fibrin gel cell culture and differentiation assay

24 well-plates were used to culture mESCs in the 3D fibrin gel. mESCs were first trypsinized using TrypLE (Invitrogen) and suspended in complete ESC culture medium as described above. For each well, 500 ESCs were prepared in 125μl of medium. Cells in suspension were then placed on ice while the subsequent steps were executed. Fibrinogen solid was dissolved in 125μl of T7 buffer (pH 7.4, 50 mM Tris, 150 mM NaCl) to a concentration of 2 mg/ml. The cells in suspension were then added to the fibrinogen mixture at a ratio of 1:1, making the resulting fibrinogen concentration 1 mg/ml. 5μl of thrombin (0.1 U/μl) was then added to each well of the 24 well-plate. The total 250μl of cell-fibrinogen mixture was added to a single well and mixed with thrombin. The plate was then incubated at 37 °C for 10 min to solidify before adding 1 ml of complete ESC culture medium. 2D fibrin gels were prepared using the same protocol as 3D fibrin gels but without premixing of cells. After the gels were made, mESCs were seeded on top of the fibrin gels. Cells were cultured in 3D or 2D fibrin gels up to 5 days. For differentiation assays, ESCs were cultured in medium without LIF (–LIF) or with medium containing 1μM of retinoic acid (all-trans, Sigma) in the absence of LIF (–LIF/+RA).

$\alpha_v\beta_3$ blocking antagonist cRGDfV (Enzo Life Sciences) was pre-diluted in normal culture medium to the indicated concentrations before being used for cell treatment.

5.4.5 Apoptosis and flow cytometry sorting

Propidium iodide (PI, Sigma) was used to label apoptotic ESCs. Cells cultured in 3D fibrin gels in –LIF/+RA medium was extracted after 5 days and labeled with PI according to

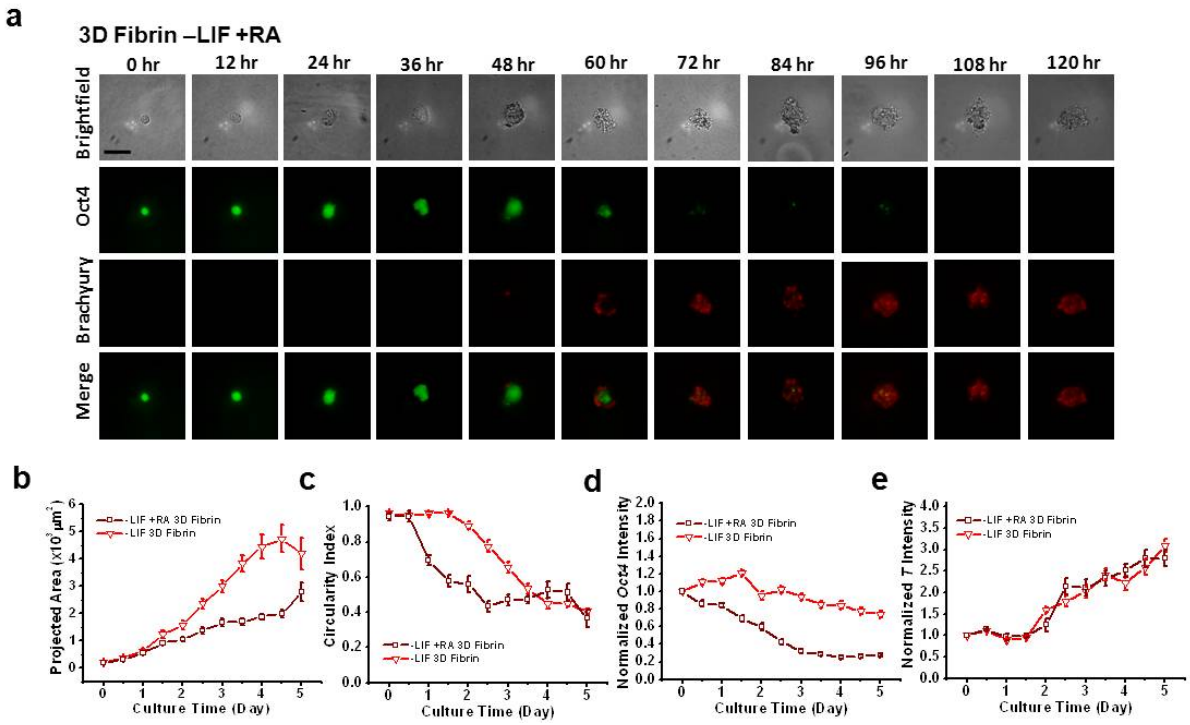

Figure 5.13: Treatment of retinoic acid (RA) induces ESC differentiation. (a) Representative images of ESCs cultured in –LIF 3D fibrin with the addition of 1μM retinoic acid. RA is known to induce differentiation of ESCs towards ectodermal lineage and is used as a positive control for differentiation. (b) The colony size of RA treated cells were significantly smaller than those without treatment. (c) Circularity index of RA treated cells decreased within day 1 as compared to the non-treated which decreased at day 2. There was no significant difference in circularity index between the RA treated cell and non-RA-treated cells at day 5 of the culture. (d) *Oct 3/4* expression of RA treated cells decrease within the first day and remained consistently lower than the non-RA-treated cells. (e) There was no significant difference in *Brachyury* intensity between RA treated and non-treated ESCs. Scale bar = 50μm. Mean+/-s.e.

manufacturers protocol. mESCs were then sorted using Beckman Coulter Epics XL system with a nozzle rate of 3000 to 5000 cells/second. Wild-type mESCs (W4, 129S6/SvEvTac) having no fluorescent protein expression served as a negative control.

Treatment of retinoic acid (RA) as a positive control for differentiation showed that the –LIF 3D soft fibrin cultured colonies are indeed differentiating (Fig 5.13 a-e). Staining of propedium iodide (PI) indicate that only a small population of colonies are apoptotic (Fig 5.14 a-c).

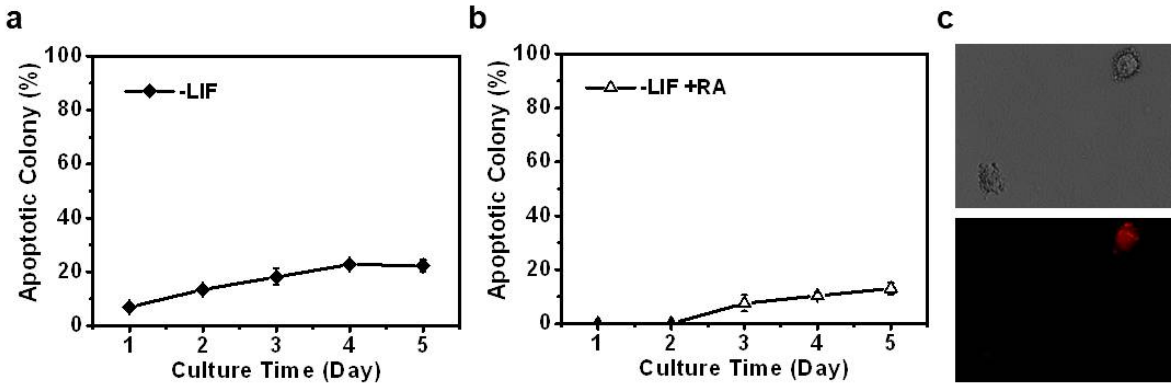

Figure 5.14: Percentage of apoptotic colonies. The number of apoptotic colonies were determined using prepedium iodide (PI). The number of PI stained colonies were counted every 24 hours. (a) ∼20% of the colonies undergo apoptosis by day 5 of –LIF 3D soft fibrin culture. Note that apoptotic colonies are visually observable under the microscope and all analysis in this study excluded them. (b) RA treated cells has ∼10% of the colonies undergo apoptosis after 5 days of culture. (c) Representative figure of a colony stained with PI while a nearby colony remains unstained. Mean+/-s.e.

5.4.6 EB formation assay

Hanging drop cultures were prepared using 25μl droplets, each having 600 cells to initiate embryoid body (EB) formation. Undifferentiated ESCs were trypsinized and were allowed to aggregate and form EBs in the bottom of the hanging drops made with the ES medium without LIF for 5 days. The number of EBs formed was then counted and the different germ layers were labeled with immunofluorescence.

5.4.7 Immunofluorescence staining

ESCs in 3D fibrin gel culture were fixed with fix beffer consisting of 4% formaldehyde (BioLegend) for 20 minutes at room temperature. Cells were then permeabilized with 0.5% Triton X-100 (BioLegend) for 2 minutes. Treat with blocking buffer made of 2% BSA in PBS for 1 hour. To examine the different germ layers, Gata6 primary antibody (Santa Cruz Biotechnology) was used to label endoderm; *Brachyury* primary antibody (Abcam) was used to label; while Sox1 primary antibody (Abcam) was used to label ectoderm. All three germ cells were detected by the donkey-anti-rabbit Alexa-488 green secondary antibody (Invitrogen). All primary antibodies were incubated with cells overnight at 4oC before the necessary

secondary antibody was incubated for 1 hour in the dark. For E-cadherin staining, a conjugated rabbit monoclonal anti-E-Cadherin antibody with Alexa-488 (Cell Signaling) was incubated with the permeabilized cells for 1 hour before examining under a fluorescence microscope.

5.4.8 RT-PCR analysis

RNA of mESC spheroids from 3D fibrin gel culture were extracted using Trizol reagent according to the suppliers instruction (Invitrogen). The relative quantity of mRNA was determined by reverse transcription-PCR (RT-PCR; 30 cycles, One-step RT-PCR kit, QIAGEN). *Nanog, Oct 3/4, Sox2, Fgf5, Otx2, Sox1, Hand1, Brachyury, Twist2, Gata4, Gata6*, and *Sox17* mRNA expressions were examined. The mRNA of glyceraldehyde-3-phosphate dehydrogenase (GAPDH) was used as the internal control. The primer sequences are shown in Fig 5.15.

5.4.9 Statistical analysis

Student's t-test was applied to all statistical analyses.

Reverse Transcription PCR		
Mus Nanog	5' primer	GTCTGCTACTGAGATGCTCTG
	3' primer	CTTGCACTTCATCCTTTGG
Mus Oct3/4	5' primer	CATACTGTGGACCTCAGGTT
	3' primer	CTCACACGGTTCTCAATGCT
Mus Sox2	5' primer	CAAGACGCTCATGAAGAAGG
	3' primer	AGTGGGAGGAAGAGGTAACC
Mus Fgf5	5' primer	ATGAGCCTGTCCTTGCTCTT
	3' primer	TCGTGGGAGCCATTGACTTT
Mus Otx2	5' primer	GACGTTCTGGAAGCTCTGTT
	3' primer	ATGGTTGGGACTGAGGTACT
Mus Sox1*	5' primer	CCAAGAGACTGCGCGCGCTG
	3' primer	GGGTGCGCCGGGTGTGCGTG
Mus Hand1	5' primer	GCTACGCACATCATCACCAT
	3' primer	GATCTTGGAGAGCTTGGTGT
Mus Brachyury (T)	5' primer	CTGCCTACCAGAATGAGGAG
	3' primer	GAGAACCAGAAGACGAGGAC
Mus Twist2	5' primer	AGAGCGACGAGATGGACAAT
	3' primer	TGTTCTGAGAGCCTTGGTC
Mus Gata4	5' primer	CAGAAGGCAGAGAGTGTGTC
	3' primer	AGTGGCATTGCTGGAGTTAC
Mus Gata6	5' primer	CCTCATCAAGCCACAGAAGC
	3' primer	CCAGAGCACACCAAGAATCC
Mus Sox17	5' primer	ATGGCACGGAATCCAACCAG
	3' primer	GAGCAAGTCCCTCAAGGCAT
Mus GAPDH	5' primer	GTGGAGATTGTTGCCATCAACG
	3' primer	CAGTGGATGCAGGGATGATGTTCTG

Figure 5.15: Primer sequences used for RT-PCR analysis of ESCs. (*, Sox1 sequence was obtained from Abranches *et. al.* [145])

CHAPTER 6

CONCLUSION

It has become evident that forces and the mechanical properties of the environment play a crucial role in cellular behavior. Whether mechanical engineering is relevant to cellular biology is no longer a question of uncertainty. Instead, we are to use engineering principles to further uncover the mysteries of cellular biology that has haunted us for many years. In this thesis, we shed some light on the understanding of mechanobiology, specifically the biophysical and gene expression change in living cells by force-induced mechanotransduction.

Mechanical force mediated gene expression is not new. Reports have shown that cells integrate physiochemical signals on the nanoscale from the local microenvironment, resulting in altered functional nuclear landscape and gene expression [29, 38, 146]. These alterations regulate diverse biological processes including cell migration, proliferation, stem cell differentiation, and germ layer organization. However, most of these studies are phenomenological where direct evidence relating mechanical force and gene alteration remains elusive. In Chapter 2, we seek to address the question as to whether mechanical stress propagate into the nucleus and alter protein-protein interaction? Our results provide the first experimental validation that cells sense mechanical forces at the apical membrane through transmembrane integrins, transmit them through the cytoskeleton, across the nuclear membrane and in to the nucleus, altering protein-protein interactions within a subnuclear complex that is important in pre-mRNA splicing. Dynamic cyclic force also induces small phase lags between various protein pairs in Cajal Bodies, suggesting viscoelastic interactions between them. As we are currently unable to detect single gene expression change, and observable protein change is detectable after a few hours; we can only postulate that our results may represent a unique mechanism of mechanotransduction that impacts on gene expression and genome maintenance. This however does not exclude gene regulation by soluble factors.

Instead, mechanical signals are transduced to the nucleus both by soluble regulatory factors via nuclear pores and by active stresses via prestressed cytoplasmic-nuclear links.

Stem cells are unique because they have the potential to become any of the various cell types. They represent a theoretically inexhaustible source of precursor cells to treat diseases and injuries and act as an invaluable research tool. As such, they can be directed to make any number of useful tissues, including nervous tissue, heart tissue or a new liver. However, working with stem cells has proved a much greater challenge than anticipated. Before the potentials of embryonic stem cells can be realized, we need to understand the fundamentals such as the coordinated interactions of chemicals, growth factors, extracellular matrices, and mechanical stimuli necessary to define and to induce directed differentiation of stem cells. Although it is known that soluble factors are critical in stem cell differentiation, growing evidence suggests that the physical microenvironment of the cells (for example, shape constraint, substrate stiffness, and topology), in addition to soluble factors, help direct the fate of mesenchymal stem cells. But whether these mechanical properties may be extended to embryonic stem cells remain to be seen. After showing how mechanical forces are transmitted in to the nucleus in Chapter 2, we explored the possibility of gene expression change via ESC differentiation in Chapter 3. We sought to explain a fundamental unanswered question on whether cell sorting during embryogenesis is dictated by the biophysical properties of cadherin bonds. Despite the widely believed idea that differential binding between cadherin subtypes mediate cell sorting during embryogenesis, there had yet to be evidence of mechanotransduction in embryonic stem cells via cadherin complexes, until the results in this chapter was published. Our findings demonstrated that biological responses of embryonic stem cells to force applied via integrins are different from those to force via E-cadherin, suggesting that mechanical forces might play different roles in different force transduction pathways to shape early embryogenesis.

In Chapter 4, we show that embryonic stem cells were cultured on substrates of different rigidity, the tractional forces generated increase accordingly but the cellular stiffness remains constant, indicating that embryonic stem cells decouple its apical cell stiffness from its basal tractional stresses. This is contrary to what has been previously established in that differentiated cells stiffen in response to elevation of substrate stiffness. The cell spreading

area of differentiated cells is associated to the traction force generated as they increase with the culture substrate stiffness. However, embryonic stem cells do not increase spreading on substrates of increasing rigidity. The stiffening of cell cytoskeleton as a result of cytoskeletal tension (prestress) increase has been established as a key feature of anchorage dependent cells. Since embryonic stem cells exhibit unique features of high intrinsic softness that dictates stress-induced cell spreading and differentiation, we therefore postulate that the pluripotency and self-renewing properties of these cells can be maintained when cultured on soft substrates. This led to our to the work presented in the following chapter.

As we have demonstrated that mouse embryonic stem cells self-renewal and pluripotency can be maintained homogeneously on soft substrates in the absence of LIF [81], and 3D soft fibrin gels provide a unique microenvironment promotes self-renewal of tumorigenic cancer cells via Sox2 [125]. This led to the work presented in Chapter 5 where we postulate that embryonic stem cells cultured in 3D soft fibrin gels in the absence of LIF may give rise to similar round self-renewing pluripotent spherical colonies. In sharp contrast, what we observed was different from what was hypothesized. It was found that ESCs not only differentiate, but they also form systematic and spatially organized germ layers with mesoderm on the outermost periphery, followed by ectoderm in the middle, and endoderm at the innermost core of the colony. A key reason for the observed phenomena is the lost of cortical tension surrounding the ES colonies leading to a decrease in colony circularity. Measurements showed that contrary to single cell stiffness where differentiated cells are stiffer and have more stress fibers, the differentiated ES colonies are significantly softer that their pluripotent counterpart. Cell-matrix tension was found to be crucial in the positioning of the endodermal layer. When $\alpha_v\beta_3$ cell-fibrin mediating integrins were inhibited, the endodermal cells moved from the inside out. We further discovered that cell-cell interaction via E-cadherin, myosin-II dependent cytoskelatal contractility, and RhoA dependent cell contractility regulate ESC colony cortical tension and germ cell organization. The results presented in this chapter shows for the first time that 3D soft fibrin gels enables the development and organization of different germ layers. Contrary to other reports on germ layer organization that begin with a group of cells [119], we begin from a single mammalian embryonic stem cell. We therefore provide a new in vitro technique for further investigation of the complex germ

layer organization process and gastrulation.

The central theme of this thesis was to further understand the how cells sense mechanical forces and convert them in to biochemical signals. The work presented in this thesis shows some of the molecular and cellular basis of mechanotransduction. Mechanical force sensing depends on how forces are distributed in the cells. The preexisting tension in the extracellular matrix, cytoskeleton, cellular membrane, nuclear membrane, and nucleoskeletal structures have been implicated in transducing stress. Mechanosensors such as integrins, cell-cell adhesion molecules such as E-cadherins, associated focal adhesions and junctional complexes, ion channels, and numerous other signaling and structural molecules also contribute to this response. However, it should be clear from the results and discussion presented here that cellular mechanotransduction cannot be studied in insolation or defined entirely in terms of mechanosenstive molecules. Thus, we need to consider how single cells fit into larger systems such as tissues, organs, and whole organisms. Contributions of multiscale microenvironments and invisible internal forces that affect cellular behavior is necessary to fully understand how physical forces influence biological form and function. Multifaceted technologies that incorporate engineering, material science, physics, chemistry, nanotechnology, and computer science are increasingly required to enhance cellular integration in vivo for therapeutic benefit. The rate at which this field of research is growing gives us hope that soluble factor strategies combined with cell mechanics will soon give rise to therapies that are safe, efficacious, and routine.

APPENDIX A

USE OF MTC AND FRET TO QUANTIFY FORCE-INDUCED PROTEIN DISSOCIATION IN THE NUCLEUS OF A LIVING CELL

A.1 Abstract

Mechanical forces are known to play a significant role in biological processes. These forces can be transmitted to the cell through the cytoskeletal filament network, inducing different biochemical responses within the cytoplasm. Although there have been ample reports showing that cytoplasmic enzymes can be directly activated by a local stress on the cell surface via integrins, there has been no evidence that mechanical forces can directly alter nuclear functions without intermediate biochemical cascades. Recently, we showed evidence that forces on the cell membrane can be transmitted directly into the nucleus, inducing structural changes of protein complexes in Cajal bodies. Here, we describe a protocol that utilizes the optical magnetic twisting cytometry (MTC) for force application and fluorescent resonance energy transfer (FRET) to monitor the dynamics and interaction of various Cajal body proteins.

A.2 Introduction

It is well known that human bodies are constantly under the influence of mechanical forces. These mechanical forces influence the growth of tissues and organs. Cells integrate both chemical and mechanical cues to regulate biological processes as diverse as differentiation, vascular development, tumor growth and malignancy [9, 29, 147–149]. However, little is known about the mechanism by which individual cells sense the mechanical forces and convert them in to biochemical signals within the cell and influence the gene expression, a process known as mechanotransduction. Advances in the field of mechanotransduction have

demonstrated that focal adhesion complex proteins such as spectrin [34], talin [35], and integrin [150] can be deformed, unfolded, and thus activated by forces of physiologic magnitudes. Proteins and enzymes within the cytoplasm can be rapidly activated and phosphorylated upon mechanical stress [12,13]. Stem cells differentiate in respond to different surface topology [151], substrate rigidity [8], and applied stress [73], a clear indication of gene expression change within the nucleus. Nonetheless, direct force-altered protein localization/activity and thus gene expression within the nucleus remains elusive.

Immunoblotting and immunostaining have been used to study mechanotransduction [75], but these techniques do not provide sufficient resolution and real time results in a single living cell. Because gene expression in a live cell involves many complicated processes in the cytoplasm and the nucleus and takes time, it is impossible, at the present time, to attribute any changes in gene expression to direct effects of the applied force at the cell surface, without involving intermediate biochemical signaling cascades. Therefore, we asked if localizations of protein complexes in the nucleus can be directly altered by a local surface force, since there is evidence that interactions among nuclear proteins are critical in regulating gene expression. We employed a FRET (fluorescence resonance energy transfer) based technique to monitor the dynamics and interaction of proteins within the Cajal Body (CB) complex in response to mechanical stress. CBs are critical for the biogenesis and recycling of several classes of small ribonucleoprotein (snRNP) complexes involved in pre-mRNA splicing and preribosomal RNA (pre-rRNA) processing15, 16, and assembly and delivery of telomerase to telomeres [42–45]. Recent advances in the dynamics, assembly, and function of CBs suggest that the CBs organize as a direct reflection of highly active genes with which they are physiologically associated [48].

Intermolecular FRET can be used to visualize protein-protein interactions. In this protocol, we labeled various CB proteins with cyan fluorescent protein (CFP) and yellow fluorescent protein (YFP). The CFP labeled protein acts as the donor while the YFP labeled protein act as the receptor. Only CFP is excited during the experiment while both CFP and YFP were monitored simultaneously. By observing the relative intensity changes of CFP and YFP, we can then quantify the distance and interaction between CB proteins. When the CFP and YFP labeled proteins are close to each another (<10nm), FRET occurs

when the emission of CFP is transferred to excite YFP. As we observe the FRET ratio of CFP/YFP, there will be a decrease in FRET ratio when the two proteins come closer to each other, because there is a decrease in CFP intensity and an increase in YFP intensity (anti-correlation). On the other hand, when the two proteins are separated and thus there is an increase in distance between the two proteins, the ratio of CFP/YFP will increase.

Here, we outline the use of magnetic twisting cytometry (MTC) [1] in detail to study the spatial and temporal mechano-chemical response within the cell nucleus. We also describe the use of a dynamic sinusoidal load to quantify the viscoelastic and dissipative behavior between protein pairs within the CB. Our results showed that mechanical force at the apical membrane can be directly transmitted through the actin microfilaments and nuclear envelope to remote cites within the nucleus. The stress induced protein dissociation was rapid and did not require intermediate biochemical signaling, diffusion, or translocation.

A.3 Reagents and Equipment

- CFP and YFP plasmid probes of coilin, SMN, fibrillarin, Nopp140, WRAP53, SART3, SmE, SmG (from Miroslav Dundr, Rosalind Franklin University of Medicine and Science, North Chicago)
- mCherry-Lamin A plasmid (from Peter Kalab, National Institute of Health)
- HeLa cells (ATCC)
- Lamin A/C -/- (LMNA-knockout) mouse embryonic fibroblast (from Colin Stewart, National University of Singapore, Singapore)
- Plectin -/- mouse fibroblast (from Gerhard Wiche, University of Vienna, Germany)
- CO_2-independent medium (Invitrogen)
- Collagen, type I from rat tail (solution, Sigma, 091M7675)

- Ferromagnetic beads (Fe_3O_4; 4.5 μm diameter) (from W. Moller, Gauting, Germany or J. Fredberg, Boston, MA; magnetic beads with various surface properties are commercially available in an assortment of sizes from Spherotech, Inc., Lake Forest, IL)
- Dimethyl sulfoxide, sterile-filtered (DMSO; Sigma)
- Fetal bovine serum (FBS; HyClone)
- Opti-MEM I medium (Invitrogen)
- Penicillin-streptomycin (Invitrogen)
- Phosphate-buffered saline (PBS; HyClone)
- L-Glutamine (100x) (Invitrogen)
- Lipofectamine 2000 (Invitrogen)
- Trolox (6-Hydroxy-2,5,7,8-tetramethylchroman-2-carboxylic acid; Sigma)
- 2% Bis solution (Bio-Rad Laboratories, 161-0142)
- 40% Acrylamide solution (Bio-Rad Laboratories, 161-0140)
- 3-aminopropyltrimethoxysilane (Aldrich, Product # 281778)
- 0.5% gluteraldehyde (Sigma-Aldrich, Product # G6257)
- 10% Ammonium persulfate (APS, Bio-Rad)
- TEMED (Bio-Rad)
- HEPES (Sigma)
- Sulfo-SANPAH (Pierce, Product # 22589)
- 0.2μm Florescent latex beads (Molecular Probes)
- 0.05M Carbonate buffer (pH 9.4; bioWORLD)

- Glass-bottomed culture dishes (35 mm diameter; Cell E&G)
- 12 mm circular cover glasses (Fisher, cat. # 12-545-80)
- Synthetic RGD-containing peptide [Ac-G(dR)GDSPASSKGGGGS(dR)LLLLLL(dR)-NH2, Peptide2000 (Telios) (18); Peptides International, Inc., Louisville, KY]
- Adobe Photoshop
- 40x 0.55 numerical aperture (N.A.) air and 63x 1.32 N.A. oil-immersion objectives (Leica)
- CCD camera (Hamamatsu; model C4742-95-12ERG)
- CFP/YFP Dual EX/EM (FRET) Filter sets for FRET experiments (Optical Insights): CFP: excitation S430/25, emission S470/30; YFP: excitation S500/20, emission S535/30. The emission filter set uses a 505nm dichroic mirror.
- DualView imaging system (Optical Insights)
- Inverted microscope (Leica, DMIRE2)
- Matlab (Mathworks)
- MTC device (Commercially available via special order from EOL Eberhard, Obervil, Switzerland)

A.4 Procedure

A.4.1 Coating magnetic beads with RGD

1. Suspend the magnetic beads stock in 95% alcohol (for sterilization) and aliquot them into small 2ml vial each containing 1mg of beads.
2. Leave a vial open and evaporate the alcohol out.

3. Add 1.5ml of PBS buffer to rinse the beads. Centrifuge it down and discard the PBS carefully.

4. Add 1ml of Cabonate buffer to the beads.

5. Add 50 μg of RGD peptides (diluted in DMSO) to the bead-buffer solution.

6. Rotate the beads at 4 °C overnight.

7. Before using beads, centrifuge the beads and discard the supernatant RGD. Then rinse it once with PBS as described in step 3.

8. Store the coated beads in serum free DMEM.

A.4.2 Cell culture and transfection

1. All cells used for experiments are preferred low passages.

2. Regular cells culture was done in T-25 flask and maintained in DMEM supplemented with 10% FBS100U/ml penicillin, 100μg/ml streptomycin, and 2mM L-Glutamine at 37 °C in 5% CO_2.

3. For experiments, cells need to be prepared 3 days in advance. Day 1, coat the 35mm glass bottom dishes with Collagen-I and store at 4 °C to allow absorption of collagen on to the glass surface.

4. Day 2, sterilize the collagen-coated culture dish by leaving it under UV light for 10 minutes. Then seed ($\sim$300,000) cells in the collagen-coated glass bottom dish such that it is $\sim$80% confluent the following day.

5. Day 3, double transfect the cells with plasmid constructs of CFP and YFP labeled proteins. Dilute 1μg of CFP plasmid and 1μg of YFP plasmid to 100μg of Opti-MEM I medium in a small vial.

6. In another vial, add 4μl of Lipofectamine 2000 to 100μg of Opti-MEM I medium in a small vial.

7. Wait 5 minutes in room temperature before mixing the contents of both vials together. Then wait another 20 minutes.

8. Add the total $\sim$200μl of DNA-Lipofectamine mixture to the dish containing cells.

9. Optional: To minimize photobleaching, 0.05mM Trolox solution was added to the dish along with the DNA-Lipofectamine mixture [74].

10. Incubate for 6 hours at 37 °C in 5% CO_2 before replacing the culture medium with regular DMEM culture medium.

11. Day 4, cells are transfected and ready for imaging.

A.4.3 Magnetic Twisting Cytometry (MTC)

1. On the day of the experiment (day 4 in the previous section), take the dish out of the incubator and remove most of the culture medium, such that only the cells in the center well (glass region) is slightly covered in medium.

2. Add 20μl of RGD-coated magnetic beads ($\sim$20μg of beads) to the center well of the dish by scattering them all over.

3. Carefully place the beads back into the incubator and leave for 10 minutes to allow for integrin clustering and formation of focal adhesions surrounding the beads.

4. Remove cells from incubator and rinse it once with PBS. Avoid disturbing cells in the center well. Add and remove PBS gently by the side of the dish.

5. Add CO_2-independent medium to the dish. This is to maintain the pH of the cell culture when it is exposed to the open while under the microscope.

6. Place the dish in the MTC stage where coils are located. Then place it on the inverted microscope.

7. Find a single cell that is well transfected with both CFP and YFP plasmids. The cell also needs to have a single bead attached to it. Exclude all cells that are not well

transfected, have more than one bead attached, or are in contact with neighboring cells.

8. After the good cell is found, magnetize the magnetic beads by applying a strong magnetic pulse (∼1000G, <0.5ms).

9. Now that the beads are polarized and magnetized, apply a magnetic field in the direction perpendicular to that of the magnetizing pulse (Figure A.1). This will cause the bead to rotate. Input the parameter for MTC. Parameters for FRET analysis are typically 17.5Pa (50G step load) or other magnitudes, where for phase lag analysis is 24.5Pa (70G oscillatory load).

10. While force is being applied, capture the necessary brightfield or fluorescence images.

A.4.4 FRET imaging and analysis

1. For FRET imaging, the Dual-View imaging system was used to split the image into two (1344 x 512 pixels each). The top view filters for YFP, while the bottom view filters for CFP. Each image is 1344 x 1024 pixels and simultaneously captures both CFP and YFP activity.

2. While force is being applied by the MTC, FRET dual-view time course images are captured to monitor the protein-protein interaction within the nucleus before and after force.

3. After experiments are done and images obtained. A customized Matlab program is used to analyze the data. The program first divides the top (YFP) and bottom (CFP) image in to two separate files.

4. The region of interest (an individual CB in our case) is then selected. The program crops this region from the CFP and YFP images, then aligns them by cross-correlation.

5. A binary mask is then created for CFP and YFP images by using Matlabs "graythresh" function. The binary mask is then multiplied with the fluorescent images generating

images that have only the fluorescing region and a black background.

6. The CFP/YFP ratio value is then calculated for each individual pixel that has been aligned and cross-correlated. An average of the region is obtained and reported. Each image or time point will generate one CFP/YFP value.

Note: More details on the Matlab program has been described by Na S et. al. [73]

A.4.5 Polyacrylamide gels for traction force measurement

1. Polyacrylamide (PA) gels with 0.2μm fluorescent beads embedded within are used to measure the traction force each cell generates. By varying the concentration of bis and acrylamide, different gel stiffness can be obtained.

2. To prepare PA gels, first smear 3-aminopropyltrimethoxysilane over the glass surface of a 35mm glass-bottom-dish using a cotton-tipped swab and let it sit there for 6 min.

3. Wash it thoroughly with water before applying 100 μl/dish of 0.5% gluteraldehyde for 30 min.

4. Wash again thoroughly and let them dry. Avoid touching the glass surface throughout the whole gel making procedure.

5. Determine the bis:acrylamide solution proportions to get the desired substrate stiffness. 0.6, 2, and 8 kPa, corresponds to 0.06% bisacrylamide and 3% acrylamide, 0.05% bisacrylamide and 5% acrylamide, 0.3% bisacrylamide and 5% acrylamide respectively. Prepare 1ml of each desired mixture in a small 2ml vial.

6. Add 10μl of 0.2μm fluorescent beads to the bis-acrylamide mixture. Before adding fluorescent beads, be sure to vortex or sonicate.

7. Add polymerizing activator/initiator to the beads-bis-acrylamide mixture. 10% APS at 1:200 volume ratio (5μl in this case). TEMED at 1:2000 volume ratio (0.5μl in this case). Mix everything together thoroughly.

8. Add 15μl of the mixture to the glass surface of the treated dish. (15 μl would give 75 μm thick substrates)

9. Flatten droplet with a 12mm circular cover glasses.

10. Turn the glass bottom dish upside down. This ensures the fluorescent beads to be closer to the top surface.

11. Place the upside down dishes in a 37 °C incubator for 30-45 minutes. Elevated temperature helps in the polymerization.

12. After the gels are fully polymerized, flood the dish with 100 mM HEPES. Then carefully remove the circular cover glass with a single edge razor.

13. Make 1mM solution of SANPAH with DMSO and 100 mM HEPES. Add DMSO to SANPAH first to dissolve the solid powder, and then add it to HEPES. For example, 5mg SANPAH + 50μl DMSO + 10ml (100mM) HEPES.

14. Take out HEPES from the glass bottom dishes, dab excess HEPES with Kim wipes from around gel edge

15. Apply 200μl of SANPAH solution the gel (center well of dish).

16. Expose surface to UV for 6 min (6" away from the lamp) to photo activate the gel surface. SANPAH color will turn dark. Without SANPAH treatment, collagen will not bind to gel surface.

17. Rinse off SANPAH with 100mM HEPES.

18. Repeat photo activation procedure once more and rinse it off with 100mM HEPES.

19. Coat the gel surface with the desired concentration of collagen and incubate at 4 ° C overnight.

20. Before seeding cells onto the gel surface, sterilize it under UV light for 10-15 minutes.

21. PA gels can be stored in PBS at 4 ° C for three weeks.

Note: To determine the ratio of bis to acrylamide for desired substrate stiffness, refer to references [101, 152, 153].

A.4.6 Traction Force Microscopy (TFM)

1. Cells are cultured on the PA gels. Depending on the PA gel stiffness, the cell will generate different traction forces, and hence different magnitude of deformation.

2. Three images need to be captured. First is the brightfield or phase contrast image of the cell which will be used to identify the cell boundary. Second is the fluorescent beads marker image while the cell is still on the substrate. Third is the reference fluorescent beads marker image after the cell has been removed or trypsinized from the AP gel surface.

3. A customize Matlab program was used to analyze the traction force generated. The displacement field induced by each individual cells tractional forces was determined by comparing the fluorescent bead positions before and after trypsinization (cell-free and thus force-free).

4. An image correlation method where the flourecent images are divided into small window areas is used to determine the displacement vectors [154].

5. The root-mean-square (RMS) traction field was then calculated from the displacement field using Fourier Transform Traction Cytometry (FTTC) based on the Boussinesq solution [155].

A.4.7 Cell stiffness measurement

1. The stress applied to the cell (in Pa) can be calculated from the applied twisting magnetic field (in G) by multiplying the bead constant (in Pa/G) with the applied twisting field (in G). The bead constant reflects the magnetic property of the bead and may differ from batch-to-batch. The beads are calibrated by immersing them in a known viscous fluid, and applying a constant magnetic field while observing the

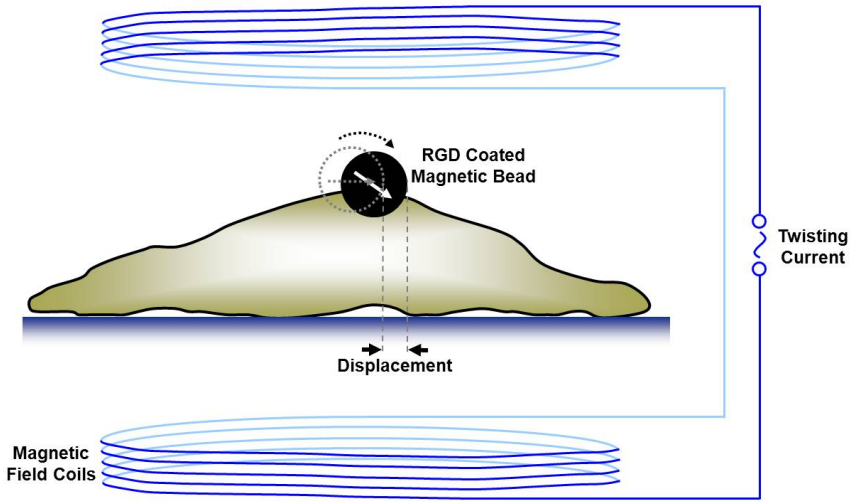

Figure A.1: Schematic of the magnetic twisting cytometry cell stiffness measurement technique. An RGD-coated ferromagnetic magnetic bead was bound to the apical surface of the cell. A controlled homogeneous magnetic field is then applied around the cell via the coils, causing the magnetic bead to displace and rotate. Based on the magnitude of the magnetic field applied, the displacement of the magnetic bead, and the bead-cell area of contact, the cell stiffness can be quantified. Gray dashed outlined bead denotes the position of bead before twisting field was applied. White arrow on bead indicates the direction of the magnetic moment.

displacement [75]. For example, a 50 G applies 17.5 Pa of stress to the cell if the bead constant is 0.35 Pa/G [12].

2. When a cell with a single bead bound to its apical surface is found under the microscope, an oscillatory stress of 0.3 Hz is applied using the MTC as shown in Figure (Figure A.1).

3. The MTC software tracks the displacement coordinates of the magnetic bead and saves them in a text file.

4. By quantifying the magnetic bead displacement, and the bead embedded area, the cell complex modulus can be estimated. A custom Matlab program is then used to calculate the cell stiffness.

5. The beads whose displacement waves are synchronized to the input sinusoidal signals were selected. This is to filter out spontaneous movements of the beads or microscope

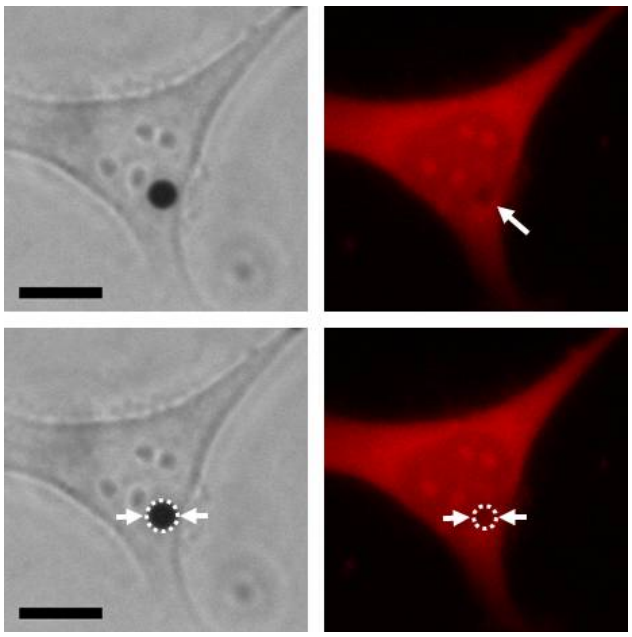

Figure A.2: Quantification of magnetic bead embedment in HeLa cells. An RGD-coated bead was bound to the apical surface of the cell for 10 minutes before it was fixed and stained with phalloidin. Integrin-mediated focal adhesions form around the bead-cell area of contact, giving rise to a noticeable actin ring. The bead embedment was estimated by measuring the actin ring diameter from the fluorescent image and comparing it to the bead diameter from the brightfield image (double arrows). Bead embedment in HeLa cells is ~30%. Scale bar = 10 μm.

stage shifts.

6. Beads with displacements less than 5 nm (detectable resolution) and loosely bound beads were not selected for analysis. To increase the signal to noise ratio, the peak amplitude of the displacement was averaged over 5 consecutive cycles for each cell.

7. The complex stiffness is calculated using the equation G*=T/d. For each bead, the elastic stiffness G' (the real part of G*) and the dissipative stiffness G" (the imaginary part of G*) was calculated based on the phase lag. The measured stiffness has the units of torque per unit bead volume per unit bead displacement (Pa/nm).

8. A finite element model is then used to convert the cell stiffness (Pa/nm) to modulus (Pa) based on the bead to cell surface contact [10] (Figure. A.2).

9. More details on how to calculate cell stiffness have been described by Fabry B et.

al. [23].

A.4.8 Phase lag quantification

1. An oscillatory stress (0.3 Hz or 0.83 Hz) is applied to a cell that is well transfected, similar to the stress used to measure cell stiffness

2. Time course images of the bead, CFP labeled protein, and YFP labeled protein are captured while the cyclic force is being applied.

3. A custom Matlab program is used to analyze the images and the displacement of bead, CFP and YFP labeled proteins are determined. The phase lag of fluorescent proteins to the bead is then calculated.

4. One complete cycle of stress corresponds to 360 °. For example, at 0.3 Hz, the period for one complete cycle is 3.33s. If CFP lags behind the bead displacement by 0.3s, that will correspond to a phase lag of ∼32 degrees.

A.4.9 Mean Square Displacement (MSD)

1. For CB dynamics, an oscillatory stress (0.3 Hz) needs to be applied. Fluorescent images used for MSD analysis were obtained using single-view fluorescence filter.

2. Time course images of the bead, CFP labeled protein, and YFP labeled protein are captured before, during and after the cyclic force is being applied.

3. Binary images of the bead, CFP and YFP are obtained by using the graythresh Matlab function. The centroid coordinates of the bead and each fluorescing protein are then obtained.

4. The coordinates of each fluorescence particle obtained was then used to calculate the mean square displacement (MSD) of Coilin and SMN. The MSD before, during, and after mechanical loading were calculated using a customized Matlab program based on Equation (A.1)

$$MSD(\Delta t) = \frac{1}{N}\sum_{i=1}^{N}\left\{\left[r(t_i+\Delta t) - r(t_i)\right]^2\right\} \tag{A.1}$$

where r(t) is the fluorescence particle position and t is the time step (0.35s in our case). The same procedure is performed on bright-field images to obtain the bead MSD.

A.4.10 Troubleshooting

Cajal bodies are dynamic and spontaneously move. There are times when the observed CB moves out of focus, especially for those that are not tethered and exhibit simple diffusion.

Intermolecular FRET is also difficult to observe because the stoichiometry of acceptors to donors can vary with transfection efficiencies [27]. On top of that, if the distance or orientations between the protein pairs are unfavorable, FRET may not be observed even if they both reside in the same CB complex.

A.4.11 Time Taken

Preparation for experiments takes up to 3 days. Dishes need to be coated with collagen or other matrix proteins. Beads need to be coated with RGD or ligands to integrins. Cells need to be transfected.

Depending on the transfection efficiency and how magnetic beads bind to the cell surface, locating an appropriate cell for data collection may take up sometime.

The whole process of making PA gels may take a day (excluding incubation time of Collagen-I).

REFERENCES

[1] N. Wang, J. P. Butler, and D. E. Ingber, "Mechanotransduction across the cell surface and through the cytoskeleton," *Science*, vol. 260, no. 5111, p. 1124, 1993.

[2] D. E. Ingber, "Cellular mechanotransduction: putting all the pieces together again," *Faseb Journal*, vol. 20, no. 7, pp. 811–827, 2006.

[3] D. E. Ingber, "Tensegrity ii. how structural networks influence cellular information processing networks," *Journal of cell science*, vol. 116, no. 8, pp. 1397–1408, 2003.

[4] B. D. Matthews, D. R. Overby, R. Mannix, and D. E. Ingber, "Cellular adaptation to mechanical stress: role of integrins, rho, cytoskeletal tension and mechanosensitive ion channels," *Journal of cell science*, vol. 119, no. 3, pp. 508–518, 2006.

[5] D. Leckband and A. Prakasam, "Mechanism and dynamics of cadherin adhesion," *Annual Review of Biomedical Engineering*, vol. 8, pp. 259–287, 2006.

[6] C. Hahn and M. A. Schwartz, "Mechanotransduction in vascular physiology and atherogenesis," *Nature Reviews Molecular Cell Biology*, vol. 10, no. 1, pp. 53–62, 2009.

[7] S. Huang and D. E. Ingber, "The structural and mechanical complexity of cell-growth control," *Nature cell biology*, vol. 1, no. 5, pp. E131–E138, 1999.

[8] A. J. Engler, S. Sen, H. L. Sweeney, and D. E. Discher, "Matrix elasticity directs stem cell lineage specification," *Cell*, vol. 126, no. 4, pp. 677–689, 2006.

[9] V. Vogel and M. Sheetz, "Local force and geometry sensing regulate cell functions," *Nature Reviews Molecular Cell Biology*, vol. 7, no. 4, pp. 265–275, 2006.

[10] S. M. Mijailovich, M. Kojic, M. Zivkovic, B. Fabry, and J. J. Fredberg, "A finite element model of cell deformation during magnetic bead twisting," *Journal of applied physiology*, vol. 93, no. 4, pp. 1429–1436, 2002.

[11] S. Hu, J. Chen, B. Fabry, Y. Numaguchi, A. Gouldstone, D. Ingber, J. Fredberg, J. Butler, and N. Wang, "Intracellular stress tomography reveals stress focusing and structural anisotropy in cytoskeleton of living cells rid b-6966-2008," *American Journal of Physiology-Cell Physiology*, vol. 285, no. 5, pp. C1082–C1090, 2003.

[12] S. Na, O. Collin, F. Chowdhury, B. Tay, M. Ouyang, Y. Wang, and N. Wang, "Rapid signal transduction in living cells is a unique feature of mechanotransduction," *Proceedings of the National Academy of Sciences of the United States of America*, vol. 105, no. 18, pp. 6626–6631, 2008.

[13] Y. C. Poh, S. Na, F. Chowdhury, M. Ouyang, Y. Wang, and N. Wang, "Rapid activation of rac gtpase in living cells by force is independent of src," *PLoS One*, vol. 4, no. 11, p. e7886, 2009.

[14] S. Hu, J. Chen, J. P. Butler, and N. Wang, "Prestress mediates force propagation into the nucleus," *Biochemical & Biophysical Research Communications*, vol. 329, no. 2, pp. 423–428, 2005.

[15] Y. C. Poh, S. P. Shevtsov, F. Chowdhury, D. C. Wu, S. Na, M. Dundr, and N. Wang, "Dynamic force-induced direct dissociation of protein complexes in a nuclear body in living cells," *Nature Communications*, vol. 3, p. 866, 2012.

[16] R. J. Pelham and Y. L. Wang, "Cell locomotion and focal adhesions are regulated by substrate flexibility," *Proceedings of the National Academy of Sciences of the United States of America*, vol. 94, no. 25, pp. 13 661–13 665, 1997.

[17] G. Giannone, B. J. Dubin-Thaler, H. G. Dobereiner, N. Kieffer, A. R. Bresnick, and M. P. Sheetz, "Periodic lamellipodial contractions correlate with rearward actin waves," *Cell*, vol. 116, no. 3, pp. 431–443, 2004.

[18] Y. Wang, J. Chang, K.-D. Chen, S. Li, J. Y.-S. Li, C. Wu, and S. Chien, "Selective adapter recruitment and differential signaling networks by vegf vs. shear stress," *Proceedings of the National Academy of Sciences of the United States of America*, vol. 104, no. 21, pp. 8875–8879, 2007.

[19] T. P. Lele, J. Pendse, S. Kumar, M. Salanga, J. Karavitis, and D. E. Ingber, "Mechanical forces alter zyxin unbinding kinetics within focal adhesions of living cells," *Journal of cellular physiology*, vol. 207, no. 1, pp. 187–194, 2006.

[20] D. Riveline, E. Zamir, N. Q. Balaban, U. S. Schwarz, T. Ishizaki, S. Narumiya, Z. Kam, B. Geiger, and A. D. Bershadsky, "Focal contacts as mechanosensors: Externally applied local mechanical force induces growth of focal contacts by an mdia1-dependent and rock-independent mechanism," *Journal of Cell Biology*, vol. 153, no. 6, pp. 1175–1185, 2001.

[21] X. Trepat, L. Deng, S. S. An, D. Navajas, D. J. Tschumperlin, W. T. Gerthoffer, J. P. Butler, and J. J. Fredberg, "Universal physical responses to stretch in the living cell," *Nature*, vol. 447, no. 7144, 2007.

[22] N. Wang and D. E. Ingber, "Probing transmembrane mechanical coupling and cytomechanics using magnetic twisting cytometry," *Biochemistry and Cell Biology-Biochimie Et Biologie Cellulaire*, vol. 73, no. 7-8, pp. 327–335, 1995.

[23] B. Fabry, G. Maksym, S. Shore, P. Moore, R. Panettieri, J. Butler, and J. Fredberg, "Signal transduction in smooth muscle - selected contribution: Time course and heterogeneity of contractile responses in cultured human airway smooth muscle cells," *Journal of applied physiology*, vol. 91, no. 2, pp. 986–994, 2001.

[24] P. A. Valberg and J. P. Butler, "Magnetic particle motions within living cells - physical theory and techniques," *Biophysical journal*, vol. 52, no. 4, pp. 537–550, 1987.

[25] G. N. Maksym, B. Fabry, J. P. Butler, D. Navajas, D. J. Tschumperlin, J. D. Laporte, and J. J. Fredberg, "Mechanical properties of cultured human airway smooth muscle cells from 0.05 to 0.4 hz," *Journal of applied physiology*, vol. 89, no. 4, pp. 1619–1632, 2000.

[26] Y. Uda, "Ligand specificity in force-induced differentiation of embryonic stem cells," *Masters Degree Thesis, Graduate School of Biomedical Engineering, Tohoku University*, 2012.

[27] K. Truong and M. Ikura, "The use of fret imaging microscopy to detect protein-protein interactions and protein conformational changes in vivo," *Current opinion in structural biology*, vol. 11, no. 5, pp. 573–578, 2001.

[28] A. Miyawaki and R. Y. Tsien, "Monitoring protein conformations and interactions by fluorescence resonance energy transfer between mutants of green fluorescent protein," *Applications of Chimeric Genes and Hybrid Proteins Pt B*, vol. 327, pp. 472–500, 2000.

[29] D. E. Discher, P. Janmey, and Y. li Wang, "Tissue cells feel and respond to the stiffness of their substrate," *Science*, vol. 310, no. 5751, pp. 1139–1143, 2005.

[30] Y. Uda, Y.-C. Poh, F. Chowdhury, D. C. Wu, T. S. Tanaka, M. Sato, and N. Wang, "Force via integrins but not e-cadherin decreases oct3/4 expression in embryonic stem cells," *Biochemical and biophysical research communications*, vol. 415, no. 2, pp. 396–400, 2011.

[31] B. Geiger, J. P. Spatz, and A. D. Bershadsky, "Environmental sensing through focal adhesions," *Nature Reviews Molecular Cell Biology*, vol. 10, no. 1, pp. 21–33, 2009.

[32] M. A. Wozniak and C. S. Chen, "Mechanotransduction in development: a growing role for contractility," *Nature Reviews Molecular Cell Biology*, vol. 10, no. 1, pp. 34–43, 2009.

[33] N. Wang, J. D. Tytell, and D. E. Ingber, "Mechanotransduction at a distance: mechanically coupling the extracellular matrix with the nucleus," *Nature Reviews Molecular Cell Biology*, vol. 10, no. 1, pp. 75–82, 2009.

[34] C. P. Johnson, H.-Y. Tang, C. Carag, D. W. Speicher, and D. E. Discher, "Forced unfolding of proteins within cells," *Science*, vol. 317, no. 5838, pp. 663–666, 2007.

[35] A. D. Rio, R. Perez-Jimenez, R. Liu, P. Roca-Cusachs, J. M. Fernandez, and M. P. Sheetz, "Stretching single talin rod molecules activates vinculin binding," *Science*, vol. 323, no. 5914, pp. 638–641, 2009.

[36] B. D. Hoffman, C. Grashoff, and M. A. Schwartz, "Dynamic molecular processes mediate cellular mechanotransduction," *Nature*, vol. 475, no. 7356, pp. 316–323, 2011.

[37] A. J. Maniotis and C. S. Chen, "Demonstration of mechanical connections between integrins, cytoskeletal filaments, and.." *Proceedings of the National Academy of Sciences of the United States of America*, vol. 94, no. 3, p. 849, 1997.

[38] J. Lammerding, P. C. Schulze, T. Takahashi, S. Kozlov, T. Sullivan, R. D. Kamm, C. L. Stewart, and R. T. Lee, "Lamin a/c deficiency causes defective nuclear mechanics and mechanotransduction," *Journal of Clinical Investigation*, vol. 113, no. 3, pp. 370–378, 2004.

[39] J. Lammerding, L. G. Fong, J. Y. Ji, K. Reue, C. L. Stewart, S. G. Young, and R. T. Lee, "Lamins a and c but not lamin b1 regulate nuclear mechanics," *Journal of Biological Chemistry*, vol. 281, no. 35, pp. 25 768–25 780, 2006.

[40] C. M. Hale, A. L. Shrestha, S. B. Khatau, P. J. Stewart-Hutchinson, L. Hernandez, C. L. Stewart, D. Hodzic, and D. Wirtz, "Dysfunctional connections between the nucleus and the actin and microtubule networks in laminopathic models rid a-6633-2009 rid a-3257-2010," *Biophysical journal*, vol. 95, no. 11, pp. 5462–5475, 2008.

[41] J. D. Pajerowski, K. N. Dahl, F. L. Zhong, P. J. Sammak, and D. E. Discher, "Physical plasticity of the nucleus in stem cell differentiation," *Proceedings of the National Academy of Sciences of the United States of America*, vol. 104, no. 40, pp. 15 619–15 624, 2007.

[42] J. G. Gall, "Cajal bodies: The first 100 years," *Annual Review of Cell & Developmental Biology*, vol. 16, no. 1, p. 273, 2000.

[43] J. Sleeman and A. Lamond, "Newly assembled snrnps associate with coiled bodies before speckles, suggesting a nuclear snrnp maturation pathway," *Current Biology*, vol. 9, no. 19, pp. 1065–1074, 1999.

[44] M. Dundr, M. D. Hebert, T. S. Karpova, D. Stanek, D. H. Xu, K. B. Shpargel, U. T. Meier, K. M. Neugebauer, A. G. Matera, and T. Misteli, "In vivo kinetics of cajal body components," *Journal of Cell Biology*, vol. 164, no. 6, pp. 831–842, 2004.

[45] T. E. Kaiser, R. V. Intine, and M. Dundr, "De novo formation of a subnuclear body," *Science*, vol. 322, no. 5908, pp. 1713–1717, 2008.

[46] M. P. Walker, L. Tian, and A. G. Matera, "Reduced viability, fertility and fecundity in mice lacking the cajal body marker protein, coilin," *Plos One*, vol. 4, no. 7, p. e6171, 2009.

[47] A. H. M. Burghes and C. E. Beattie, "Spinal muscular atrophy: why do low levels of survival motor neuron protein make motor neurons sick?" *Nature Reviews Neuroscience*, vol. 10, no. 8, pp. 597–609, 2009.

[48] M. Platani, I. Goldberg, A. I. Lamond, and J. R. Swedlow, "Cajal body dynamics and association with chromatin are atp-dependent," *Nature cell biology*, vol. 4, no. 7, p. 502, 2002.

[49] A. G. Matera, M. Izaguire-Sierra, K. Praveen, and T. K. Rajendra, "Nuclear bodies: Random aggregates of sticky proteins or crucibles of macromolecular assembly?" *Developmental Cell*, vol. 17, no. 5, pp. 639–647, 2009.

[50] S. P. Shevtsov and M. Dundr, "Nucleation of nuclear bodies by rna," *Nature cell biology*, vol. 13, no. 2, pp. 167–U134, 2011.

[51] S. Hu, L. Eberhard, J. Chen, J. C. Love, J. P. Bulter, J. J. Fredberg, G. M. Whitesides, and N. Wang, "Mechanical anisotropy of adherent cells probed by a three-dimensional magnetic twisting device," *American Journal of Physiology: Cell Physiology*, vol. 56, no. 5, pp. C1184–C1191, 2004.

[52] M. Hebert, P. Szymczyk, K. Shpargel, and A. Matera, "Coilin forms the bridge between cajal bodies and smn, the spinal muscular atrophy protein," *Genes & development*, vol. 15, no. 20, pp. 2720–2729, 2001.

[53] S. Mahmoudi, S. Henriksson, I. Weibrecht, S. Smith, O. Soderberg, S. Stromblad, K. G. Wiman, and M. Farnebo, "Wrap53 is essential for cajal body formation and for targeting the survival of motor neuron complex to cajal bodies," *Plos Biology*, vol. 8, no. 11, p. e1000521, 2010.

[54] C. G. Toyota, M. D. Davis, A. M. Cosman, and M. D. Hebert, "Coilin phosphorylation mediates interaction with smn and smb'," *Chromosoma*, vol. 119, no. 2, pp. 205–215, 2010.

[55] C. Isaac, Y. F. Yang, and U. T. Meier, "Nopp140 functions as a molecular link between the nucleolus and the coiled bodies," *Journal of Cell Biology*, vol. 142, no. 2, pp. 319–329, 1998.

[56] I. Novotny, M. Blazikova, D. Stanek, P. Herman, and J. Malinsky, "In vivo kinetics of u4/u6.u5 tri-snrnp formation in cajal bodies," *Molecular biology of the cell*, vol. 22, no. 4, pp. 513–523, 2011.

[57] L. Pellizzoni, J. Baccon, B. Charroux, and G. Dreyfuss, "The survival of motor neurons (smn) protein interacts with the snornp proteins fibrillarin and gar1," *Current Biology*, vol. 11, no. 14, pp. 1079–1088, 2001.

[58] E. Kiseleva, "Cell of the month - nuclear pore complexes and cajal bodies in xenopus laevis oocytes," *Nature cell biology*, vol. 5, no. 3, pp. 193–193, 2003.

[59] K. N. Dahl and A. Kalinowski, "Nucleoskeleton mechanics at a glance," *Journal of cell science*, vol. 124, no. 5, pp. 675–678, 2011.

[60] M. Brosig, J. Ferralli, L. Gelman, M. Chiquet, and R. Chiquet-Ehrismann, "Interfering with the connection between the nucleus and the cytoskeleton affects nuclear rotation, mechanotransduction and myogenesis," *International Journal of Biochemistry & Cell Biology*, vol. 42, no. 10, pp. 1717–1728, 2010.

[61] T. J. Chancellor, J. Lee, C. K. Thodeti, and T. Lele, "Actomyosin tension exerted on the nucleus through nesprin-1 connections influences endothelial cell adhesion, migration, and cyclic strain-induced reorientation," *Biophysical journal*, vol. 99, no. 1, pp. 115–123, 2010.

[62] C. Grashoff, B. D. Hoffman, M. D. Brenner, R. Zhou, M. Parsons, M. T. Yang, M. A. McLean, S. G. Sligar, C. S. Chen, T. Ha, and M. A. Schwartz, "Measuring mechanical tension across vinculin reveals regulation of focal adhesion dynamics," *Nature*, vol. 466, no. 7303, pp. 263–266, 2010.

[63] S. M. Hearst, A. S. Gilder, S. S. Negi, M. D. Davis, E. M. George, A. A. Whittom, C. G. Toyota, A. Husedzinovic, O. J. Gruss, and M. D. Hebert, "Cajal-body formation correlates with differential coilin phosphorylation in primary and transformed cell lines," *Journal of cell science*, vol. 122, no. 11, pp. 1872–1881, 2009.

[64] K. Hayakawa, H. Tatsumi, and M. Sokabe, "Actin stress fibers transmit and focus force to activate mechanosensitive channels," *Journal of cell science*, vol. 121, no. 4, pp. 10–10, 2008.

[65] M. Platani and I. Goldberg, "In vivo analysis of cajal body movement, separation, and joining in live human cells," *Journal of Cell Biology*, vol. 151, no. 7, p. 1561, 2000.

[66] L. Hernandez, K. J. Roux, E. S. M. Wong, L. C. Mounkes, R. Mutalif, R. Navasankari, B. Rai, S. Cool, J.-W. Jeong, H. Wang, H.-S. Lee, S. Kozlov, M. Grunert, T. Keeble, C. M. Jones, M. D. Meta, S. G. Young, I. O. Daar, B. Burke, A. O. Perantoni, and C. L. Stewart, "Functional coupling between the extracellular matrix and nuclear lamina by wnt signaling in progeria," *Developmental Cell*, vol. 19, no. 3, pp. 413–425, 2010.

[67] M. J. Paszek, N. Zahir, K. R. Johnson, J. N. Lakins, G. I. Rozenberg, A. Gefen, C. A. Reinhart-King, S. S. Margulies, M. Dembo, D. Boettiger, D. A. Hammer, and V. M. Weaver, "Tensional homeostasis and the malignant phenotype," *Cancer Cell*, vol. 8, no. 3, pp. 241–254, 2005.

[68] K. R. Levental, H. Yu, L. Kass, J. N. Lakins, M. Egeblad, J. T. Erler, S. F. T. Fong, K. Csiszar, A. Giaccia, W. Weninger, M. Yamauchi, D. L. Gasser, and V. M. Weaver, "Matrix crosslinking forces tumor progression by enhancing integrin signaling," *Cell*, vol. 139, no. 5, pp. 891–906, 2009.

[69] M. S. Samuel, J. I. Lopez, E. J. McGhee, D. R. Croft, D. Strachan, P. Timpson, J. Munro, E. Schroeder, J. Zhou, V. G. Brunton, N. Barker, H. Clevers, O. J. Sansom, K. I. Anderson, V. M. Weaver, and M. F. Olson, "Actomyosin-mediated cellular tension drives increased tissue stiffness and beta-catenin activation to induce epidermal hyperplasia and tumor growth," *Cancer Cell*, vol. 19, no. 6, pp. 776–791, 2011.

[70] J. Sleeman, P. Ajuh, and A. Lamond, "snrnp protein expression enhances the formation of cajal bodies containing p80-coilin and smn," *Journal of cell science*, vol. 114, no. 24, pp. 4407–4419, 2001.

[71] M. Hebert and A. Matera, "Self-association of coilin reveals a common theme in nuclear body localization," *Molecular biology of the cell*, vol. 11, no. 12, pp. 4159–4171, 2000.

[72] M. Dundr and T. Misteli, "The dynamics of postmitotic reassembly of the nucleolus," *Journal of Cell Biology*, vol. 150, no. 3, p. 433, 2000.

[73] F. Chowdhury, S. Na, D. Li, Y.-C. Poh, T. S. Tanaka, F. Wang, and N. Wang, "Material properties of the cell dictate stress-induced spreading and differentiation in embryonic stem cells," *Nature Materials*, vol. 9, no. 1, pp. 82–88, 2010.

[74] I. Rasnik, S. A. McKinney, and T. Ha, "Nonblinking and longlasting single-molecule fluorescence imaging," *Nature Methods*, vol. 3, no. 11, pp. 891–893, 2006.

[75] S. Na and N. Wang, "Application of fluorescence resonance energy transfer and magnetic twisting cytometry to quantify mechanochemical signaling activities in a living cell," *Science Signaling*, vol. 1, no. 34, p. pl1, 2008.

[76] R. McBeath, D. M. Pirone, C. M. Nelson, K. Bhadriraju, and C. S. Chen, "Cell shape, cytoskeletal tension, and rhoa regulate stem cell lineage commitment," *Developmental Cell*, vol. 6, no. 4, pp. 483–495, 2004.

[77] K. Kurpinski, J. Chu, C. Hashi, and S. Li, "Anisotropic mechanosensing by mesenchymal stem cells," *Proceedings of the National Academy of Sciences of the United States of America*, vol. 103, no. 44, pp. 16 095–16 100, 2006.

[78] I.-H. Park, R. Zhao, J. A. West, A. Yabuuchi, H. Huo, T. A. Ince, P. H. Lerou, M. W. Lensch, and G. Q. Daley, "Reprogramming of human somatic cells to pluripotency with defined factors," *Nature*, vol. 451, no. 7175, pp. 141–U1, 2008.

[79] Y. C. Poh, F. Chowdhury, T. S. Tanaka, and N. Wang, "Embryonic stem cells do not stiffen on rigid substrates," *Biophysical journal*, vol. 99, no. 2, pp. L19–L21, 2010.

[80] J. Nichols, B. Zevnik, K. Anastassiadis, H. Niwa, D. Klewe-Nebenius, I. Chambers, H. Scholer, and A. Smith, "Formation of pluripotent stem cells in the mammalian embryo depends on the pou transcription factor oct4," *Cell*, vol. 95, no. 3, pp. 379–391, 1998.

[81] F. Chowdhury, Y. Li, Y. C. Poh, T. Yokohama-Tamaki, N. Wang, and T. S. Tanaka, "Soft substrates promote homogeneous self-renewal of embryonic stem cells via downregulating cell-matrix tractions," *PLoS One*, vol. 5, no. 12, p. e15655, 2010.

[82] Q. le Duc, Q. Shi, I. Blonk, A. Sonnenberg, N. Wang, D. Leckband, and J. de Rooij, "Vinculin potentiates e-cadherin mechanosensing and is recruited to actin-anchored sites within adherens junctions in a myosin ii-dependent manner (vol 189, pg 1107, 2010)," *Journal of Cell Biology*, vol. 191, no. 4, pp. 891–891, 2010.

[83] D. Choquet, D. P. Felsenfeld, and M. P. Sheetz, "Extracellular matrix rigidity causes strengthening of integrin-cytoskeleton linkages," *Cell*, vol. 88, no. 1, pp. 39–48, 1997.

[84] K. Saha, A. J. Keung, E. F. Irwin, Y. Li, L. Little, D. V. Schaffer, and K. E. Healy, "Substrate modulus directs neural stem cell behavior," *Biophysical journal*, vol. 95, no. 9, pp. 4426–4438, 2008.

[85] H. Niwa, K. Yamamura, and J. Miyazaki, "Efficient selection for high-expression transfectants with a novel eukaryotic vector," *Gene*, vol. 108, no. 2, pp. 193–199, 1991.

[86] E. L. George, E. N. Georgeslabouesse, R. S. Patelking, H. Rayburn, and R. O. Hynes, "Defects in mesoderm, neural-tube and vascular development in mouse embryos lacking fibronectin," *Development*, vol. 119, no. 4, pp. 1079–1091, 1993.

[87] I. Leivo, A. Vaheri, R. Timpl, and J. Wartiovaara, "Appearance and distribution of collagens and laminin in the early mouse embryo," *Developmental biology*, vol. 76, no. 1, pp. 100–114, 1980.

[88] E. H. J. Danen, P. Sonneveld, C. Brakebusch, R. Fassler, and A. Sonnenberg, "The fibronectin-binding integrins alpha 5 beta 1 and alpha v beta 3 differentially modulate rhoa-gtp loading, organization of cell matrix adhesions, and fibronectin fibrillogenesis," *Journal of Cell Biology*, vol. 159, no. 6, pp. 1071–1086, 2002.

[89] L. M. T. Sterk, C. A. W. Geuijen, J. G. van den Berg, N. Claessen, J. J. Weening, and A. Sonnenberg, "Association of the tetraspanin cd151 with the laminin-binding integrins alpha 3 beta 1, alpha 6 beta 1, alpha 6 beta 4 and alpha 7 beta 1 in cells in culture and in vivo," *Journal of cell science*, vol. 115, no. 6, pp. 1161–1173, 2002.

[90] P. Singh, C. Carraher, and J. E. Schwarzbauer, "Assembly of fibronectin extracellular matrix," *Annual Review of Cell and Developmental Biology, Vol 26*, vol. 26, pp. 397–419, 2010.

[91] S. Yonemura, Y. Wada, T. Watanabe, A. Nagafuchi, and M. Shibata, "alpha-catenin as a tension transducer that induces adherens junction development," *Nature cell biology*, vol. 12, no. 6, pp. 533–U35, 2010.

[92] H. Obama and M. Ozawa, "Identification of the domain of alpha-catenin involved in its association with beta-catenin and plakoglobin (gamma-catenin)," *Journal of Biological Chemistry*, vol. 272, no. 17, pp. 11 017–11 020, 1997.

[93] K. A. DeMali, C. A. Barlow, and K. Burridge, "Recruitment of the arp2/3 complex to vinculin: coupling membrane protrusion to matrix adhesion," *Journal of Cell Biology*, vol. 159, no. 5, pp. 881–891, 2002.

[94] M. A. Partridge and E. E. Marcantonio, "Initiation of attachment and generation of mature focal adhesions by integrin-containing filopodia in cell spreading," *Molecular biology of the cell*, vol. 17, no. 10, pp. 4237–4248, 2006.

[95] M. Nagaoka, U. Koshimizu, S. Yuasa, F. Hattori, H. Chen, T. Tanaka, M. Okabe, K. Fukuda, and T. Akaike, "E-cadherin-coated plates maintain pluripotent es cells without colony formation," *Plos One*, vol. 1, no. 1, p. e15, 2006.

[96] B. Ladoux, E. Anon, M. Lambert, A. Rabodzey, P. Hersen, A. Buguin, P. Silberzan, and R.-M. Mege, "Strength dependence of cadherin-mediated adhesions," *Biophysical journal*, vol. 98, no. 4, pp. 534–542, 2010.

[97] A. Ralston and J. Rossant, "Genetic regulation of stem cell origins in the mouse embryo," *Clinical genetics*, vol. 68, no. 2, pp. 106–112, 2005.

[98] A. M. Wobus and K. R. Boheler, "Embryonic stem cells: Prospects for developmental biology and cell therapy," *Physiological Reviews*, vol. 85, no. 2, pp. 635–678, 2005.

[99] N. Desprat, W. Supatto, P.-A. Pouille, E. Beaurepaire, and E. Farge, "Tissue deformation modulates twist expression to determine anterior midgut differentiation in drosophila embryos," *Developmental Cell*, vol. 15, no. 3, pp. 470–477, 2008.

[100] M. Rauzi, P.-F. Lenne, and T. Lecuit, "Planar polarized actomyosin contractile flows control epithelial junction remodelling," *Nature*, vol. 468, no. 7327, pp. 1110–U515, 2010.

[101] T. Yeung, P. C. Georges, L. A. Flanagan, B. Marg, M. Ortiz, M. Funaki, N. Zahir, W. Y. Ming, V. Weaver, and P. A. Janmey, "Effects of substrate stiffness on cell morphology, cytoskeletal structure, and adhesion," *Cell motility and the cytoskeleton*, vol. 60, no. 1, pp. 24–34, 2005.

[102] N. Wang, I. M. Tolic-Norrelykke, J. X. Chen, S. M. Mijailovich, J. P. Butler, J. J. Fredberg, and D. Stamenovic, "Cell prestress. i. stiffness and prestress are closely associated in adherent contractile cells," *American Journal of Physiology-Cell Physiology*, vol. 282, no. 3, pp. C606–C616, 2002.

[103] A. J. Engler, M. A. Griffin, S. Sen, C. G. Bonnetnann, H. L. Sweeney, and D. E. Discher, "Myotubes differentiate optimally on substrates with tissue-like stiffness: pathological implications for soft or stiff microenvironments," *Journal of Cell Biology*, vol. 166, no. 6, pp. 877–887, 2004.

[104] J. Solon, I. Levental, K. Sengupta, P. C. Georges, and P. A. Janmey, "Fibroblast adaptation and stiffness matching to soft elastic substrates," *Biophysical journal*, vol. 93, no. 12, pp. 4453–4461, 2007.

[105] J. X. Chen, B. Fabry, E. L. Schiffrin, and N. Wang, "Twisting integrin receptors increases endothelin-1 gene expression in endothelial cells," *American Journal of Physiology-Cell Physiology*, vol. 280, no. 6, pp. C1475–C1484, 2001.

[106] Y. Numaguchi, S. Huang, T. R. Polte, G. S. Eichler, N. Wang, and D. E. Ingber, "Caldesmon-dependent switching between capillary endothelial cell growth and apoptosis through modulation of cell shape and contractility." *Angiogenesis*, vol. 6, no. 1, pp. 55–64, 2003.

[107] S. B. Khatau, C. M. Hale, P. J. Stewart-Hutchinson, M. S. Patel, C. L. Stewart, P. C. Searson, D. Hodzic, and D. Wirtz, "A perinuclear actin cap regulates nuclear shape," *Proceedings of the National Academy of Sciences of the United States of America*, vol. 106, no. 45, pp. 19 017–19 022, 2009.

[108] J. S. H. Lee, C. M. Hale, P. Panorchan, S. B. Khatau, J. P. George, Y. Tseng, C. L. Stewart, D. Hodzic, and D. Wirtz, "Nuclear lamin a/c deficiency induces defects in cell mechanics, polarization, and migration," *Biophysical journal*, vol. 93, no. 7, pp. 2542–2552, 2007.

[109] F. J. Byfield, Q. Wen, I. Levental, K. Nordstrom, P. E. Arratia, R. T. Miller, and P. A. Janmey, "Absence of filamin a prevents cells from responding to stiffness gradients on gels coated with collagen but not fibronectin," *Biophysical journal*, vol. 96, no. 12, pp. 5095–5102, 2009.

[110] G. Q. Daley and D. T. Scadden, "Prospects for stem cell-based therapy," *Cell*, vol. 132, no. 4, pp. 544–548, 2008.

[111] J. T. Dimos, K. T. Rodolfa, K. K. Niakan, L. M. Weisenthal, H. Mitsumoto, W. Chung, G. F. Croft, G. Saphier, R. Leibel, R. Goland, H. Wichterle, C. E. Henderson, and K. Eggan, "Induced pluripotent stem cells generated from patients with als can be differentiated into motor neurons," *Science*, vol. 321, no. 5893, pp. 1218–1221, 2008.

[112] F. Soldner, D. Hockemeyer, C. Beard, Q. Gao, G. W. Bell, E. G. Cook, G. Hargus, A. Blak, O. Cooper, M. Mitalipova, O. Isacson, and R. Jaenisch, "Parkinson's disease patient-derived induced pluripotent stem cells free of viral reprogramming factors," *Cell*, vol. 136, no. 5, pp. 964–977, 2009.

[113] M. Pekkanen-Mattila, M. Pelto-Huikko, V. Kujala, R. Suuronen, H. Skottman, K. Aalto-Setala, and E. Kerkela, "Spatial and temporal expression pattern of germ layer markers during human embryonic stem cell differentiation in embryoid bodies," *Histochemistry and cell biology*, vol. 133, no. 5, pp. 595–606, 2010.

[114] C. E. Murry and G. Keller, "Differentiation of embryonic stem cells to clinically relevant populations: Lessons from embryonic development," *Cell*, vol. 132, no. 4, pp. 661–680, 2008.

[115] P. L. Townes and J. Holtfreter, "Directed movements and selective adhesion of embryonic amphibian cells," *Journal of Experimental Zoology*, vol. 128, no. 1, pp. 53–120, 1955.

[116] M. S. Steinberg, "Differential adhesion in morphogenesis: a modern view," *Current opinion in genetics & development*, vol. 17, no. 4, pp. 281–286, 2007.

[117] A. K. Harris, "Is cell sorting caused by differences in work of intercellular-adhesion - critique of steinberg hypothesis," *Journal of theoretical biology*, vol. 61, no. 2, pp. 267–285, 1976.

[118] J. D. Amack and M. L. Manning, "Knowing the boundaries: Extending the differential adhesion hypothesis in embryonic cell sorting," *Science*, vol. 338, no. 6104, pp. 212–215, 2012.

[119] M. Krieg, Y. Arboleda-Estudillo, P. H. Puech, J. Kaefer, F. Graner, D. J. Mueller, and C. P. Heisenberg, "Tensile forces govern germ-layer organization in zebrafish," *Nature cell biology*, vol. 10, no. 4, pp. 429–U122, 2008.

[120] A. G. Smith, J. Nichols, M. Robertson, and P. D. Rathjen, "Differentiation inhibiting activity (dia/lif) and mouse development," *Developmental biology*, vol. 151, no. 2, pp. 339–351, 1992.

[121] H. Niwa, K. Ogawa, D. Shimosato, and K. Adachi, "A parallel circuit of lif signalling pathways maintains pluripotency of mouse es cells," *Nature*, vol. 460, no. 7251, pp. 118–122, 2009.

[122] J. Zoldan, E. D. Karagiannis, C. Y. Lee, D. G. Anderson, R. Langer, and S. Levenberg, "The influence of scaffold elasticity on germ layer specification of human embryonic stem cells," *Biomaterials*, vol. 32, no. 36, pp. 9612–9621, 2011.

[123] R. Uibo, I. Laidmaee, E. S. Sawyer, L. A. Flanagan, P. C. Georges, J. P. Winer, and P. A. Janmey, "Soft materials to treat central nervous system injuries: Evaluation of the suitability of non-mammalian fibrin gels," *Biochimica Et Biophysica Acta-Molecular Cell Research*, vol. 1793, no. 5, pp. 924–930, 2009.

[124] Y.-E. Ju, P. A. Janmey, M. E. McCormick, E. S. Sawyer, and L. A. Flanagan, "Enhanced neurite growth from mammalian neurons in three-dimensional salmon fibrin gels," *Biomaterials*, vol. 28, no. 12, pp. 2097–2108, 2007.

[125] J. Liu, Y. Tan, H. Zhang, Y. Zhang, P. Xu, J. Chen, Y. C. Poh, K. Tang, N. Wang, and B. Huang, "Soft fibrin gels promote selection and growth of tumorigenic cells," *Nature Materials*, vol. 11, no. 8, pp. 734–741, 2012.

[126] J. P. Winer, S. Oake, and P. A. Janmey, "Non-linear elasticity of extracellular matrices enables contractile cells to communicate local position and orientation," *Plos One*, vol. 4, no. 7, p. e6382, 2009.

[127] C. Fuchs, M. Scheinast, W. Pasteiner, S. Lagger, M. Hofner, A. Hoellrigl, M. Schultheis, and G. Weitzer, "Self-organization phenomena in embryonic stem cell-derived embryoid bodies: Axis formation and breaking of symmetry during cardiomyogenesis," *Cells Tissues Organs*, vol. 195, no. 5, pp. 377–391, 2012.

[128] M. A. Schwartz and C. S. Chen, "Deconstructing dimensionality," *Science*, vol. 339, no. 6118, pp. 402–404, 2013.

[129] H. Hong and J. P. Stegemann, "2d and 3d collagen and fibrin biopolymers promote specific ecm and integrin gene expression by vascular smooth muscle cells," *Journal of Biomaterials Science-Polymer Edition*, vol. 19, no. 10, pp. 1279–1293, 2008.

[130] P. M. Gilbert, K. L. Havenstrite, K. E. G. Magnusson, A. Sacco, N. A. Leonardi, P. Kraft, N. K. Nguyen, S. Thrun, M. P. Lutolf, and H. M. Blau, "Substrate elasticity regulates skeletal muscle stem cell self-renewal in culture," *Science*, vol. 329, no. 5995, pp. 1078–1081, 2010.

[131] V. Maruthamuthu, B. Sabass, U. S. Schwarz, and M. L. Gardel, "Cell-ecm traction force modulates endogenous tension at cell-cell contacts," *Proceedings of the National Academy of Sciences of the United States of America*, vol. 108, no. 12, pp. 4708–4713, 2011.

[132] A. F. Mertz, S. Banerjee, Y. Che, G. K. German, Y. Xu, C. Hyland, M. C. Marchetti, V. Horsley, and E. R. Dufresne, "Scaling of traction forces with the size of cohesive cell colonies," *Physical Review Letters*, vol. 108, no. 19, p. 198101, 2012.

[133] S. F. G. Krens, S. Moellmert, and C.-P. Heisenberg, "Enveloping cell-layer differentiation at the surface of zebrafish germ-layer tissue explants," *Proceedings of the National Academy of Sciences of the United States of America*, vol. 108, no. 3, pp. E9–E10, 2011.

[134] Y. Cai, O. Rossier, N. C. Gauthier, N. Biais, M.-A. Fardin, X. Zhang, L. W. Miller, B. Ladoux, V. W. Cornish, and M. P. Sheetz, "Cytoskeletal coherence requires myosin-iia contractility," *Journal of cell science*, vol. 123, no. 3, pp. 413–423, 2010.

[135] P. P. L. Tam and D. A. F. Loebel, "Gene function in mouse embryogenesis: get set for gastrulation," *Nature Reviews Genetics*, vol. 8, no. 5, pp. 368–381, 2007.

[136] S. Koelle, S. Reese, and W. Kummer, "New aspects of gamete transport, fertilization, and embryonic development in the oviduct gained by means of live cell imaging," *Theriogenology*, vol. 73, no. 6, pp. 786–795, 2010.

[137] J. Nichols and A. Smith, "Pluripotency in the embryo and in culture," *Cold Spring Harbor Perspectives in Biology*, vol. 4, no. 8, p. a008128, 2012.

[138] M. Marsden and D. W. DeSimone, "Integrin-ecm interactions regulate cadherin-dependent cell adhesion and are required for convergent extension in xenopus," *Current Biology*, vol. 13, no. 14, pp. 1182–1191, 2003.

[139] S. Yamada and W. J. Nelson, "Localized zones of rho and rac activities drive initiation and expansion of epithelial cell-cell adhesion," *Journal of Cell Biology*, vol. 178, no. 3, pp. 517–527, 2007.

[140] T. Manshouri, A. Quintas-Cardama, R. H. Nussenzveig, A. Gaikwad, Z. Estrov, J. Prchal, J. E. Cortes, H. M. Kantarjian, and S. Verstovsek, "The jak kinase inhibitor cp-690,550 supresses the growth of human polycythemia vera cells carrying the jak2(v617f) mutation," *Cancer Science*, vol. 99, no. 6, pp. 1265–1273, 2008.

[141] S. Dupont, L. Morsut, M. Aragona, E. Enzo, S. Giulitti, M. Cordenonsi, F. Zanconato, J. L. Digabel, M. Forcato, S. Bicciato, N. Elvassore, and S. Piccolo, "Role of yap/taz in mechanotransduction," *Nature*, vol. 474, no. 7350, pp. 179–U212, 2011.

[142] D. ten Berge, W. Koole, C. Fuerer, M. Fish, E. Eroglu, and R. Nusse, "Wnt signaling mediates self-organization and axis formation in embryoid bodies," *Cell Stem Cell*, vol. 3, no. 5, pp. 508–518, 2008.

[143] S. Hu and N. Wang, "Control of stress propagation in the cytoplasm by prestress and loading frequency," *Molecular & Cellular Biomechanics*, vol. 3, no. 2, pp. 49–60, 2006.

[144] L. Chen, Z. Xiao, Y. Meng, Y. Zhao, J. Han, G. Su, B. Chen, and J. Dai, "The enhancement of cancer stem cell properties of mcf-7 cells in 3d collagen scaffolds for modeling of cancer and anti-cancer drugs," *Biomaterials*, vol. 33, no. 5, pp. 1437–1444, 2012.

[145] E. Abranches, M. Silva, L. Pradier, H. Schulz, O. Hummel, D. Henrique, and E. Bekman, "Neural differentiation of embryonic stem cells in vitro: A road map to neurogenesis in the embryo," *Plos One*, vol. 4, no. 7, p. e6286, 2009.

[146] G. Shivashankar, "Mechanosignaling to the cell nucleus and gene regulation," *Annual review of biophysics*, vol. 40, pp. 361–378, 2011.

[147] S. Kumar and V. M. Weaver, "Mechanics, malignancy, and metastasis: The force journey of a tumor cell," *Cancer and metastasis reviews*, vol. 28, no. 1-2, pp. 113–127, 2009.

[148] A. D. Bershadsky, N. Q. Balaban, and B. Geiger, "Adhesion-dependent cell mechanosensitivity," *Annual Review of Cell and Developmental Biology*, vol. 19, pp. 677–695, 2003.

[149] T. Lecuit and P.-F. Lenne, "Cell surface mechanics and the control of cell shape, tissue patterns and morphogenesis," *Nature Reviews Molecular Cell Biology*, vol. 8, no. 8, pp. 633–644, 2007.

[150] J. C. Friedland, M. H. Lee, and D. Boettiger, "Mechanically activated integrin switch controls alpha(5)beta(1) function," *Science*, vol. 323, no. 5914, pp. 642–644, 2009.

[151] M. J. Dalby, N. Gadegaard, R. Tare, A. Andar, M. O. Riehle, P. Herzyk, C. D. W. Wilkinson, and R. O. C. Oreffo, "The control of human mesenchymal cell differentiation using nanoscale symmetry and disorder," *Nature Materials*, vol. 6, no. 12, pp. 997–1003, 2007.

[152] A. Engler, L. Bacakova, C. Newman, A. Hategan, M. Griffin, and D. Discher, "Substrate compliance versus ligand density in cell on gel responses," *Biophysical journal*, vol. 86, no. 1, pp. 617–628, 2004.

[153] J. R. Tse and A. J. Engler, "Preparation of hydrogel substrates with tunable mechanical properties." *Current protocols in cell biology / editorial board, Juan S.Bonifacino ...[et al.]*, vol. Chapter 10, 2010.

[154] I. M. Tolic-Norrelykke, J. P. Butler, J. X. Chen, and N. Wang, "Spatial and temporal traction response in human airway smooth muscle cells," *American Journal of Physiology-Cell Physiology*, vol. 283, no. 4, pp. C1254–C1266, 2002.

[155] J. P. Butler, I. M. Tolic-Norrelykke, B. Fabry, and J. J. Fredberg, "Traction fields, moments, and strain energy that cells exert on their surroundings," *American Journal of Physiology-Cell Physiology*, vol. 282, no. 3, pp. C595–C605, 2002.